

UNIVERSIDADE ESTADUAL PAULISTA “JÚLIO DE MESQUITA FILHO”

FACULDADE DE ENGENHARIA

CAMPUS DE ILHA SOLTEIRA

PABLO TORREZ CABALLERO

**INCLUSION OF THE FREQUENCY DEPENDENCE IN THE BERGERON MODEL:
REPRESENTATION OF SHORT AND LONG TRANSMISSION LINES CONSIDERING
ELECTROMAGNETIC TRANSIENTS RESULTING FROM SWITCHING
OPERATIONS AND LIGHTNING STRIKES**

**INCLUSÃO DO EFEITO DA FREQUÊNCIA NO MODELO DE BERGERON:
REPRESENTAÇÃO DE LINHAS DE TRANSMISSÃO CURTAS E LONGAS
CONSIDERANDO TRANSITÓRIOS ELETROMAGNÉTICOS RESULTANTES DE
OPERAÇÕES DE MANOBRAS E DE DESCARGAS ATMOSFÉRICAS**

Ilha Solteira

2018

PABLO TORREZ CABALLERO

**INCLUSION OF THE FREQUENCY DEPENDENCE IN THE BERGERON MODEL:
REPRESENTATION OF SHORT AND LONG TRANSMISSION LINES CONSIDERING
ELECTROMAGNETIC TRANSIENTS RESULTING FROM SWITCHING
OPERATIONS AND LIGHTNING STRIKES**

**INCLUSÃO DO EFEITO DA FREQUÊNCIA NO MODELO DE BERGERON:
REPRESENTAÇÃO DE LINHAS DE TRANSMISSÃO CURTAS E LONGAS
CONSIDERANDO TRANSITÓRIOS ELETROMAGNÉTICOS RESULTANTES DE
OPERAÇÕES DE MANOBRAS E DE DESCARGAS ATMOSFÉRICAS**

Tese apresentada à Faculdade de Engenharia de Ilha Solteira, Campus de Ilha Solteira - UNESP, como parte dos requisitos para obtenção do título de Doutor em Engenharia Elétrica.

Área de Conhecimento: Automação

Prof. Dr. Sérgio Kurokawa
Orientador

Ilha Solteira

2018

FICHA CATALOGRÁFICA

Desenvolvido pelo Serviço Técnico de Biblioteca e Documentação

T694i Torrez Caballero, Pablo.
Inclusão do efeito da frequência no modelo de Bergeron: representação de linhas de transmissão curtas e longas considerando transitórios eletromagnéticos resultantes de operações de manobras e de descargas atmosféricas / Pablo Torrez Caballero. -- Ilha Solteira: [s.n.], 2018
174 f. : il.

Tese (doutorado) - Universidade Estadual Paulista. Faculdade de Engenharia de Ilha Solteira. Área de conhecimento: Automação, 2018

Orientador: Sérgio Kurokawa
Inclui bibliografia

1. Modelo de linha de transmissão. 2. Modelo de Bergeron. 3. Análise de transitórios.

Raiane da Silva Santos
Raiane da Silva Santos

Supervisora Técnica de Saúde
Serviço Técnico de Biblioteca, Arquivo e Documentação
Diretoria Técnica de Biblioteca e Documentação
CUBA - 999


CERTIFICADO DE APROVAÇÃO

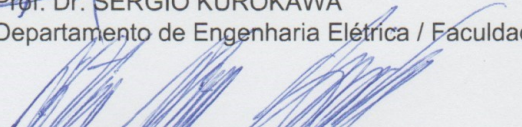
TÍTULO DA TESE: Inclusion of the frequency effect in the Bergeron line model: Representation of short and long transmission lines considering eletromagnetic transientes resulting from switching operations and lightning strikes

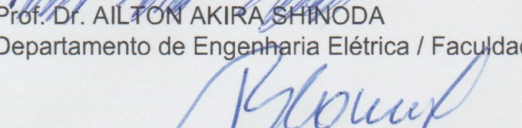
AUTOR: PABLO TORREZ CABALLERO

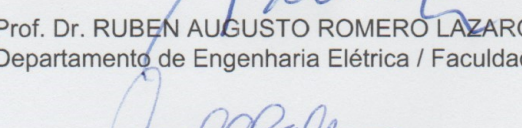
ORIENTADOR: SERGIO KUROKAWA

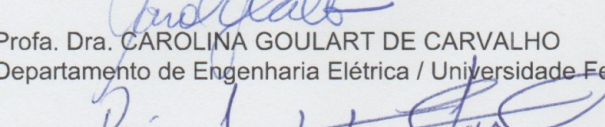
Aprovado como parte das exigências para obtenção do Título de Doutor em ENGENHARIA ELÉTRICA, área: Automação pela Comissão Examinadora:


Prof. Dr. SERGIO KUROKAWA
Departamento de Engenharia Elétrica / Faculdade de Engenharia de Ilha Solteira


Prof. Dr. AILTON AKIRA SHINODA
Departamento de Engenharia Elétrica / Faculdade de Engenharia de Ilha Solteira


Prof. Dr. RUBEN AUGUSTO ROMERO LAZARO
Departamento de Engenharia Elétrica / Faculdade de Engenharia de Ilha Solteira


Profa. Dra. CAROLINA GOULART DE CARVALHO
Departamento de Engenharia Elétrica / Universidade Federal do Mato Grosso do Sul


Prof. Dr. ROGERIO ANDRADE FLAUZINO
Departamento de Engenharia Elétrica e de Computação / Escola de Engenharia de São Carlos - USP

Ilha Solteira, 17 de dezembro de 2018

ACKNOWLEDGEMENTS

To Fundação de Amparo à Pesquisa do Estado de São Paulo – FAPESP for the financial support, without which this research project would not be possible. Project 2014/17051-0. The author would also like to acknowledge the Coordination for the Improvement of Higher Education Personnel CAPES for the support.

Gratitude and greetings to the supervisor, who dedicates part of his time to this project.

The author would also like to thank all the family and friends for all the help and support provided through the years.

RESUMO

O objetivo deste projeto é desenvolver um modelo de linha de transmissão que leva em conta as principais características exigidas de um modelo deste componente do sistema elétrico, ou seja, ser desenvolvido diretamente no domínio do tempo, considerar que os parâmetros da linha são distribuídos ao longo de seu comprimento e levar em conta que os parâmetros longitudinais variam em função da frequência. O modelo proposto é baseado no modelo de Bergeron, que é um modelo de linha de transmissão desenvolvido diretamente no domínio do tempo e que leva em conta que os parâmetros de uma linha de transmissão são distribuídos ao longo de seu comprimento. No modelo proposto será levado em consideração que, devido aos efeitos solo e pelicular, os parâmetros longitudinais da linha (resistência longitudinal e indutância longitudinal) são variáveis em relação à frequência. Estes parâmetros serão aproximados por funções racionais e inseridos no modelo de Bergeron. O modelo desenvolvido será utilizado para representar linhas curtas e longas em simulações de transitórios eletromagnéticos resultantes de operações de manobras e de incidências de descargas atmosféricas. Por ser desenvolvido diretamente no domínio do tempo, o modelo proposto pode ser facilmente inserido em aplicativos do tipo ATP (*Alternative Transients Program*) e será uma ferramenta útil em simulações e análises de transitórios eletromagnéticos em sistemas de energia elétrica.

Keywords: Modelo de linha de transmissão. Modelo de Bergeron. Análise de transitórios.

ABSTRACT

The main objective of our project is to develop a transmission line model that takes into account the main characteristics demanded by a model of this electrical system component, i.e., be developed directly in the time-domain, consider the distributed nature of the line parameters and take into account the frequency dependence of the longitudinal parameters. The proposed model is based on the Bergeron model, which is a transmission line model directly developed in the time domain that takes into account that the transmission line parameters are distributed along its length. In the proposed model it will be taken into account that, due to earth-return effect and skin impedance, the longitudinal parameters (longitudinal resistance and longitudinal inductance) vary in relation to the frequency. These parameters will be approximated by rational functions and will be added to the Bergeron model. The developed model will be used to represent short and long transmission lines in simulations resulting from switching operations and lightning strikes. Because of the model being directly developed in the time-domain, the proposed model can be easily implemented in programs ATP-like (*Alternative Transients Program*) and will be a useful tool in power system transient analysis.

Keywords: Transmission line model. Bergeron model. Transient analysis.

LIST OF FIGURES

FIGURE 1 – CONDUCTORS I AND K, OVER AN IDEAL SOIL, WITH ITS IMAGES I' AND K'	7
FIGURE 2 – NORMALIZED CURRENT FOR VARIOUS FREQUENCIES.....	10
FIGURE 3 – NORMALIZED CURRENT DISTRIBUTION COMPARISON.	11
FIGURE 4 – TYPES OF CONDUCTORS.....	13
FIGURE 5 – INTERNAL RESISTANCE FOR DIFFERENT EXTERNAL-INTERNAL RADII RATIOS.....	15
FIGURE 6 – INTERNAL INDUCTANCE FOR DIFFERENT EXTERNAL-INTERNAL RADII RATIOS	15
FIGURE 7 – ACSR CABLE AND ACCC CABLE.....	16
FIGURE 8 – CONDUCTORS I K, OVER A NON-IDEAL SOIL, WITH ITS RESPECTIVE IMAGES	17
FIGURE 9 – GROUND RESISTANCE AND INDUCTANCE FOR VARIOUS VALUES OF THE SOIL RESISTIVITY P	21
FIGURE 10 – GROUND RESISTANCE AND INDUCTANCE FOR VARIOUS VALUES OF THE SOIL RESISTIVITY P	22
FIGURE 11 – CHARGE DISTRIBUTION IN A GENERIC BIPHASIC LINE	24
FIGURE 12 – SHUNT CAPACITANCE CIRCUIT.....	26
FIGURE 13 – BUNDLING OF CONDUCTORS.....	29
FIGURE 14 – CASCADED TRANSMISSION LINE WITH TOWER RESISTANCES	33
FIGURE 15 – SEGMENTED GROUND WIRE.....	34
FIGURE 16 – PHASE TRANSPOSITIONS.....	35
FIGURE 17 – 400kV TRANSMISSION LINE	40
FIGURE 18 – PHASE 1'S SELF-IMPEDANCE.....	41
FIGURE 19 – MUTUAL IMPEDANCES.....	42
FIGURE 20 – SINGLE-PHASE TRANSMISSION LINE.....	44
FIGURE 21 – TRANSMISSION LINE'S INFINITESIMAL SEGMENT	45
FIGURE 22 – COMMON LOW FREQUENCY WAVEFORMS USED IN TRANSIENT ANALYSIS	50
FIGURE 23 – COMMON HIGH FREQUENCY WAVEFORMS USED IN TRANSIENT ANALYSIS	50
FIGURE 24 – FREQUENCY DEPENDENT TRANSFORMATION MATRICES RESPONSE.....	56
FIGURE 25 – CONSTANT TRANSFORMATION MATRICES RESPONSE IN A TRANSPOSED LINE.....	62
FIGURE 26 – CONSTANT TRANSFORMATION MATRICES RESPONSE IN AN UNTRANSPOSED LINE.....	63

FIGURE 27 – FREQUENCY DOMAIN SOLUTION FLOWCHART.....	68
FIGURE 28 – CESP’S TRANSMISSION LINE MODES.....	69
FIGURE 29 – INFINITESIMAL PORTION OF THE TRANSMISSION LINE.....	73
FIGURE 30 – LINE’S TWO PORT NETWORK.....	76
FIGURE 31 – EQUIVALENT IMPEDANCES NETWORK.....	77
FIGURE 32 – MODIFIED QUADRUPOLE.....	78
FIGURE 33 – BERGERON’S MODEL WITH LOSSES CONCENTRATED ON BOTH TERMINALS.....	79
FIGURE 34 – BERGERON’S MODEL WITH LOSSES LUMPED IN THREE POINTS.....	79
FIGURE 35 – ADMITTANCE-TYPE DIRECT CIRCUIT TOPOLOGY.....	89
FIGURE 36 – IMPEDANCE-TYPE DIRECT CIRCUIT TOPOLOGY.....	90
FIGURE 37 – IMPEDANCE-TYPE MODIFIED-FITTING EQUIVALENT CIRCUIT.....	93
FIGURE 38 – ERROR REDUCTION AS A FUNCTION OF THE NUMBER OF TERMS.....	97
FIGURE 39 – MODIFIED CIRCUIT FITTING FLOWCHART.....	99
FIGURE 40 – MODIFIED CIRCUIT FITTING.....	100
FIGURE 41 – ACCURACY OF THE MODIFIED CIRCUIT FITTING.....	101
FIGURE 42 – MODIFIED TWO-PORT NETWORK.....	104
FIGURE 43 – MODIFIED BERGERON CIRCUIT.....	106
FIGURE 44 – DIRECT-CIRCUIT TOPOLOGY.....	106
FIGURE 45 – INDIRECT CIRCUIT TOPOLOGY.....	106
FIGURE 46 – FIRST-ORDER CIRCUIT OF A DIRECT FITTING.....	107
FIGURE 47 – FIRST-ORDER CIRCUIT OF AN INDIRECT FITTING.....	108
FIGURE 48 – SECOND-ORDER CIRCUIT OF A DIRECT FITTING.....	108
FIGURE 49 – SECOND-ORDER CIRCUIT OF AN INDIRECT FITTING.....	109
FIGURE 50 – FITTED CIRCUIT INCLUDING STATE SPACE EQUATIONS.....	110
FIGURE 51 – TRANSMISSION LINE DIVIDED IN B BLOCKS.....	111
FIGURE 52 – COMPOSITION OF EACH BLOCK.....	111
FIGURE 53 – SINGLE FREQUENCY-DEPENDENT BERGERON MODEL.....	113
FIGURE 54 – CASCADED FREQUENCY DEPENDENT METHOD OF CHARACTERISTICS.....	113
FIGURE 55 – INPUT MESH.....	114

FIGURE 56 – OUTPUT MESH	115
FIGURE 57 – CONNECTION MESH	117
FIGURE 58 – FIRST-ORDER EQUIVALENT CIRCUIT	117
FIGURE 59 – SECOND-ORDER EQUIVALENT CIRCUIT	118
FIGURE 60 – SIMPLIFIED CONNECTION MESH	118
FIGURE 61 – GUIDE TO ASSEMBLE VECTORS OF INDEXES	128
FIGURE 62 – ERROR STACKED DUE TO TIME DISCRETIZATION AND PROPOSED SOLUTION.....	129
FIGURE 64 – MULTICONDUCTOR TRANSMISSION LINE WITH VERTICAL CONFIGURATION.....	131
FIGURE 65 – MULTICONDUCTOR TRANSMISSION LINE LAYOUT.....	132
FIGURE 66 – INDUCED VOLTAGE IN A TRANSMISSION LINE WITH VERTICAL CONFIGURATION.....	132
FIGURE 67 – INDUCED ERROR AS A FUNCTION OF THE FREQUENCY AT WHICH THE TRANSFORMATION MATRICES ARE CALCULATED.	133
FIGURE 68 – RESPONSE OF THE PROPOSED MODEL SEGMENTING THE LINE IN 1, 5 AND 50 BLOCKS.	135
FIGURE 69 – ERROR OF THE PROPOSED MODEL AS A FUNCTION OF THE NUMBER OF CASCADED BLOCKS.....	136
FIGURE 70 – MULTICONDUCTOR TRANSMISSION LINE LAYOUT.....	137
FIGURE 71 – ENERGIZING OF A 100KM OPEN-CIRCUITED TRANSMISSION LINE.....	138
FIGURE 72 – ENERGIZING OF A 1000KM OPEN-CIRCUITED TRANSMISSION LINE.....	139
FIGURE 73 – HIGH FREQUENCY TEST LAYOUT.....	140
FIGURE 74 – INDUCED VOLTAGE DURING A FAST TRANSIENT.....	140
FIGURE 75 – INPUT CURRENT DURING A FAST TRANSIENT.....	141
FIGURE 76 – OUTPUT CURRENT DURING A FAST TRANSIENT.....	141
FIGURE 77 – A THREE PHASE TRANSMISSION LINE TERMINATED BY A NONLINEAR LOAD.....	143
FIGURE 78 – SIMULATION RESULTS: VOLTAGES AT THE RECEIVING TERMINAL.....	143
FIGURE 79 – SIMULATION RESULTS: CURRENTS AT THE RECEIVING TERMINAL.....	144

LIST OF TABLES

TABLE 1 – A CAPACITANCE ASSOCIATED TO EACH MODE	70
TABLE 2 – CONSTANT IN THE LINEAR TERM FOR DIRECT AND INDIRECT CIRCUIT TOPOLOGIES	95
TABLE 3 – CONSTANT TERM OBTAINED FOR DIFFERENT TYPES OF CIRCUIT FITTING	95
TABLE 4 – FITTING RAW-NRMSE FOR VARIOUS NUMBERS OF TERMS	96
TABLE 5 – A COMPARISON OF FLOPS PER ITERATION FOR DIFFERENT METHODS. B IS THE NUMBER OF CASCADED BLOCKS AND M IS THE NUMBER OF POLES USED TO FIT THE LONGITUDINAL IMPEDANCE.....	124
TABLE 5 – SIMULATION TIMES	125
TABLE 6 – PROCESSING TIMES FOR VARIOUS TRANSMISSION LINE MODELS.....	142

SUMMARY

1	INTRODUCTION	1
1.1	TRANSMISSION LINE MODELING	1
1.2	ORGANIZATION	4
1.3	PUBLISHED PAPERS	5
2	TRANSMISSION LINE PARAMETERS	6
2.1	INTRODUCTION	6
2.2	LONGITUDINAL IMPEDANCE	6
2.2.1	External impedance	7
2.2.2	Internal impedance	9
2.2.3	Earth-return impedance	16
2.3	TRANVERSAL ADMITTANCE	20
2.3.1	Transversal capacitance	23
2.4	STRANDED CONDUCTORS	27
2.5	BUNDLING OF CONDUCTORS	28
2.6	GROUND WIRES	31
2.6.1	Continuous Ground wires	32
2.6.2	Segmented Ground wires	33
2.7	TRANSPOSITION OF SINGLE-CIRCUIT THREE-PHASE LINES	34
2.8	APPLICATION	39
2.9	CONCLUSION	43
3	FREQUENCY DOMAIN MODEL OF A MULTICONDUCTOR TRANSMISSION LINE	44
3.1	INTRODUCTION	44
3.2	SINGLE PHASE TRANSMISSION LINE DIFFERENTIAL EQUATIONS	44
3.3	GENERAL SOLUTION OF THE TRANSMISSION LINE EQUATIONS	46
3.4	FREQUENCIES INVOLVED IN PRACTICAL CASES	49
3.5	MODAL TRANSFORMATION OF MULTICONDUCTOR TRANSMISSION LINES	50
3.6	TRANSFORMATION MATRICES	53
3.6.1	Frequency-Dependent Transformation Matrices	55
3.6.2	Constant Transformation Matrices	57
3.6.3	Two-Phase Constant Transformation Matrices	57
3.6.4	Three-phase Constant Transformation Matrices	58
3.6.5	Multi-phase constant transformation matrices	62
3.7	PHASE-DOMAIN SOLUTION OF A TRANSMISSION LINE IN THE FREQUENCY DOMAIN	64
3.8	IMPLEMENTATION	67
3.9	CONSIDERATIONS ON MODAL TRANSFORMATION	68
3.10	CONCLUSION	70

4	TIME DOMAIN TRANSMISSION LINE MODELS	72
4.1	INTRODUCTION	72
4.2	TRANSMISSION LINE DIFFERENTIAL EQUATIONS IN THE TIME DOMAIN	72
4.3	BERGERON'S LINE MODEL	74
4.4	CONCLUSION	80
5	PARAMETER REPRESENTATION USING RATIONAL FUNCTIONS	81
5.1	INTRODUCTION	81
5.2	FITTING MODELS	81
5.2.1	The Model-Based Parameter Estimation (MBPE)	82
5.2.2	The Vector Fitting VF	83
5.2.3	The Debye's type Fitting DF	84
5.2.4	Modified Vector Fitting MVF	85
5.2.5	Fast Vector Fitting FVF	86
5.2.6	Fast Relaxed Vector Fitting FRVF	87
5.3	EQUIVALENT CIRCUIT TOPOLOGIES	87
5.3.1	Direct-Circuit Topology	88
5.3.2	Indirect-Circuit Topology	92
5.3.3	Equivalent Circuit for longitudinal impedance in transmission lines	94
5.4	NUMBER OF POLES-RESIDUES	95
5.5	INITIAL POLES	97
5.6	POLE REFINEMENT	98
5.7	IMPLEMENTATION	98
5.8	APPLICATION	100
5.9	CONCLUSION	102
6	OUR APPROACH: INCLUSION OF THE FREQUENCY EFFECT IN THE METHOD OF CHARACTERISTICS FOR MULTICONDUCTOR TRANSMISSION LINES	103
6.1	INTRODUCTION	103
6.2	MODIFIED METHOD OF CHARACTERISTICS	103
6.3	STATE SPACE REPRESENTATION OF THE FITTED LONGITUDINAL IMPEDANCE	105
6.3.1	First-Order Branch Circuit	107
6.3.2	Second-Order Circuit	108
6.3.3	State Space Matrix Assembly	110
6.4	CASCADED FREQUENCY DEPENDENT METHOD OF CHARACTERISTICS	111
6.4.1	Input mesh	114
6.4.2	Output Mesh	115
6.4.3	Simplified Connection Mesh	116
6.5	STATE EQUATIONS OF THE FITTED LONGITUDINAL IMPEDANCE	119
6.6	SOLUTION OF THE STATE-SPACE EQUATIONS	121
6.6.1	Heun's method	122

6.7	FAST IMPLEMENTATION OF THE FREQUENCY-DEPENDENT METHOD OF CHARACTERISTICS	123
6.7.1	Global Solution	123
6.7.2	Variable storage	125
6.7.3	Correction due to Time Discretization	128
6.8	MODAL TRANSFORMATION APPLIED TO THE MODEL	129
6.9	CONCLUSION	133
7	VALIDATION AND RESULTS	134
7.1	TRANSMISSION LINE USED AND VALIDATION	134
7.2	QUANTITY OF CASCADED BLOCKS	134
7.3	STEP SIZE	136
7.4	LONG VS. SHORT LINES	136
7.5	FAST TRANSIENTS	137
7.6	QUALITY AND PROCESSING TIMES	142
7.7	COMPATIBILITY	142
7.8	CONCLUSION	144
8	CONCLUSIONS	145
	REFERENCES	146

1 INTRODUCTION

1.1 TRANSMISSION LINE MODELING

One of the most important aspects in transmission line modeling for electromagnetic transient studies is taking into account the frequency dependence and the distributed nature of the transmission line parameters. By aiming to accurately describe the transmission line behavior, many models had been proposed and enhanced in technical literature through time: the method of characteristics, distributed-parameters models, frequency domain methods, convolution methods, finite element methods and others.

First, the method of characteristics was applied by Bergeron ¹ to solve hydraulic problems and later was used by Branin ² to accurately and efficiently simulate transients in lossless transmission lines. Afterwards, Dommel ³ implemented the lossy lumped method of characteristics in the nodal admittance matrix method, and so created the first flexible algorithm to solve circuits with non-linear elements, switching operations and non-zero initial conditions through the trapezoidal rule of integration. This algorithm rapidly evolved to become one of the first computational programs for transient simulations, the EMTP ⁴.

One of the issues with Dommel's method ³ to represent transmission lines is that the line parameters are fixed in a predetermined frequency. Transmission line parameters are strongly dependent on the frequency effect, specially the earth-return impedance as showed by Carson ⁵. In order to overcome this limitation, Budner ⁶ developed an alternative method that considers the frequency dependence of the line parameters. Budner solved the hyperbolic equations in the time domain using weighting functions based on the convolution integrals present in the inverse transform. Afterwards, Meyer ⁷ applied the convolution theory and inverse transform theory to enhance the weighting functions developed by Budner, improving accuracy and processing time.

Another limitation of time-domain methods is that multiphase transmission lines have to be simulated as set of single-phase transmission lines due to coupling between its parameters. Aiming

to overcome this issue, Saied⁸ modeled the mutual impedances as a transformer in cascade with the line.

The basic approach to represent transmission lines was to formulate it in the frequency-domain and then solve the convolution integrals existing in the inverse transform, which is needed to see the time-domain response of the line. Many authors developed different ways of solving the convolution integrals: Semlyen^{9,10} proposed to avoid them by approximating the characteristic admittances with exponential functions, that can be solved through simpler expressions. Marti¹¹ used rational functions to approach the frequency-dependent parameters so they can be solved in the time-domain with recursive methods. Breiholtz¹² avoided the convolution integrals by solving the transmission line equations using the Galerkin method.

Within the models based on the method of characteristics, Snelson's contribution¹³ was to propose the usage of traveling waves instead of voltages and currents as variables of interest in Dommel's proposal³, giving great computational dividends. Marti¹⁴ modified the Bergeron model to include weighting functions so the line can be represented by a single Bergeron. Modern literature still improves the method of characteristics in order to expand its capabilities^{15,16}.

Due to the advantages of time-domain methods, other lumped parameters models were developed in technical literature. Colvin¹⁷ formulated the cascade of lumped parameters and solved the resulting matrices using Cramer's rule. Nelms¹⁸ opted to use the trapezoidal rule of integration to solve the resulting state equations of the cascade of lumped parameters, including the capability of modeling surge arresters¹⁹, tower resistances and transformers²⁰. Considering that the lumped parameter model may have oscillations, one way of avoiding the oscillations is by connecting filters in the system's input or output²¹. Gustavsen²² modeled the transmission line and, by applying the Vector Fitting, managed to obtain the realization of the equations directly in the time-domain. Morched²³ opted to adjust the variables in the phase-domain and express the result in terms of convolutions, to represent both cables and overhead lines. Most of the time-domain methods depend on the time step used in the simulations²⁴ and on the method used to include the frequency dependence in the line parameters²⁵. The most complex models require smaller time steps. Many

of these models depend on a constant real transformation matrix to decouple multiphase lines into its modes and represent each mode individually as a single phase line ^{26,27,28,29}.

Modern time-domain models take into account the frequency effect by solving the convolution integrals by means of fitting methods and directly solving the equations using recursive techniques ^{30,31,32,33,34,35,36,37}.

Time-domain methods are preferred to represent transmission lines over frequency-domain methods because they can also represent non-linear elements (surge arresters, power electronic devices, saturable inductors, switching devices and others) and parameter changing factors (such as the effect of corona). Protection and insulator sizing depend on the voltages and currents that exceed the nominal values of the line, which normally happens in transient state. The most modern time-domain models in technical literature consider the effect of corona ³⁸, the errors due to iterative integration methods ^{39,40}, non-uniformities in the line ^{41,42}, surge arresters ⁴³, explicit integration methods ⁴⁴, fault arcs ⁴⁵, towers ⁴², transformers ⁴⁶, frequency-dependence of the longitudinal parameters ^{47,48} and others.

One of the main limitations of the frequency-domain models is the complexity in the representation of non-linear elements, multiple switching, non-uniformities in the line, faults, time-variant devices and other devices. Because of that, frequency-domain models are not widely used in power systems and time-domain models are preferred for simulating transients. Despite the fact that time-domain models are more flexible and versatile than frequency-domain models, the latter serve to validate new time-domain based models. Frequency-domain methods allow us to identify if the oscillations of a time-domain model are due to the transients or due to the model itself ^{49,50,51}. This is accomplished by using the superposition principle ⁴⁹, window functions, dampening coefficients and the inverse Numerical Laplace Transform ^{52,53}.

Taking into account the advantages, flexibility and versatility of the time-domain models, the main objective of our research is to propose a new time-domain multiconductor transmission line model, based on the method of characteristics and modal transformation, that can accurately represent short and long transmission lines under slow and fast transients, including the frequency-

dependence of the longitudinal parameters. The inclusion of the frequency effect is performed by using the Fast Relaxed Vector Fitting ^{25,54,55} to find an equivalent circuit whose impedance accurately represents the longitudinal impedance of the transmission line. Modal transformation is conducted by finding real and constant transformation matrices such as Clarke's matrix ⁵⁶.

1.2 ORGANIZATION

This doctoral dissertation is developed in nine chapters. The current chapter presents the state of art of transmission line modeling. The second chapter addresses the computation of the transmission line parameters and compares the effect and importance of each part of the line's parameters. It also introduces the study case used for this dissertation: CESP's Araraquara-Bauru transmission line ⁵⁷.

Chapter 3 develops the frequency-domain differential equations of a generic multiconductor transmission line and its solution.

Chapter 4 introduces the method of characteristics, its advantages and limitations.

Chapter 5 introduces the methods available to fit a rational function to a sampled function. It also explores the circuit topologies available in technical literature to represent a rational functions. We introduce a highly efficient computational algorithm to accurately fit any set of data into enhanced circuit topologies.

Chapter 6 enhances the method of characteristics described in chapter 4, and then incorporates the frequency effect by fitting of rational functions presented in chapter 5. The resulting state space representation is efficiently solved using computational and numerical techniques. We propose tailored real and constant transformation matrices for decoupling symmetrical, vertical and asymmetrical overhead transmission lines.

Chapter 7 validates the proposed model by comparing it with the reference model presented in chapter 3. Finally, chapter 8 presents the conclusions obtained so far with our research and chapter 9 the references used in this doctoral dissertation.

1.3 PUBLISHED PAPERS

Through the development of this doctoral dissertation, the following papers were published in chronological order:

- CABALLERO, P.T.; COSTA, E.C.M.; KUROKAWA, S. “*Frequency-dependent multiconductor line model based on the Bergeron method*”. *Electric Power Systems Research (Print)*, v. 127, p. 314-322, 2015. ⁵⁸
- CABALLERO, P.T., COSTA, E.C.M., KUROKAWA, S. “*Using the Frequency-Dependent Bergeron Line Model to simulate transients*”. XI Conferência Brasileira sobre Qualidade da Energia Elétrica- CBQEE, Campina Grande, PB, Brasil (2015). ⁵⁹
- CABALLERO, P.T.; COSTA, E.C.M.; KUROKAWA, S. “*Frequency-dependent line model in the time domain for simulation of fast and impulsive transients*”. *International Journal of Electrical Power & Energy Systems*, v. 80, p. 179-189, 2016. ⁶⁰
- CABALLERO, P.T.; COSTA, E.C.M.; KUROKAWA, S. “*Análise de Desempenho de Modelos de Linhas de Transmissão a Parâmetros Discretos*” VI Simpósio Brasileiro de Sistemas Elétrico-SBSE, Natal, RN, Brasil (2016). ⁶¹
- HAFNER, A. A.; CABALLERO, P.T. et al. “*Modeling of Power Cables with Arbitrary Cross Section: From Parameter Calculation to Electromagnetic Transients Simulation*”. *Journal of Control, Automation and Electrical Systems*, v. 28, n. 3, p. 405–417, 2017bh. ⁶²
- CABALLERO, P.T.; COSTA, E.C.M.; KUROKAWA, S. “*Modal decoupling of overhead transmission lines using real and constant matrices: Influence of the line length*”. *International Journal of Electrical Power & Energy Systems*, v. 92, p. 202–211, nov. 2017bk. ⁶³
- CABALLERO, P.T.; KUROKAWA, S.; KORDI, B. “*Routine for Simulating Transmission Lines with Symmetrical and Asymmetrical Configurations Using a Real and Constant Modal Transformation Matrix*”. *Proceedings of the 18th annual IEEE Canada Electrical Power and Energy Conference. Anais...Toronto: IEEE, 2018bl.* ⁶⁴
- CABALLERO, P.T.; KUROKAWA, S.; KORDI, B. “*Accelerated frequency-dependent method of characteristics for the simulation of multiconductor transmission lines in the time domain*”. *Electric Power Systems Research*, v. 168, p. 55–66, mar. 2019bi. ⁶⁵

2 TRANSMISSION LINE PARAMETERS

2.1 INTRODUCTION

The behavior of a $(n + 1)$ -conductor multiconductor transmission line MTL (*i.e.*, n conductors plus ground) is defined by its longitudinal impedance matrix \mathbf{Z} and transversal admittance matrix \mathbf{Y} that are given by

$$\mathbf{Z} = \begin{bmatrix} Z_{11} & Z_{12} & \cdots & Z_{1n} \\ Z_{21} & Z_{22} & \cdots & Z_{2n} \\ \vdots & \vdots & \ddots & \vdots \\ Z_{n1} & Z_{n2} & \cdots & Z_{nn} \end{bmatrix} \quad (1)$$

$$\mathbf{Y} = \begin{bmatrix} Y_{11} & Y_{12} & \cdots & Y_{1n} \\ Y_{21} & Y_{22} & \cdots & Y_{2n} \\ \vdots & \vdots & \ddots & \vdots \\ Y_{n1} & Y_{n2} & \cdots & Y_{nn} \end{bmatrix} \quad (2)$$

where diagonal and non-diagonal terms represent the self-parameters and mutual-parameters between conductors, respectively.

The longitudinal impedance \mathbf{Z} and transversal admittance \mathbf{Y} of a MTL are described in this chapter as well as the methods used to compute them.

2.2 LONGITUDINAL IMPEDANCE

Self and mutual impedances, in the frequency domain, can be calculated from Maxwell equations using the 3 contact surfaces as boundary conditions: conductor, air and soil ⁶⁶.

External impedance $\mathbf{Z}(\omega)_{ext}$, inner impedance $\mathbf{Z}(\omega)_{inn}$ and earth-return impedance $\mathbf{Z}(\omega)_{gnd}$ compose the frequency-dependent longitudinal impedance matrix $\mathbf{Z}(\omega)_{ext}$ as given by

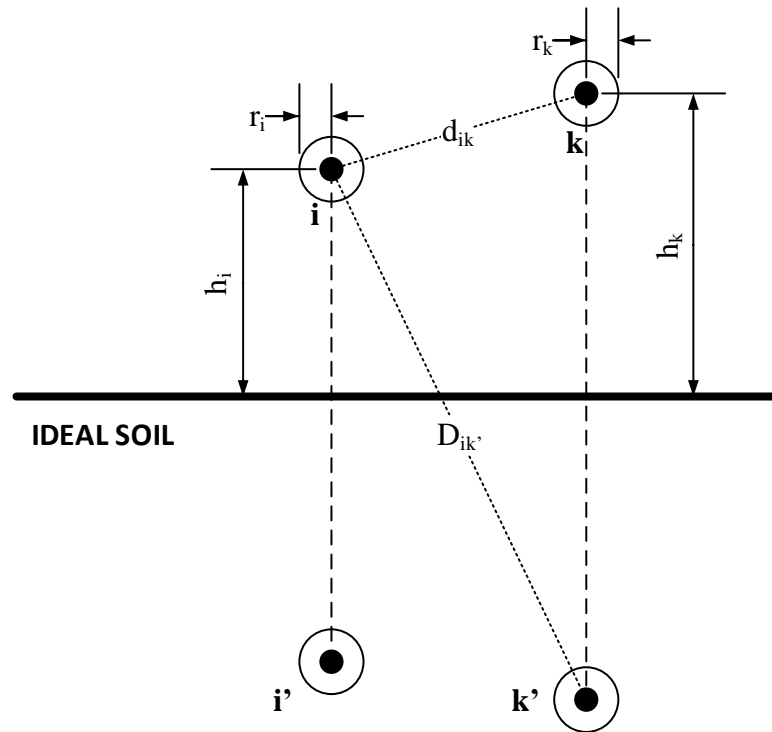
$$\mathbf{Z}(\omega)_{ext} = \mathbf{Z}(\omega)_{ext} + \mathbf{Z}(\omega)_{inn} + \mathbf{Z}(\omega)_{gnd}. \quad (3)$$

Self-impedances fall into all three components of equation (3), whereas mutual impedances are only present in the external impedance $\mathbf{Z}(\omega)_{ext}$ and earth-return impedance $\mathbf{Z}(\omega)_{gnd}$.

2.2.1 External impedance

Let i and k be the conductors of a generic transmission line with an ideal earth-return (lossless ground). For an ideal soil, conductors i' and k' are the images of i and k respectively as shown in Figure 1.

Figure 1 – Conductors i and k , over an ideal soil, with its images i' and k'



Source: Compiled by author

External impedance appears due to the magnetic fields enveloping the conductors in the air⁶⁶. External impedance can be divided into two components: its real part (resistance) and its imaginary part (reactance) as given by

$$\mathbf{Z}_{ext} = \mathbf{R}_{ext} + j\mathbf{X}_{ext} \quad (4)$$

Assuming lossless conductors and an ideal ground (an earth-return with infinite conductance), *i.e.* disregarding line's resistance \mathbf{R}_{ext} , leaves \mathbf{Z}_{ext} only with its imaginary component, the external reactance \mathbf{X}_{ext} . The external reactance matrix \mathbf{X}_{ext} contains self-

impedance terms (diagonal terms) and mutual-impedance terms (non-diagonal terms). Self-impedance terms are given by

$$Z_{ext(ii)}(\omega) = j\omega \frac{\mu}{2\pi} \ln\left(\frac{2h_i}{r_i}\right) \quad (5)$$

where:

$r_i = \text{radius of conductor } i$

$r_k = \text{radius of conductor } k$

$\mu = \mu_r \mu_o \text{ medium's magnetic permeability}$

$h_i = \text{conductor } i\text{'s height}$

$h_k = \text{conductor } k\text{'s height}$

For air and nonmagnetic metallic materials, relative magnetic permeability μ_r is approximately 1.

Mutual impedances occur due to the interaction between conductors i and k and are calculated based on the distance between conductors d_{ik} and their images $D_{ik'}$ as follows

$$Z_{ext(ik)}(\omega) = j\omega \frac{\mu}{2\pi} \ln\left(\frac{D_{ik'}}{d_{ik}}\right) \quad (6)$$

For a MTL with $(n + 1)$ conductors (*i.e.*, n conductors plus ground) assuming lossless conductors and an ideal soil, external impedance matrix \mathbf{Z}_{ext} is given by

$$\mathbf{Z}_{ext} = j\omega \mathbf{L}_{ext} = j\omega \left(\frac{\mu}{2\pi} \begin{bmatrix} \ln \frac{2h_1}{r_1} & \ln \frac{D_{12}}{d_{12}} & \dots & \ln \frac{D_{1n}}{d_{1n}} \\ \ln \frac{D_{21}}{d_{21}} & \ln \frac{2h_2}{r_2} & \dots & \ln \frac{D_{2n}}{d_{2n}} \\ \vdots & \vdots & \ddots & \vdots \\ \ln \frac{D_{n1}}{d_{n1}} & \ln \frac{D_{n2}}{d_{n2}} & \dots & \ln \frac{2h_n}{r_n} \end{bmatrix} \right) \quad (7)$$

The inductive reactance X_{ext} is function of the external inductance L_{ext} , which depends only on the conductor's geometric parameters and on the magnetic permeability of the medium.

2.2.2 Internal impedance

The internal impedance due to skin effect occurs when a conductor has alternating current passing through it ⁶⁷.

When alternating current AC at certain frequency passes through a cylindrical conductor, the current density is maximum in the outer surface of the conductor and minimum at the center as it is shown in Figure 2. In consequence, the resistance of the conductor increases while the inductance of the conductor decreases when the frequency of the input signals increase ⁶⁸.

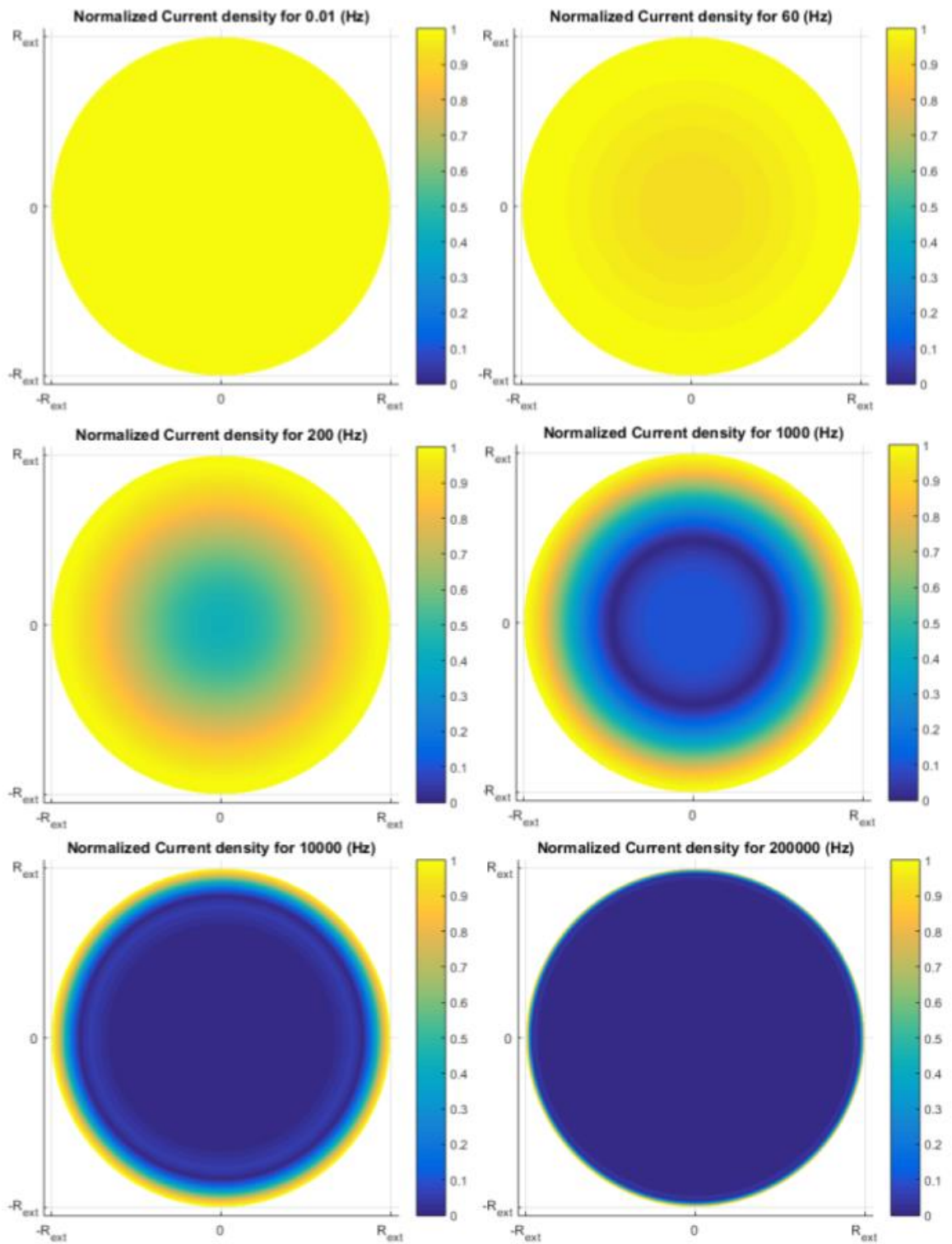
In Figure 2, we show the normalized current density distribution passing through a cylindrical conductor for various frequencies. The current density was normalized in each point using the following equation

$$J_{normalized}(r, \theta) = \frac{|J(r, \theta)|}{\max(|J|)} \quad (8)$$

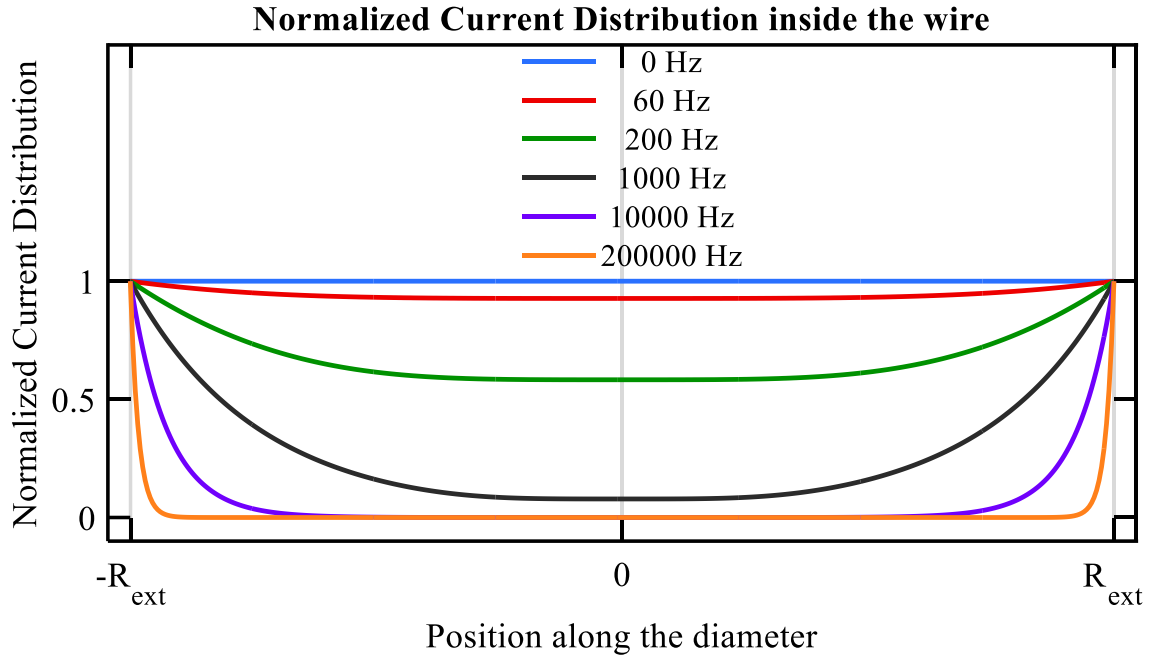
so that the maximum current density has a unitary value and all other current densities range from 0 to 1. We can see that for lower frequencies, the current density is almost uniform across the conductor. As the frequency increases, the current distribution is more accentuated, having the largest current density in the outer surface and the lowest current density in the center of the conductor.

We combined all the current distributions at various frequencies along the diameter of the conductor in a single plot presented in Figure 3. Here, it is more evident how the higher the frequency, the more accentuated is the current density curve along the diameter of the conductor. At low frequencies, the current density is almost uniform across the conductor. At high frequencies, almost all current goes through the outer surface of the conductor. This results in an increase in the effective resistance and a decrease in the internal inductance of the conductor ⁶⁹.

Figure 2 – Normalized current for various frequencies.



Source: Compiled by author

Figure 3 – Normalized current distribution comparison.

Source: Compiled by author

The impedance due to skin effect can be approximated as a function of Kelvin functions for solid cylindrical conductors⁷⁰ as follows

$$Z_{int}(\omega) = \frac{jm}{2\pi r\sigma} \left[\frac{ber(mr) + jbei(mr)}{ber(mr) + jbei'(mr)} \right] \quad (9)$$

$$m = \sqrt{\omega\mu\sigma} \quad (10)$$

where

$\mu = \mu_r\mu_o$ magnetic permeability of the conductor [H/m]

r = radius of the conductor [m]

σ = conductivity of the conductor [ohm/m]

$\omega = 2\pi f$, angular velocity [rad/s]

Equations (9) and (10) can also be written in terms of Bessel functions for cylindrical conductors as given by

$$Z_{int}(\omega) = \frac{m}{2\pi r \sigma} \frac{J_0(mr)}{J_1(mr)} \quad (11)$$

$$m = \sqrt{-j\omega\mu\sigma} \quad (12)$$

where

$J_0(x)$ = Bessel function of the first kind of zeroth order

$J_1(x)$ = Bessel function of the first kind of first order

It should be noted that equations (9) and (11) describe the internal impedance for a solid conductor which is special case of the tubular cylinder with internal radius q equal to 0. For tubular conductors with external radius r and internal radius q , as shown in Figure 4, the internal impedance can be expressed as a function of Kelvin functions ⁷⁰ as follows

$$Z_{int}(\omega) = \frac{jm}{2\pi r \sigma} \left[\frac{(ber(mr) + jbei(mr)) - \lambda(ker(mr) + jkei(mr))}{(ber'(mr) + jbei'(mr)) - \lambda(ker'(mr) + jkei'(mr))} \right] \quad (13)$$

$$\lambda = \frac{ber'(mq) + jbei'(mq)}{ker'(mq) + jkei'(mq)} \quad (14)$$

$$m = \sqrt{\omega\mu\sigma} \quad (15)$$

All arguments in equation (13) can be expressed in terms of modified Bessel functions I_0 , I_1 , K_0 , K_1 as follows ⁴

$$ber(x) + jbei(x) = I_0(x\sqrt{j}) \quad (16)$$

$$ber'(x) + jbei'(x) = \sqrt{j} I_1(x\sqrt{j}) \quad (17)$$

$$ker(x) + jkei(x) = K_0(x\sqrt{j}) \quad (18)$$

$$ker'^{(x)} + jkei'(x) = -\sqrt{j} K_1(x\sqrt{j}) \quad (19)$$

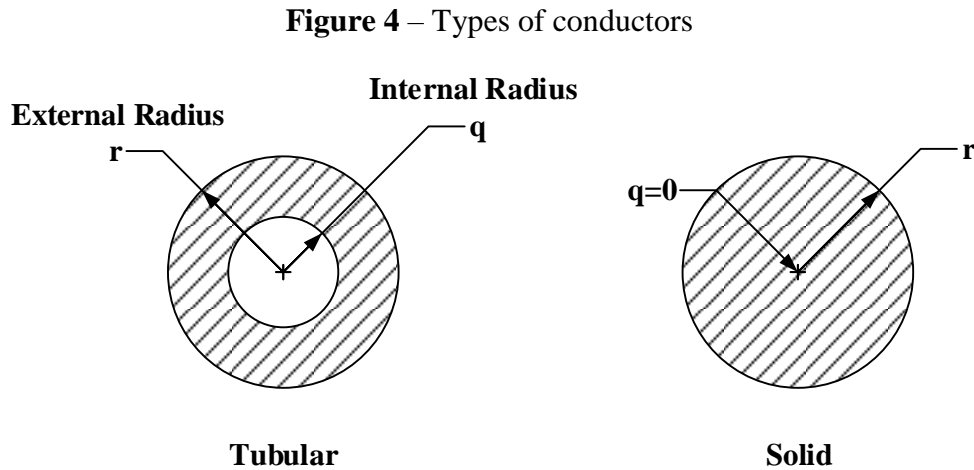
where

$I_0(x)$ = Modified Bessel function of the first kind of zeroth order

$I_1(x)$ = Modified Bessel function of the first kind of first order

$K_0(x)$ = Modified Bessel function of the second kind of zeroth order

$K_1(x)$ = Modified Bessel function of the second kind of first order



Source: Compiled by author

The internal impedance consists of an internal resistance R_{int} and an internal reactance X_{int} , with the internal resistance R_{int} being of more practical interest than the internal reactance X_{int} . That is because the internal reactance X_{int} is only a very small part of the total reactance for nonmagnetic conductors and its accurate determination is somewhat academic ⁴.

For a fixed external ratio and different internal-external radii ratios (tubular conductor), we show in Figure 5 the internal resistance R_{int} and in Figure 6 the inductance L_{int} , both components of the internal impedance due to skin effect Z_{int} as shown in equation (20).

$$Z_{int}(\omega) = R_{int} + j\omega L_{int} \quad (20)$$

In both figures, we computed the internal impedance for a solid conductor (internal ratio equal to 0) and other 3 internal-external radii ratios.

Furthermore, we computed the internal impedance for a practical conductor considering it as a tubular conductor and approximating it as a solid conductor. It has been claimed that stranded conductors can usually be approximated as solid conductors of the same conducting cross-sectional area (shaded area in Figure 4). However, there are cases where this approximation is not good enough. In consequence, more accurate formulas are needed ⁴.

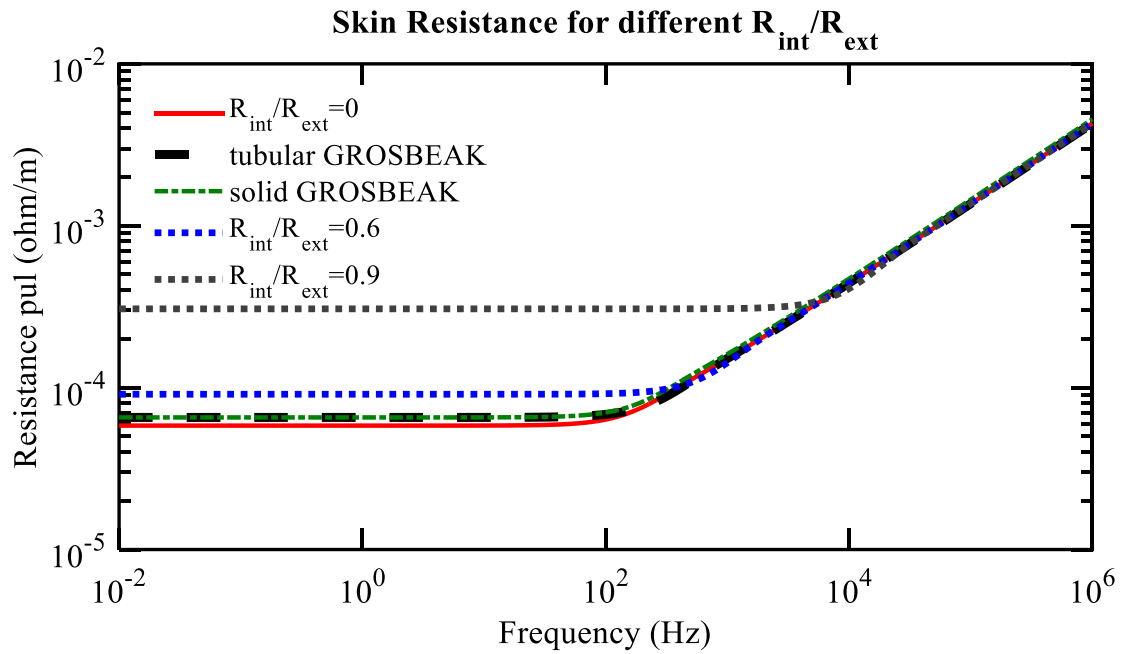
In order to approximate a tubular conductor as a solid conductor, both Aluminum Conductor Steel-Reinforced cables (ACSR) and modern Aluminum Conductor Composite Core cables ACCC show in its datasheets the information needed to perform the approximation (core diameter, outer diameter and cross-sectional area of the Aluminum). For the purpose of showing the difference between ACSR cables and ACCC cables, we show in Figure 7 a photo of both conductors.

Additional to the internal impedance computed for different internal-external radii ratios, we show in Figure 4 the internal impedance of a grosbeak conductor considering it tubular and approximating it as a solid conductor. The grosbeak conductor will be used in further simulations in this dissertation.

We can note from Figure 5 and Figure 6 that the internal resistance at high frequencies is practically the same in all cases at high frequencies for conductors with the same external diameter. Only at low frequencies, where the skin effect has more value in the total longitudinal impedance, the external-internal radii ratio has some effect.

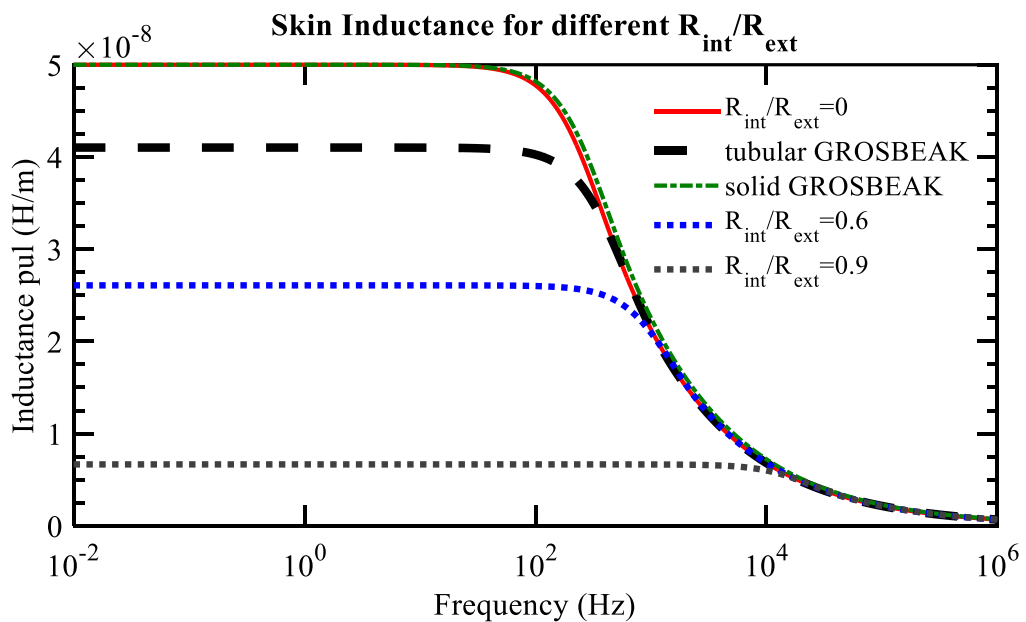
It can also be seen that by approximating a tubular conductor as a solid conductor, the internal resistance is practically the same but there are differences in the internal inductance. Nonetheless, these variations as well as the internal inductance itself are negligible compared to the other inductances (external and earth-return) as it is shown in section 2.8 of this document. Therefore, approximating a tubular as a solid conductor is valid for overhead conductors.

Figure 5 – Internal resistance for different external-internal radii ratios



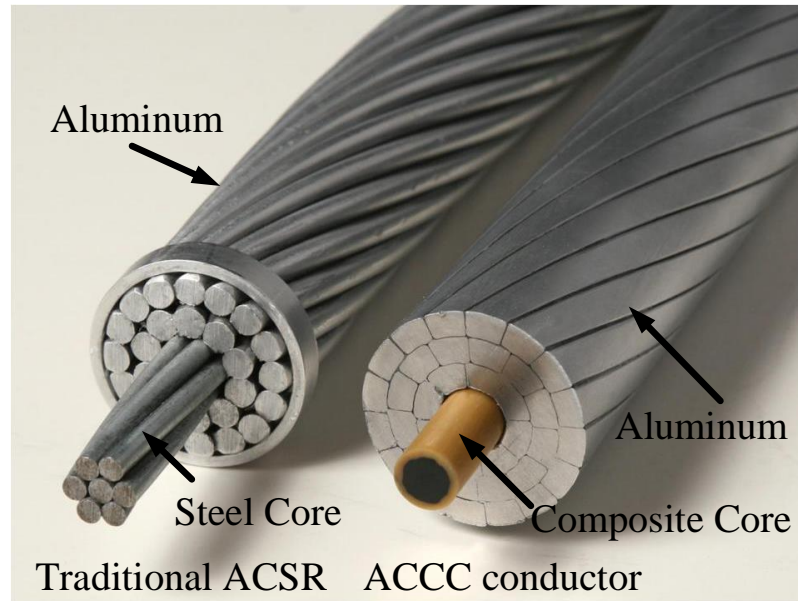
Source: Compiled by author

Figure 6 – Internal inductance for different external-internal radii ratios



Source: Compiled by author

Figure 7 – ACSR cable and ACCC cable



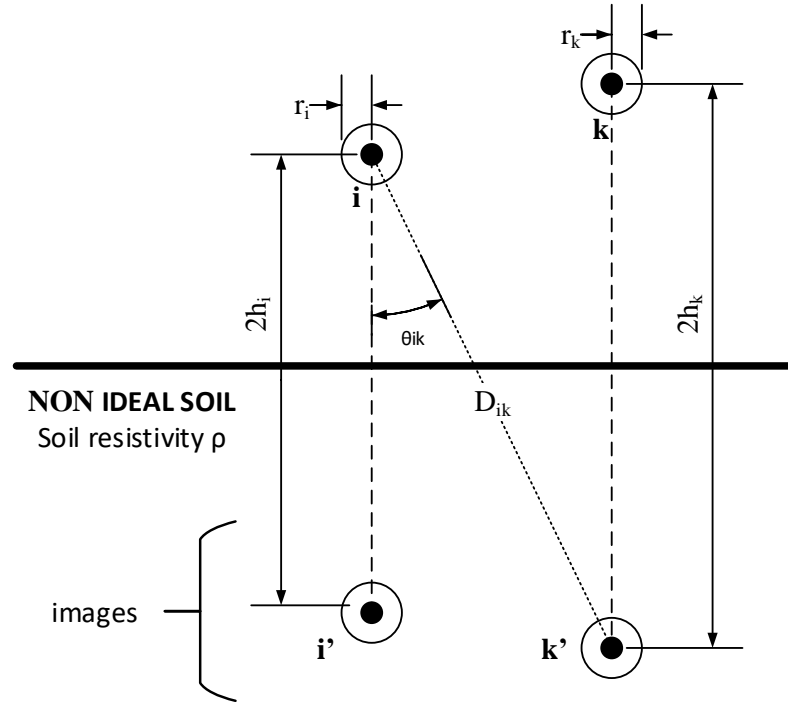
Source: Edited by author from Wikimedia Commons Contributors ⁷¹

2.2.3 Earth-return impedance

Earth-return impedance, also known as ground-return impedance, its formulas were first developed by Carson ⁵ and Pollaczek for telephone circuits and also can be used for power aerial lines. At 60 Hz, Carson's formulas give the same result as Pollaczek's most complicated equations⁴. Both author's equations can be used to compute the earth-return impedance in aerial transmission lines but Pollaczek formulas are preferred for cables.

Carson's solution ⁵ considered for its calculations conductors parallel to the ground and soil resistivity uniform across an infinite area (no stratification). It was proven that a non-ideal earth-return (lossy) circuit is equal to the same circuit considering an ideal earth-return, with conductor images, plus a correction factor due to the non-ideal soil effect ^{69,5}. The depth under the soil surface of the conductor's images is the conductor's height. The resulting circuit is shown in Figure 8. The correction factor is applied to both internal and external impedances computed considering an ideal soil.

Figure 8 – Conductors i k , over a non-ideal soil, with its respective images



Source: Compiled by author

Carson's work ⁵ proved that the impedance in earth-return circuits is composed by the impedance due to the metallic circuit $Z = R_c + j\omega L$ plus a correction factor $\Delta R + j\omega\Delta L$ that represents the earth-return effect on the circuit as follows ⁶⁹

$$Z = R_c + \Delta R + j\omega\{L + \Delta L\} \quad (21)$$

The correction factor was denominated as impedance due to earth-return or ground impedance as shown in equation (22).

$$Z_{gnd} = \Delta R + j\omega\Delta L = \Delta R + j\Delta X \quad (22)$$

The components of ΔR and ΔX , are function of the angle Θ ($\Theta=0$ for self-impedance, $\Theta=\theta_{ik}$ for mutual impedances) and of the a parameter ⁴. The a parameter is given by

$$a = 4 \pi \sqrt{5} 10^{-4} D \sqrt{\frac{f}{\rho}} \quad (23)$$

where

$D = 2h_i$ [m] for self – impedance

$D = D_{ik}$ [m] for mutual – impedance

$\rho =$ soil resistivity [Ωm]

$f =$ frequency [Hz]

When $a \leq 5$, ΔR and ΔX in [Ω/km] and [H/km] respectively, are given by

$$\begin{aligned} \Delta R = 4\omega 10^{-4} \left\{ \frac{\pi}{8} - b_1 a \cos \theta + b_2 [(c_2 - \ln a) a^2 \cos 2\theta + \theta a^2 \sin 2\theta] + b_3 a^3 \cos 3\theta \right. \\ \left. - d_4 a^4 \cos 4\theta - b_5 a^5 \cos 5\theta \right. \\ \left. + b_6 [(c_6 - \ln a) a^6 \cos 6\theta + \theta a^6 \sin(6\theta)] + b_7 a^7 \cos 7\theta \right. \\ \left. - d_8 a^8 \cos 8\theta + \dots \right\} \end{aligned} \quad (24)$$

$$\begin{aligned} \Delta X = 4\omega 10^{-4} \left\{ \frac{1}{2} (0.6159315 - \ln a) + b_1 a \cos \theta - d_2 a^2 \cos 2\theta + b_3 a^3 \cos 3\theta \right. \\ \left. - b_4 [(c_4 - \ln a) a^4 \cos 4\theta + \theta a^4 \sin 4\theta] + b_5 a^5 \cos 5\theta - d_6 a^6 \cos 6\theta \right. \\ \left. + b_7 a^7 \cos 7\theta - b_8 [(c_8 - \ln a) a^8 \cos 8\theta + \theta a^8 \sin(8\theta)] + \dots \right\} \end{aligned} \quad (25)$$

where coefficients b_i , c_i e d_i are calculated as follows

$$b_1 = \frac{\sqrt{2}}{6} \quad (26)$$

$$b_2 = \frac{1}{16} \quad (27)$$

$$b_i = |b_{i-2}| \frac{sign}{i(i+2)}; sign = +1 + 1 + 1 + 1, -1 - 1 - 1 - 1, +1 \dots \quad (28)$$

$$c_2 = 1.3659315 \quad (29)$$

$$c_i = c_{i-2} + \frac{1}{i} + \frac{1}{i+2} \quad (30)$$

$$d_i = \frac{\pi}{4} b_i \quad (31)$$

When $a > 5$, the following finite series are best used to calculate ΔR and ΔX as follows

$$\Delta R = \frac{4\omega 10^{-4}}{\sqrt{2}} \left(\frac{\cos \theta}{a} - \frac{\sqrt{2} \cos 2\theta}{a^2} + \frac{\cos 3\theta}{a^3} + \frac{3 \cos 5\theta}{a^5} + \frac{5 \cos 7\theta}{a^7} \right) \quad (32)$$

$$\Delta X = \frac{4\omega 10^{-4}}{\sqrt{2}} \left(\frac{\cos \theta}{a} - \frac{\cos 3\theta}{a^3} + \frac{3 \cos 5\theta}{a^5} - \frac{5 \cos 7\theta}{a^7} \right) \quad (33)$$

Both ΔR and ΔX are functions of the angular frequency ω , the soil resistivity ρ and the geometrical configuration of the line. However, ground-return impedance is not sensitive to wide variations of the soil resistivity ρ , a fortunate circumstance in view of its wide variability and our lack of precise information about it ⁵. We show in Figure 9 the resistance and inductance of a common air transmission line configuration for various values of the soil resistivity ρ . We can see in both plots that the variations on the ground resistance are minimal along the frequency range and that the soil resistivity ρ mainly affects the ground inductance.

Regarding the number of terms, for power circuits at power frequency only few terms are needed in the infinite series (24) and (25). However, more terms must be taken into account as the parameter becomes larger. Note that the number of terms are only needed while computing the infinite series (24) and (25) since the finite series (32) and (33) have only 5 and 4 terms respectively. The infinite series (24) and (25) is used when $a \leq 5$ which means that it is possible to compute the maximum value of the frequencies involved while using (24) and (25), i.e., when $a = 5$ as follows

$$f_{max} = 5\rho \left(\frac{1}{4\pi D} 10^4 \right)^2 \quad (34)$$

By applying scale analysis (or order-of-magnitude analysis) to equation (34) for overhead transmission lines, we can estimate that the order of the maximum frequency involved using the infinite series for computing ground-return impedance is approximately

$$f_{max} \sim 10^3 \rho \quad (35)$$

Expression (35) suggests that the infinite series (24) and (25) will be partially used in the transient analysis spectrum if the soil resistivity is equal or less than $10^3[\text{ohm} \cdot \text{m}]$.

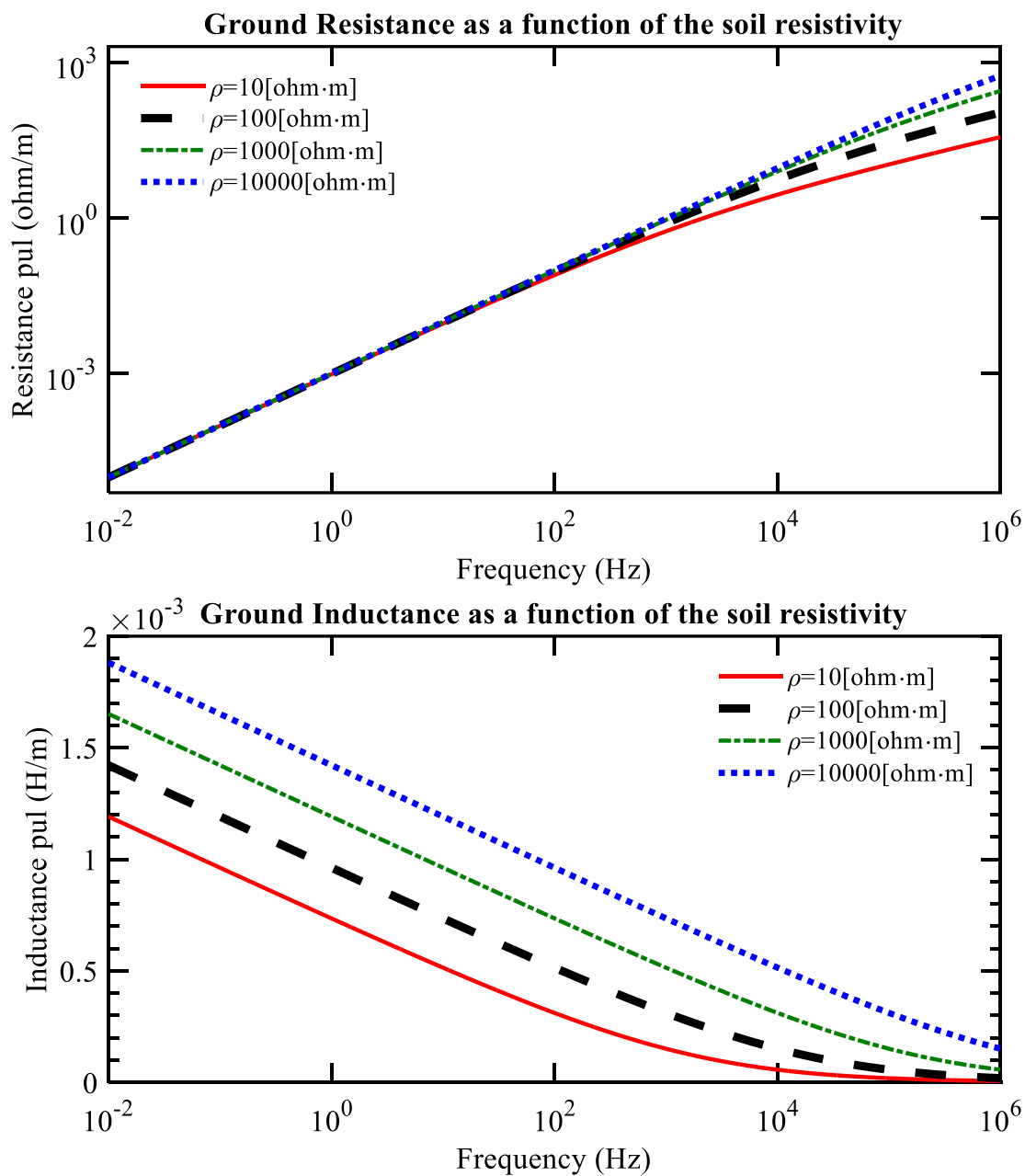
As an example, we show in Figure 10 the ground-return resistance and inductance for various numbers of terms for a conductor 27 [m] above the ground with a soil resistivity of 100[ohm · m].

As expected, the maximum frequency f_{max} , at which the infinite series (24) and (25) is used, has the order of 10^5 [Hz] for a soil resistivity of 100[ohm · m]. We can confirm in Figure 10 that once Carson's infinite series starts to converge, it does so fairly rapidly⁴. With 12 terms we obtain a result as good as using 100 terms.

2.3 TRANVERSAL ADMITTANCE

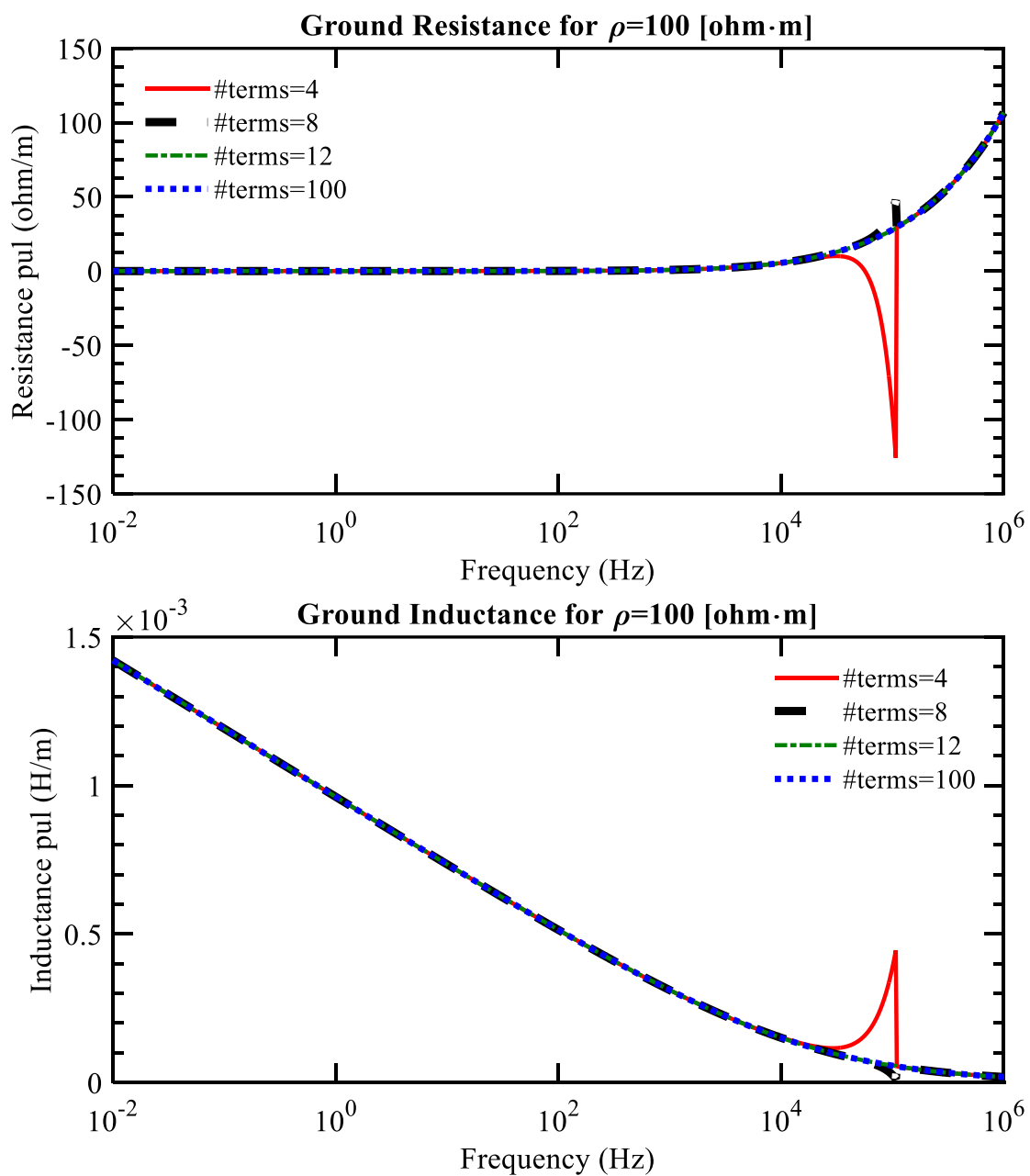
Transmission line's parameters are usually calculated using the subroutines available in most transient analysis software. The parameters calculated are function of many parameters, most of them based on the geometrical configuration of the line. The longitudinal parameters are heavily dependent on the frequency effect. However, the transversal capacitance can be assumed as constant and the conductance is usually neglected³⁸.

Figure 9 – Ground Resistance and inductance for various values of the soil resistivity ρ



Source: Compiled by author

Figure 10 – Ground Resistance and inductance for various values of the soil resistivity ρ



Source: Compiled by author

2.3.1 Transversal capacitance

Transmission line conductors have potential differences between them as well as with the ground. This differences exist due to distributed electrical charges along the conductors. Therefore, the transmission line behaves as a multielectrode capacitor, having the conductors and the ground as electrodes. Thus, an energized transmission line absorbs from the source the electrical charges needed to charge itself, as a capacitor ⁶⁹.

This capacitive effect exists within the conductors and the ground.

The capacitance between parallel conductors is a constant that depends on the geometrical properties of the conductors. For line lengths smaller than 80km, the capacitance is minimal and in consequence the leakage currents can be neglected, i.e., the input and output currents are the same. For longer lines, the capacitance effect is more relevant and should be considered ⁷².

Figure 11 shows a generic biphasic line. Applying a voltage in conductors i and k generates a potential difference between them. Due to the potential difference, an electrical field will envelope the dielectric medium between conductors, causing a charge $+q_i$ in conductor i and a negative charge $-q_i$ in its image i' . Similarly, the potential difference will generate a positive charge $+q_k$ and a negative charge $-q_i$ in conductor k and in its image k' .

Charges $+q_i$ and $+q_k$ between conductors i and k , and charges $-q_i$ and $-q_k$ between its images define the instantaneous potential between conductors i and his image i' as well as conductor k and its image k' :

$$V_i = \frac{Q_i}{2\pi\epsilon_0} \ln \frac{2h_i}{r_i} + \frac{Q_k}{2\pi\epsilon_0} \ln \frac{D_{ik}}{d_{ik}} \quad (36)$$

$$V_k = \frac{Q_k}{2\pi\epsilon_0} \ln \frac{2h_k}{r_k} + \frac{Q_i}{2\pi\epsilon_0} \ln \frac{D_{ik}}{d_{ik}} \quad (37)$$

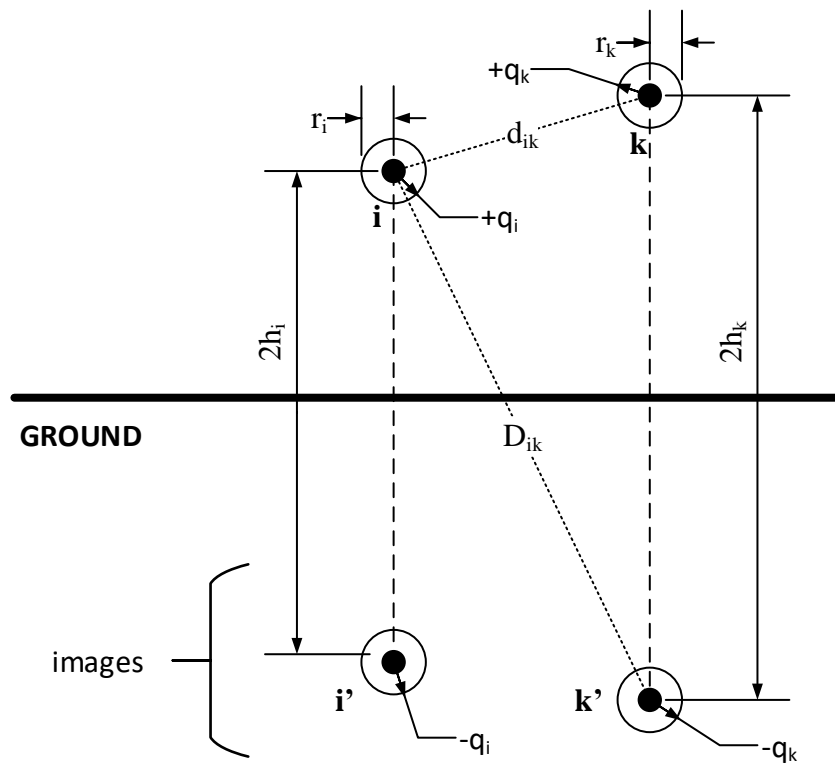
where

$Q_i = \text{charge in conductor } i$

$Q_k = \text{charge in conductor } k$

$\epsilon_0 = \frac{1}{36\pi} 10^{-6} [F/Km]$ Vacuum permittivity

Figure 11 – Charge distribution in a generic biphasic line



Source: Compiled by author

For a generic n -phases MTL, the potential difference between a conductor and its image is given by

$$V_i = \frac{1}{2\pi\epsilon_0} \left(Q_1 \ln \frac{D_{i1}}{d_{i1}} + Q_2 \ln \frac{D_{i2}}{d_{i2}} + \dots + Q_i \ln \frac{2h_i}{r_i} + \dots + Q_n \ln \frac{D_{in}}{d_{in}} \right) \quad (38)$$

Rearranging terms in equation (38) for each conductor and expressing it in matricial form with respect to ground gives

$$\begin{bmatrix} V_1 \\ V_2 \\ \vdots \\ V_n \end{bmatrix} = \frac{1}{2\pi\epsilon_0} \begin{bmatrix} \ln \frac{2h_1}{r_1} & \ln \frac{D_{12}}{d_{12}} & \dots & \ln \frac{D_{1n}}{d_{1n}} \\ \ln \frac{D_{21}}{d_{21}} & \ln \frac{2h_2}{r_2} & \dots & \ln \frac{D_{2n}}{d_{2n}} \\ \vdots & \vdots & \ddots & \vdots \\ \ln \frac{D_{n1}}{d_{n1}} & \ln \frac{D_{n2}}{d_{n2}} & \dots & \ln \frac{2h_n}{r_n} \end{bmatrix} \begin{bmatrix} Q_1 \\ Q_2 \\ \vdots \\ Q_n \end{bmatrix} \quad (39)$$

Equation (39) in matrix form becomes

$$\mathbf{V} = \mathbf{E} \mathbf{Q} \quad (40)$$

Potential difference within conductors and ground with respect to ground is function of the electric field \mathbf{E} and the charge in each conductor \mathbf{Q} .

From the definition of capacitance, an ideal capacitor is defined by its capacitance C which relates the charges $\pm q$ in each conductor and the voltage V between them. Equation (41) describes this relationship in matrix form.

$$\mathbf{Q} = \mathbf{C} \mathbf{V} \quad (41)$$

We can infer from equations (40) and (41) that:

$$\mathbf{C} = \mathbf{E}^{-1} \quad (42)$$

Capacitance matrix \mathbf{C} in equation (42) is symmetrical. By expanding it, we find that all off-diagonal terms are negative:

$$\mathbf{C} = \begin{bmatrix} C_{11} & -C_{12} & \dots & -C_{1n} \\ -C_{12} & C_{22} & \dots & -C_{2n} \\ \vdots & \vdots & \ddots & \vdots \\ -C_{1n} & -C_{2n} & \dots & C_{nn} \end{bmatrix} \quad (43)$$

The negative signs for the off-diagonal capacitance terms are due to the matrices being in nodal form. As an example of this, let us consider a three-phase transmission line as shown in Figure 12. The injected current into node 1 is given by ⁷³

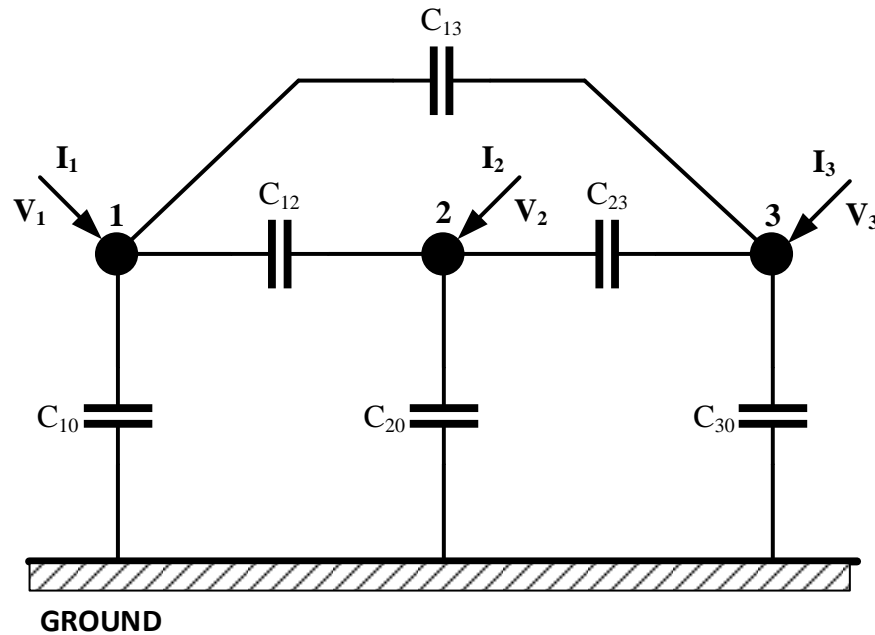
$$I_1 = j\omega C_{10}V_1 + j\omega C_{12}(V_1 - V_2) + j\omega C_{13}(V_1 - V_3) \quad (44)$$

$$I_1 = j\omega C_{11}V_1 - j\omega C_{12}V_2 - j\omega C_{13}V_3 \quad (45)$$

where

$$C_{11} = C_{10} + C_{12} + C_{13} \quad (46)$$

Figure 12 – Shunt capacitance circuit



Source: Compiled by author

The injected currents for nodes 2 and 3 are obtained in a similar fashion. By expanding the nodal analysis equations to a generic n – phase MTL, we obtain the nodal capacitance matrix \mathbf{C} in equation (43) as follows ⁷³

$$\mathbf{C} = \begin{bmatrix} C_{10} + C_{12} + \dots + C_{1n} & -C_{12} & \dots & -C_{1n} \\ -C_{12} & C_{12} + C_{20} + \dots + C_{2n} & \dots & -C_{2n} \\ \vdots & \vdots & \ddots & \vdots \\ -C_{1n} & -C_{2n} & \dots & C_{n1} + C_{n2} + \dots + C_{n0} \end{bmatrix} \quad (47)$$

Capacitance matrix (47) is symmetrical and expressed in nodal form, meaning that diagonal elements C_{ii} are the sum of all capacitances per-unit-of-length p.u.l. between conductor i and all other conductors as well as the ground ⁷³. Non-diagonal elements C_{ik} are the p.u.l. negative capacitance between conductors i and k ⁴.

The elements of the capacitance matrix (47) must be equal to the elements corresponding to the inverted field matrix \mathbf{E}^{-1} in equation (42) because both matrices represent the same physical system. Therefore, after calculating the matrix \mathbf{E}^{-1} , we obtain by simple comparison the partial capacitances C_{i0} and C_{ij} that contain the circuit values of the capacitances ^{73,74,69}.

Assuming that the conductance in overhead MTL can be neglected ³⁸, we can conclude that the transversal admittance is given by

$$\mathbf{Y} = \mathbf{G} + j\mathbf{B} = j\omega\mathbf{C} \quad (48)$$

2.4 STRANDED CONDUCTORS

Stranded conductors can usually be approximated as solid conductors of the same cross-sectional area as shown in section 2.2.2. Therefore, in most cases, equation (9) can be used for computing the inner impedance (skin effect) within the conductor.

It has been claimed that steel-reinforced aluminum cables (ACSR) can be approximated as tubular conductors when the influence of the steel core is negligible, which is more likely to be the case with an even number of layers of aluminum strands since magnetization effect of the steel core caused by one layer of spiraled aluminum strands is approximately canceled by the next layer spiraled in the opposite direction ⁴.

As shown in Figure 5, it makes almost no difference for inner impedance to consider the stranded conductor as a solid conductor or as a tubular conductor as long as the inner-outer radii

ratio is small, which happens in most practical cases. However, for any type of conductor, e.g., Aluminum Conductor Composite Core ACCC, if the influence of the core can be considered negligible, we can approximate the conductor as a tubular conductor and compute its inner impedance with equation (13). All other impedances and admittances are based on the Geometric Mean Radius GMR as explained in the next section of this document.

If the magnetic material of the core is of influence, then calculations may be unreliable and current-dependent, measured values should be used instead.

2.5 BUNDLING OF CONDUCTORS

Bundled conductors are usually used in high voltage power lines. Each bundle consists of two or more subconductors held together by spacers usually located every 100 meters ⁴.

Bundling of conductors can be done symmetrically or not. Asymmetrical bundling was proposed to reduce audible noise but its advantage is offset by the unequal current distribution in each conductor within the bundle. Therefore, symmetrical bundles are preferred in practical applications.

Since the voltages are equal for the subconductors within the bundle, we can use this to reduce the order of the matrices to the number of “equivalent phase conductors”. One of the methods for reducing the order of the system is replacing bundled subconductors with equivalent single conductors.

This method is theoretically not limited to symmetrical bundles, but equations had been derived for the more practical case, which is symmetrical bundles. Formulas are based on the assumptions that the bundles are symmetrical and that the current distribution amongst the conductors within the bundle is uniform.

If the steel core was of influence, then calculations become current-dependent making equations unreliable. To avoid that, measured values should be used ⁴.

First, we need to consider the single conductor or unbundled conductor's geometry, i.e., we consider its single conductor Geometrical Mean Radius GMR (equivalent radius r_x). Usually, the conductor's equivalent radius r_x is tabulated because it depends on the exact composition of the conductor and its inductive properties as well. However, if this information is not available, we may compute it using equation (49) assuming the conductor as a solid, round conductor.

$$GMR_{unbundled\ conductor} = r_x = r e^{-\mu_r/4} \quad (49)$$

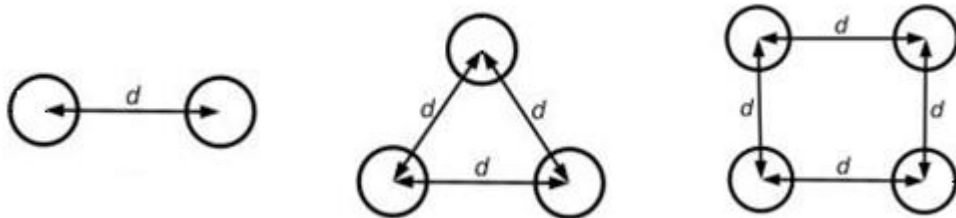
Where

$r = \text{radius of the conductor}$

$\mu_r = \text{conductor's relatively permeability, 1 for non - magnetic conductors}$

Then, we need to consider the conductors bundling by calculating the equivalent phase conductor's GMR, that depends purely on the bundling configuration. Assuming uniformly distributed conductors as in Figure 13, we can calculate the GMR of the bundle, from now on referred simply as GMR, using equation (50).

Figure 13 – Bundling of conductors



Source: Compiled by author

$$GMR_{bundle} = GMR = \frac{d}{2 \sin\left(\frac{\pi}{n}\right)} \sqrt[n]{\frac{2 n r_x \sin\left(\frac{\pi}{n}\right)}{d}} \quad (50)$$

where

$r_x = \text{conductor's equivalent radius (GMR}_{unbundled \text{ conductor}})$

$n = \text{number of conductors in the bundle}$

$d = \text{distance between conductors in the bundle}$

After considering the properties of the conductor and its bundling, i.e., computing the equivalent phase conductor's GMR (r_x for single unbundled conductor), we include it on impedance and admittance computation. Equivalent phase conductor's outer impedance can be calculated with equation (51).

$$\mathbf{Z}_{ext} = j\omega \mathbf{L}_{ext} = j\omega \left(\frac{\mu}{2\pi} \begin{bmatrix} \ln \frac{2h_1}{GMR_1} & \ln \frac{D_{12}}{d_{12}} & \dots & \ln \frac{D_{1n}}{d_{1n}} \\ \ln \frac{D_{21}}{d_{21}} & \ln \frac{2h_2}{GMR_2} & \dots & \ln \frac{D_{2n}}{d_{2n}} \\ \vdots & \vdots & \ddots & \vdots \\ \ln \frac{D_{n1}}{d_{n1}} & \ln \frac{D_{n2}}{d_{n2}} & \dots & \ln \frac{2h_n}{GMR_n} \end{bmatrix} \right) \quad (51)$$

Note that all distances in equation (51) are measured from the center of the bundle.

In order to calculate the equivalent phase internal impedance \mathbf{Z}_{int} , we first compute the inner impedance for each conductor within the bundle. Then we calculate the phase equivalent inner impedance by reducing all conductor's individual inner impedances as parallel impedances, because all of them represent longitudinal impedances. If all n_{bundle} conductors within the bundle are equal, the phase equivalent internal impedance is calculated as follows

$$Z_{int-bundle} = \frac{1}{n_{bundle}} Z_{int-individual} \quad (52)$$

Note that each bundle's equivalent inner impedance represents a diagonal element in the equivalent inner impedance matrix \mathbf{Z}_{int} .

Ground impedance can be calculated for each equivalent phase conductor using the formulas explained in the earth-return impedance section of this chapter (section 2.2.3). Note that distances should be measured from the center of the bundle.

Similarly, equivalent phase conductor's capacitance matrix can be calculated using bundle's GMR instead of radius r for each bundle and measuring distances from the center of the bundle.

2.6 GROUND WIRES

Transmission lines are usually equipped with a ground set of conductors (shield wires or overhead earth wires). If we consider a set of ground wires in the system, the total impedance and admittance of the system becomes

$$\mathbf{Z} = \begin{bmatrix} \mathbf{Z}_{uu} & \mathbf{Z}_{ug} \\ \mathbf{Z}_{ug}^T & \mathbf{Z}_{gg} \end{bmatrix} \quad (53)$$

$$\mathbf{Y} = j\omega\mathbf{C} \quad (54)$$

where \mathbf{Z}_{uu} represents the impedance of the system without the set of ground wires (grounded-less), terms \mathbf{Z}_{ug} represent the mutual impedance of the grounded-less system with the ground wires, and terms \mathbf{Z}_{gg} represent the self-impedance of the set of ground wires. Term \mathbf{Y} represent the admittance of the entire circuit, including ground wires.

Normally, ground wires are continuous and grounded at every tower, which are typically 250 to 350 meters apart. Because of that, it is safe to assume that the potential of the ground wires V_g is continuously zero for frequencies up to 250 kHz. In this case, total impedance \mathbf{Z} in (53) can be reduced to:

$$\mathbf{Z} = \mathbf{Z}_{uu} - \mathbf{Z}_{ug}\mathbf{Z}_{gg}^{-1}\mathbf{Z}_{ug}^T \quad (55)$$

In order to reduce the admittance matrix \mathbf{Y} in equation (54), first, the capacitance matrix \mathbf{C} must be reduced from the set of ground wires. At first sight it may appear that we can discard rows and columns from the capacitance matrix \mathbf{C} associated to the ground wires set but that task is not that simple. Capacitance matrix \mathbf{C} must be obtained from inverting the electric field \mathbf{E} in equation (40). In order to do that, the potential difference in equation (39) including all wires is written as

$$\begin{bmatrix} \mathbf{V}_u \\ \mathbf{V}_g \end{bmatrix} = \begin{bmatrix} \mathbf{E}_{uu} & \mathbf{E}_{ug} \\ \mathbf{E}_{ug}^T & \mathbf{E}_{gg} \end{bmatrix} \begin{bmatrix} \mathbf{Q}_u \\ \mathbf{Q}_g \end{bmatrix} \quad (56)$$

All terms in equation (56) containing the subscript u are associated to the grounded-less system and terms containing the subscript g are associated to the set of ground wires. Normally, we may consider \mathbf{V}_g equal to zero and reduce the ground wires from the field matrix \mathbf{E} . Only after reducing the system of equations (56), we can invert the reduced field matrix $\mathbf{E}_{reduced}$ and obtain the reduced capacitance matrix in nodal form $\mathbf{C}_{reduced}$ as follows

$$\mathbf{C}_{reduced} = [\mathbf{E}_{uu} - \mathbf{E}_{ug}\mathbf{E}_{gg}^{-1}\mathbf{E}_{ug}^T]^{-1} \quad (57)$$

If the ground wires do not have the normal configuration described above, they can still be reduced from the equations. For that purpose, two different types of ground wire configurations, continuous and segmented, are discussed in the next subsections of this document.

2.6.1 Continuous Ground wires

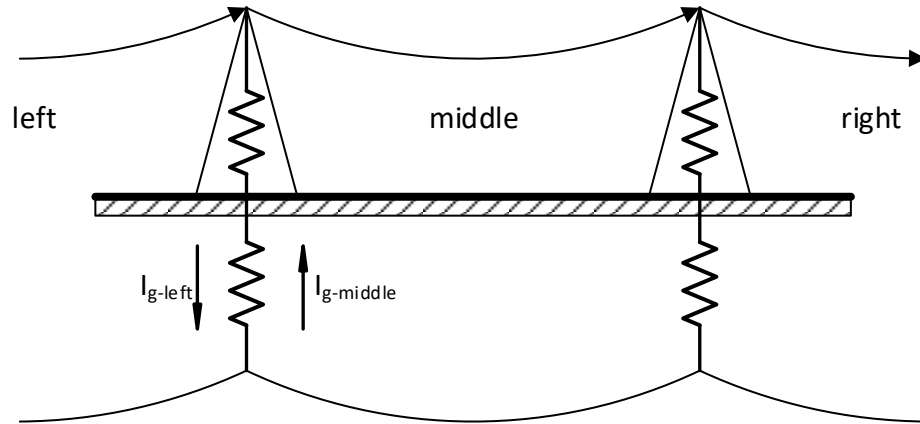
If tower and footing resistances are neglected, then the voltage in the ground wire set can be considered constant and its derivative will be zero as long as $\text{span} \ll \text{wavelength}^4$. In that case currents in the ground wire set \mathbf{I}_g are given by

$$\mathbf{I}_g = -\mathbf{Z}_{gg}^{-1}\mathbf{Z}_{ug}\mathbf{I}_u \quad (58)$$

Since the mutual impedances \mathbf{Z}_{ug} from the phase conductors to the ground wire are never exactly equal, equation (58) does never add up to zero even if the phase currents are symmetrical. In consequence there are non-zero currents in \mathbf{I}_g circulating through ground conductors. This

circulating currents produce additional losses, which are translated in increased grounded-less impedance Z_{ug} . In one particular case of a single-circuit 500kV line, this increase was 6.5%⁴.

Figure 14 – Cascaded transmission line with tower resistances



Source: Compiled by author

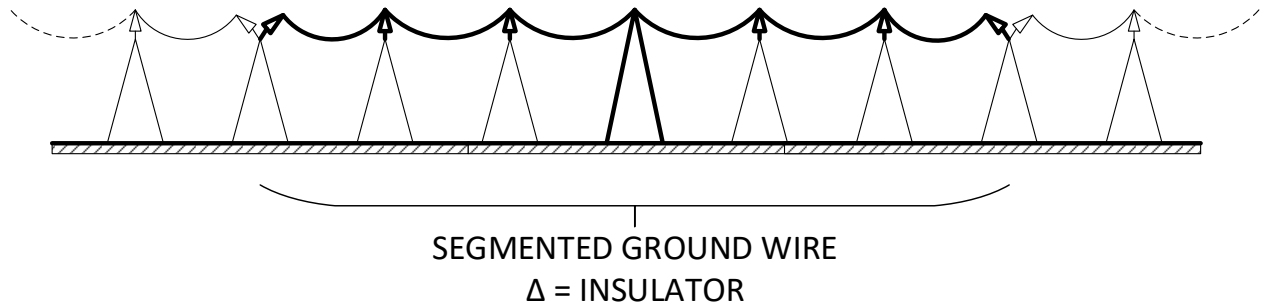
If tower and tower footing resistances were considered in the analysis, currents would circulate in loops as shown in Figure 14. We can see that the voltage drop produced by the current in the left loop is canceled by the voltage drop produced by the current in the middle loop. Then the voltage drops between loops would be neglected except in the very first and very last span of the line. In consequence, the phase currents do not change from one span to the next, which is reasonable up to a certain frequency⁴.

2.6.2 Segmented Ground wires

To avoid losses associated to ground wire currents I_g , some utility companies use segmented ground wires as showed in Figure 15. In this model, ground wire is grounded in one tower (middle bold tower of the bold segment) and insulated at the towers in both ends of the segmented interval, where they are interrupted as well.

They still act as shields for lightning protection and when they are struck by lightning, the segmentation gaps and the small insulators will flash over, thereby making the ground wire continuous again ⁴.

Figure 15 – Segmented Ground wire



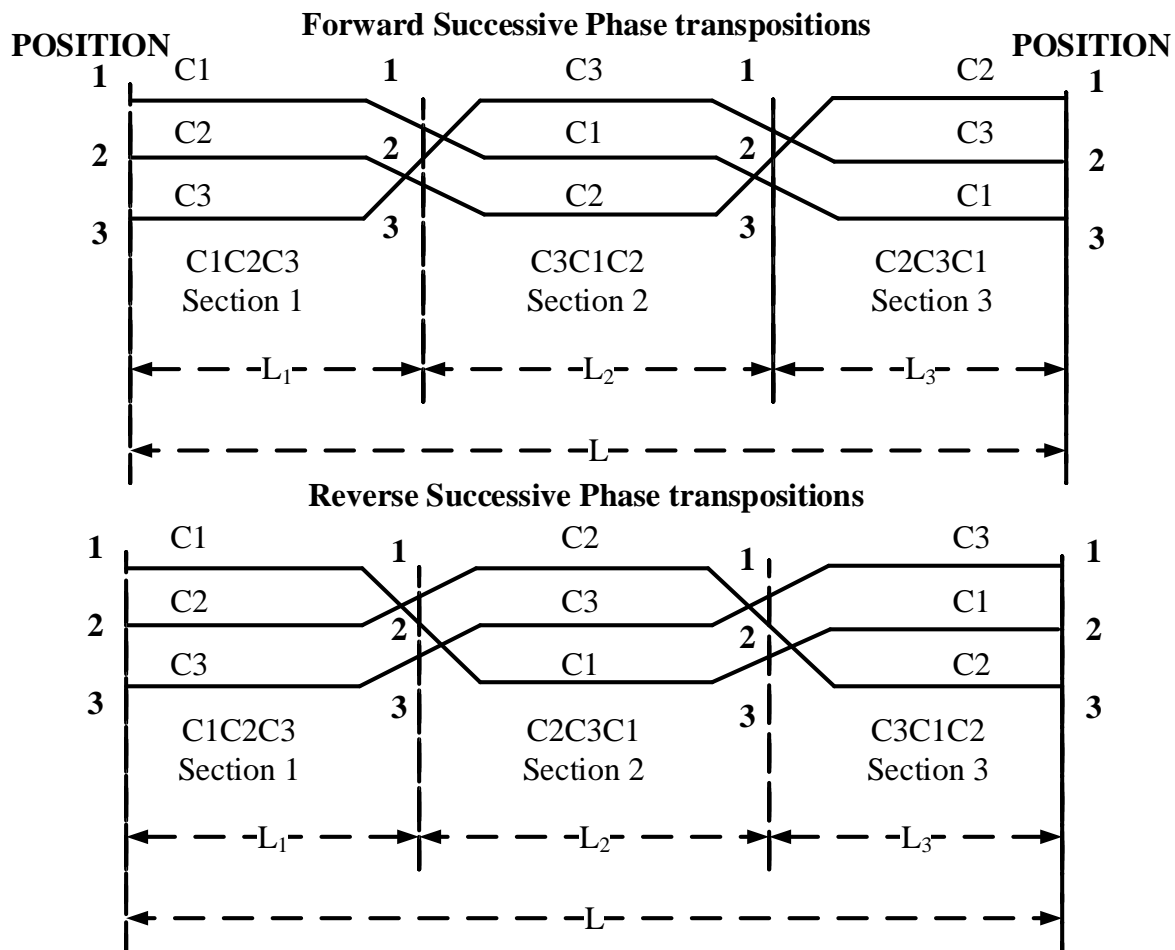
Source: Compiled by author

Since wire currents I_g are suppressed by cutting the continuity of the ground wire, calculation of the impedance matrix ignores the rows and columns associated to the ground wire set. However, ground wires set still should be still taken into account for calculating the capacitance matrix because the electrostatic fields are not influenced by segmentation.

2.7 TRANSPOSITION OF SINGLE-CIRCUIT THREE-PHASE LINES

We have shown so far in this chapter how to calculate the sequence series impedance and shunt admittance matrices including full intersequence mutual coupling for an untransposed transmission line. One powerful tool to analyze transmission line is the sequence component reference frame analysis, which is based on the positive phase sequence, negative phase sequence and zero phase sequence. In order to eliminate the intersequence couplings, it can be assumed that the line is perfectly transposed. The objective of transposition is to produce equal series self-impedances and equal series mutual impedance. Same for shunt self-admittances and shunt mutual admittances. Perfect transposition means that each conductor occupies successively the same physical position as others conductors as exemplified in Figure 16 ⁷³.

Figure 16 – Phase Transpositions



Source: Compiled by author

However, in practice, lines are rarely perfectly transposed because of the expense and the inconvenience. The general case where the line may be semi-transposed at some points is considered as follows. If we consider a three-phase transmission line of length L transposed in two points dividing the line section in three sections L_1 , L_2 and L_3 where $L_1 + L_2 + L_3 = L$ as shown in Figure 16. Then we can write the voltage drops for each conductor as follows

$$\begin{bmatrix} \Delta V_{C1} \\ \Delta V_{C2} \\ \Delta V_{C3} \end{bmatrix}_{Section-1} = L_1 \begin{bmatrix} Z_{11} & Z_{12} & Z_{13} \\ Z_{12} & Z_{22} & Z_{23} \\ Z_{13} & Z_{23} & Z_{33} \end{bmatrix} \begin{bmatrix} I_{C1} \\ I_{C2} \\ I_{C3} \end{bmatrix} \quad (59)$$

$$\begin{bmatrix} \Delta V_{C1} \\ \Delta V_{C2} \\ \Delta V_{C3} \end{bmatrix}_{Section-2} = L_2 \begin{bmatrix} Z_{22} & Z_{23} & Z_{12} \\ Z_{23} & Z_{33} & Z_{13} \\ Z_{12} & Z_{13} & Z_{11} \end{bmatrix} \begin{bmatrix} I_{C1} \\ I_{C2} \\ I_{C3} \end{bmatrix} \quad (60)$$

$$\begin{bmatrix} \Delta V_{C1} \\ \Delta V_{C2} \\ \Delta V_{C3} \end{bmatrix}_{Section-3} = L_3 \begin{bmatrix} Z_{33} & Z_{13} & Z_{23} \\ Z_{13} & Z_{11} & Z_{12} \\ Z_{23} & Z_{12} & Z_{22} \end{bmatrix} \begin{bmatrix} I_{C1} \\ I_{C2} \\ I_{C3} \end{bmatrix} \quad (61)$$

where each Z_{ij} represent the p.u.l. impedance of a conductor in its current physical position.

Note that all p.u.l. impedances are written respecting the positions defined in Figure 16. By summing the voltage drops in each section, we obtain the total voltage drop:

$$\begin{bmatrix} \Delta V_{C1} \\ \Delta V_{C2} \\ \Delta V_{C3} \end{bmatrix} = \mathbf{Z}_{total} \begin{bmatrix} I_{C1} \\ I_{C2} \\ I_{C3} \end{bmatrix} \quad (62)$$

where \mathbf{Z}_{total} represents the total phase impedance matrix of the transposed line:

$$\mathbf{Z}_{total} = \begin{bmatrix} L_1 Z_{11} + L_2 Z_{22} + L_3 Z_{33} & L_1 Z_{12} + L_2 Z_{23} + L_3 Z_{13} & L_1 Z_{13} + L_2 Z_{12} + L_3 Z_{23} \\ L_1 Z_{12} + L_2 Z_{23} + L_3 Z_{13} & L_1 Z_{22} + L_2 Z_{33} + L_3 Z_{11} & L_1 Z_{23} + L_2 Z_{13} + L_3 Z_{12} \\ L_1 Z_{13} + L_2 Z_{12} + L_3 Z_{23} & L_1 Z_{23} + L_2 Z_{13} + L_3 Z_{12} & L_1 Z_{33} + L_2 Z_{11} + L_3 Z_{22} \end{bmatrix} \quad (63)$$

In (63), we define the p.u.l. impedance matrix of the transposed line \mathbf{Z} of length L as:

$$\mathbf{Z} = \frac{1}{L} \begin{bmatrix} L_1 Z_{11} + L_2 Z_{22} + L_3 Z_{33} & L_1 Z_{12} + L_2 Z_{23} + L_3 Z_{13} & L_1 Z_{13} + L_2 Z_{12} + L_3 Z_{23} \\ L_1 Z_{12} + L_2 Z_{23} + L_3 Z_{13} & L_1 Z_{22} + L_2 Z_{33} + L_3 Z_{11} & L_1 Z_{23} + L_2 Z_{13} + L_3 Z_{12} \\ L_1 Z_{13} + L_2 Z_{12} + L_3 Z_{23} & L_1 Z_{23} + L_2 Z_{13} + L_3 Z_{12} & L_1 Z_{33} + L_2 Z_{11} + L_3 Z_{22} \end{bmatrix} \quad (64)$$

Note that each diagonal term contains the same value Z_S and each off-diagonal term contains the same value Z_M :

$$\mathbf{Z} = \begin{bmatrix} Z_S & Z_M & Z_M \\ Z_M & Z_S & Z_M \\ Z_M & Z_M & Z_S \end{bmatrix} \quad (65)$$

The diagonal terms Z_S are defined as the weighted arithmetic mean of the diagonal terms:

$$Z_S = \frac{\sum_{i=1}^n L_i Z_{ii}}{\sum_{i=1}^n L_i} \quad (66)$$

And the off-diagonal terms Z_M are defined as the weighted arithmetic mean of the off-diagonal terms:

$$Z_M = \frac{\sum_{i=1}^n L_i Z_{ij}}{\sum_{i=1}^n L_i} \quad \text{for } j = i + 1, \quad \text{if } j > n \text{ then } j = 1 \quad (67)$$

For a three-phase transposed transmission line with $L_1 = L_2 = L_3$:

$$Z_S = \frac{1}{3} (Z_{11} + Z_{22} + Z_{33}) \quad (68)$$

$$Z_M = \frac{1}{3} (Z_{12} + Z_{23} + Z_{13}) \quad (69)$$

We have shown how to calculate the phase impedance matrix \mathbf{Z} from first principles. However, a general matrix analysis approach is more suitable for modern calculations. Let us define a transposition matrix for a three-phase system as follows

$$\mathbf{T} = \begin{bmatrix} 0 & 0 & 1 \\ 1 & 0 & 0 \\ 0 & 1 & 0 \end{bmatrix} \quad (70)$$

which has the following properties

$$\mathbf{T}^{-1} = \mathbf{T}^T = \mathbf{T}^2 = \begin{bmatrix} 0 & 1 & 0 \\ 0 & 0 & 1 \\ 1 & 0 & 0 \end{bmatrix} \quad (71)$$

$$\mathbf{T}^3 = \mathbf{U} = \begin{bmatrix} 1 & 0 & 0 \\ 0 & 1 & 0 \\ 0 & 0 & 1 \end{bmatrix} \quad (72)$$

Noting the successive changing positions of the three conductors in Figure 16 and the order of its respective impedance matrices in (59)-(61), we can rewrite the voltage drops of each section using the transposition matrix (70):

$$\begin{bmatrix} \Delta V_{C1} \\ \Delta V_{C2} \\ \Delta V_{C3} \end{bmatrix}_{Section-1} = L_1 \mathbf{Z}_{Section-1} \begin{bmatrix} I_{C1} \\ I_{C2} \\ I_{C3} \end{bmatrix} \quad (73)$$

$$\begin{bmatrix} \Delta V_{C3} \\ \Delta V_{C1} \\ \Delta V_{C2} \end{bmatrix}_{Section-2} = \mathbf{T} \begin{bmatrix} \Delta V_{C1} \\ \Delta V_{C2} \\ \Delta V_{C3} \end{bmatrix}_{Section-2} = L_2 \mathbf{Z}_{Section-1} \mathbf{T} \begin{bmatrix} I_{C1} \\ I_{C2} \\ I_{C3} \end{bmatrix} \quad (74)$$

$$\begin{bmatrix} \Delta V_{C2} \\ \Delta V_{C3} \\ \Delta V_{C1} \end{bmatrix}_{Section-3} = \mathbf{T}^{-1} \begin{bmatrix} \Delta V_{C1} \\ \Delta V_{C2} \\ \Delta V_{C3} \end{bmatrix}_{Section-3} = L_3 \mathbf{Z}_{Section-1} \mathbf{T}^{-1} \begin{bmatrix} I_{C1} \\ I_{C2} \\ I_{C3} \end{bmatrix} \quad (75)$$

Thus, we can write impedance phase matrices as a function of the first section's impedance phase matrix $\mathbf{Z}_{Section-1}$ as follows

$$\mathbf{Z}_{Section-2} = \mathbf{T}^T \mathbf{Z}_{Section-1} \mathbf{T} \quad (76)$$

$$\mathbf{Z}_{Section-3} = \mathbf{T} \mathbf{Z}_{Section-1} \mathbf{T}^T \quad (77)$$

and the p.u.l. total phase impedance matrix of the transposed line as

$$\mathbf{Z} = \frac{1}{L} (L_1 \mathbf{Z}_{Section-1} + L_2 \mathbf{T}^T \mathbf{Z}_{Section-1} \mathbf{T} + L_3 \mathbf{T} \mathbf{Z}_{Section-1} \mathbf{T}^T) \quad (78)$$

The effect of pre-multiplying a matrix by \mathbf{T} or \mathbf{T}^T is to shift its rows and the effect of post-multiplying a matrix by \mathbf{T} or \mathbf{T}^T is to shift its columns.

The same procedure using transposition matrix $[\mathbf{T}]$ could be used to find the reverse successive transposition cycle as shown in Figure 16. In summary, the p.u.l. phase impedance matrix for any section in a Forward Successive Phase transpositions is given by⁷³

$$[Z]_{Section-i} = \begin{cases} \mathbf{Z}_{Section-1} & \text{for } i = 1n_{barrel} \\ \mathbf{T}^T \mathbf{Z}_{Section-1} \mathbf{T} & \text{for } i = 2n_{barrel} \\ \mathbf{T} \mathbf{Z}_{Section-1} \mathbf{T}^T & \text{for } i = 3n_{barrel} \end{cases} \quad (79)$$

where n_{barrel} is the number of barrels, which is equal to 3 sections or one cycle of the transposition scheme. The length of a barrel may be 80 to 160 km on long lines but it is recommended to be no longer than 80 km at 50 Hz or 67 km at 60 Hz ⁴.

Analogously, the p.u.l. phase impedance matrix for any section in a Reverse Successive Phase transpositions is given by ⁷³

$$[Z]_{Section-i} = \begin{cases} \mathbf{Z}_{Section-1} & \text{for } i = 1n_{barrel} \\ \mathbf{T} \mathbf{Z}_{Section-1} \mathbf{T}^T & \text{for } i = 2n_{barrel} \\ \mathbf{T}^T \mathbf{Z}_{Section-1} \mathbf{T} & \text{for } i = 3n_{barrel} \end{cases} \quad (80)$$

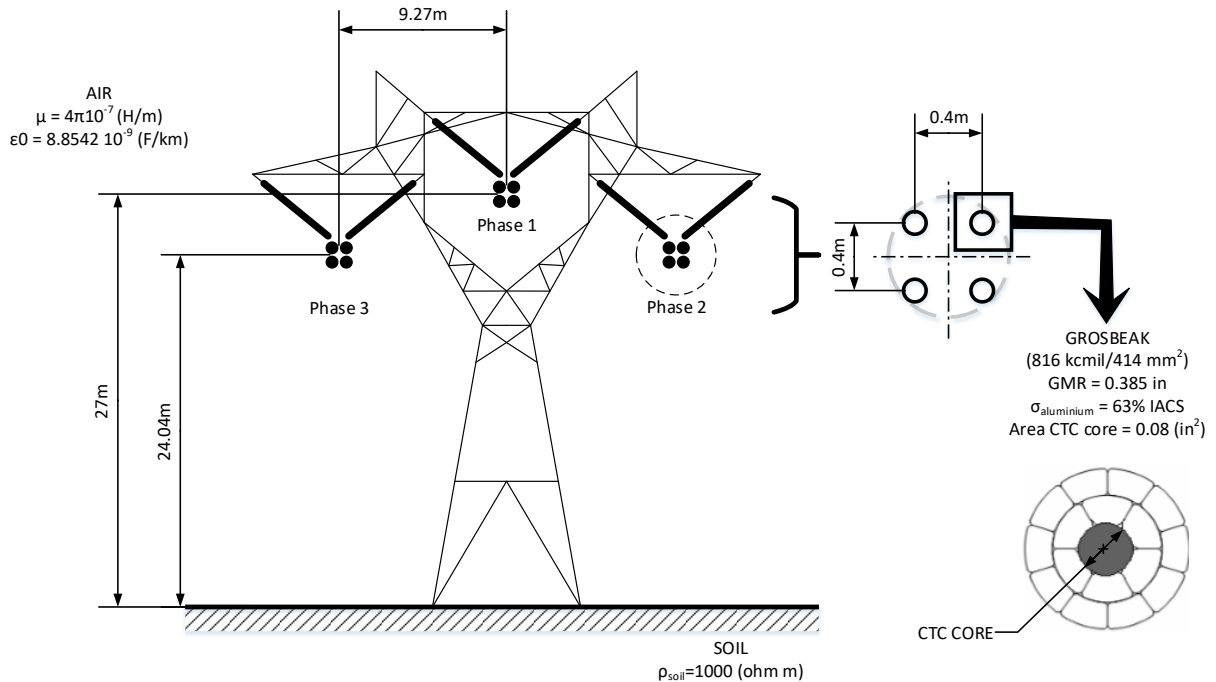
If a barrel length is much shorter than the wavelength, then the series impedances can be averaged by themselves through three sections ⁴. Otherwise, the weighted average mean (68) and (69) must be applied for all sections.

Note that the exact procedure is applied to the shunt capacitances in order to find the diagonal terms Y_S and the off-diagonal terms Y_M .

2.8 APPLICATION

With all formulas developed in this chapter, we compute the parameters for the 400kV CESP's Araraquara-Bauru transmission line shown in Figure 17 ^{57,75}.

Figure 17 – 400kV Transmission line

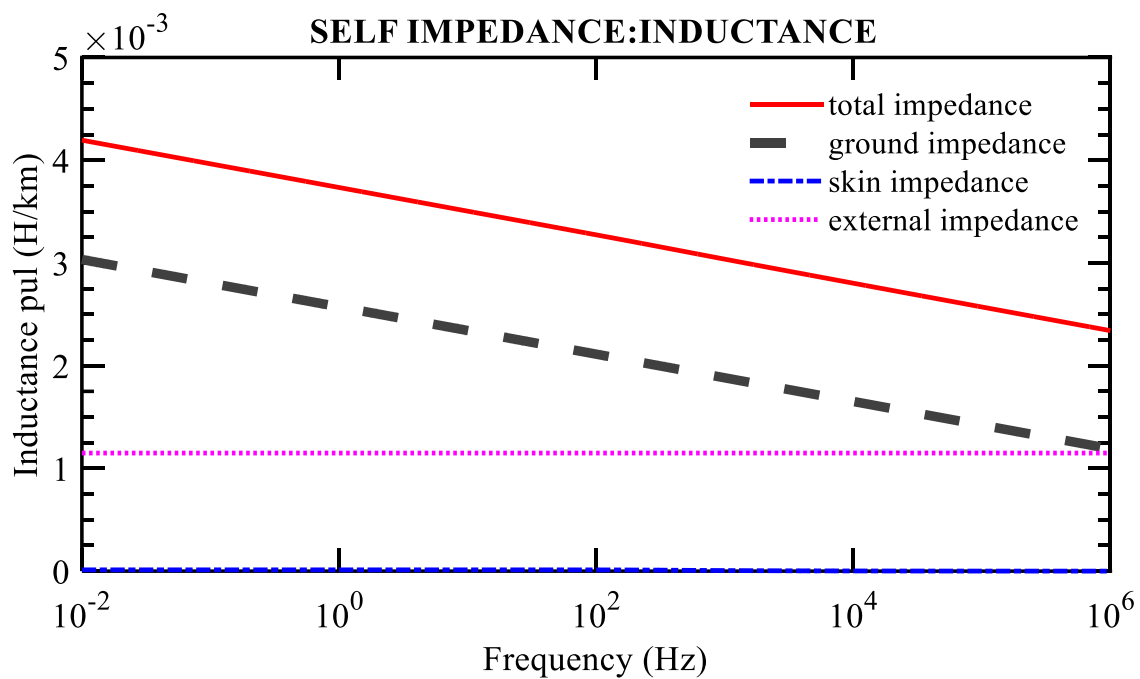
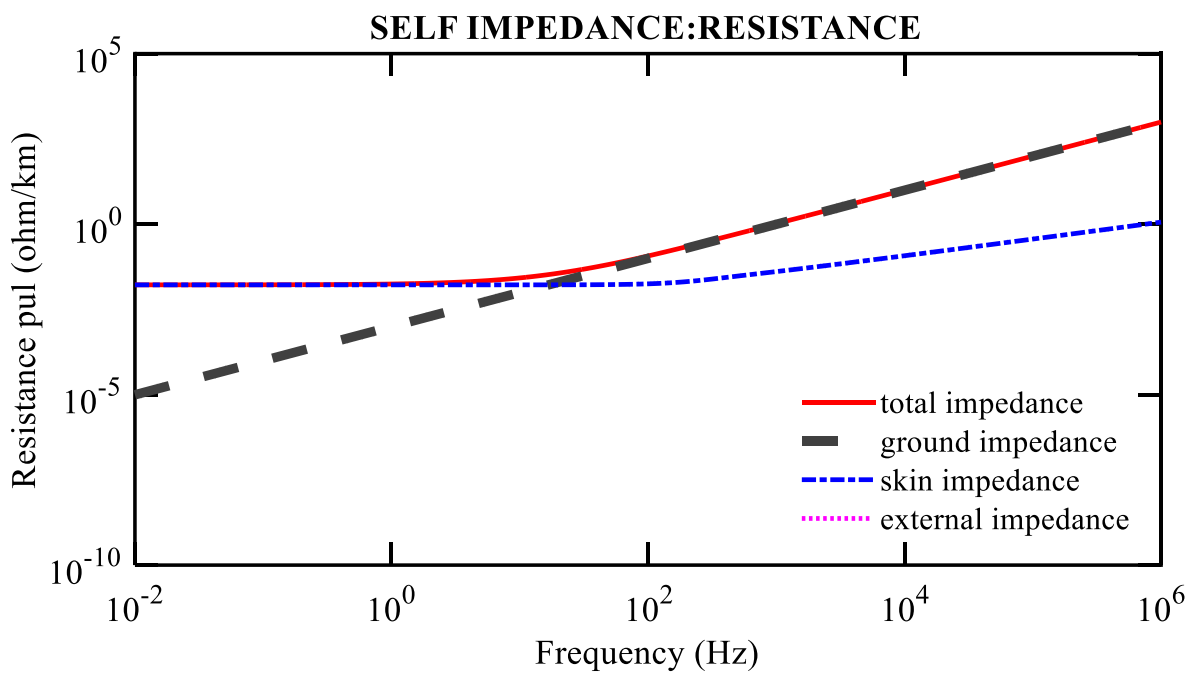


Source: Compiled by author

First, we show in Figure 18 the self-impedance of phase 1 decomposed into its three parts: the external impedance, the inner impedance and the earth-return impedance.

We can note from the resistance and inductance plots in Figure 18 that all three components of the self-impedance are equally important. Each one of the components has a resistance and an inductance except for the external impedance, which only has an inductance contribution to the total impedance. Skin resistance is the most important component at low frequencies while ground resistance prevails over skin resistance at high frequencies. We can also confirm from the inductance plots in Figure 18 that skin inductance is indeed very small compared to other component's inductances to the point where it could be dismissed without affecting the total inductance of the line. Contrary to skin inductance, both external and ground inductance define the phase's self-inductance.

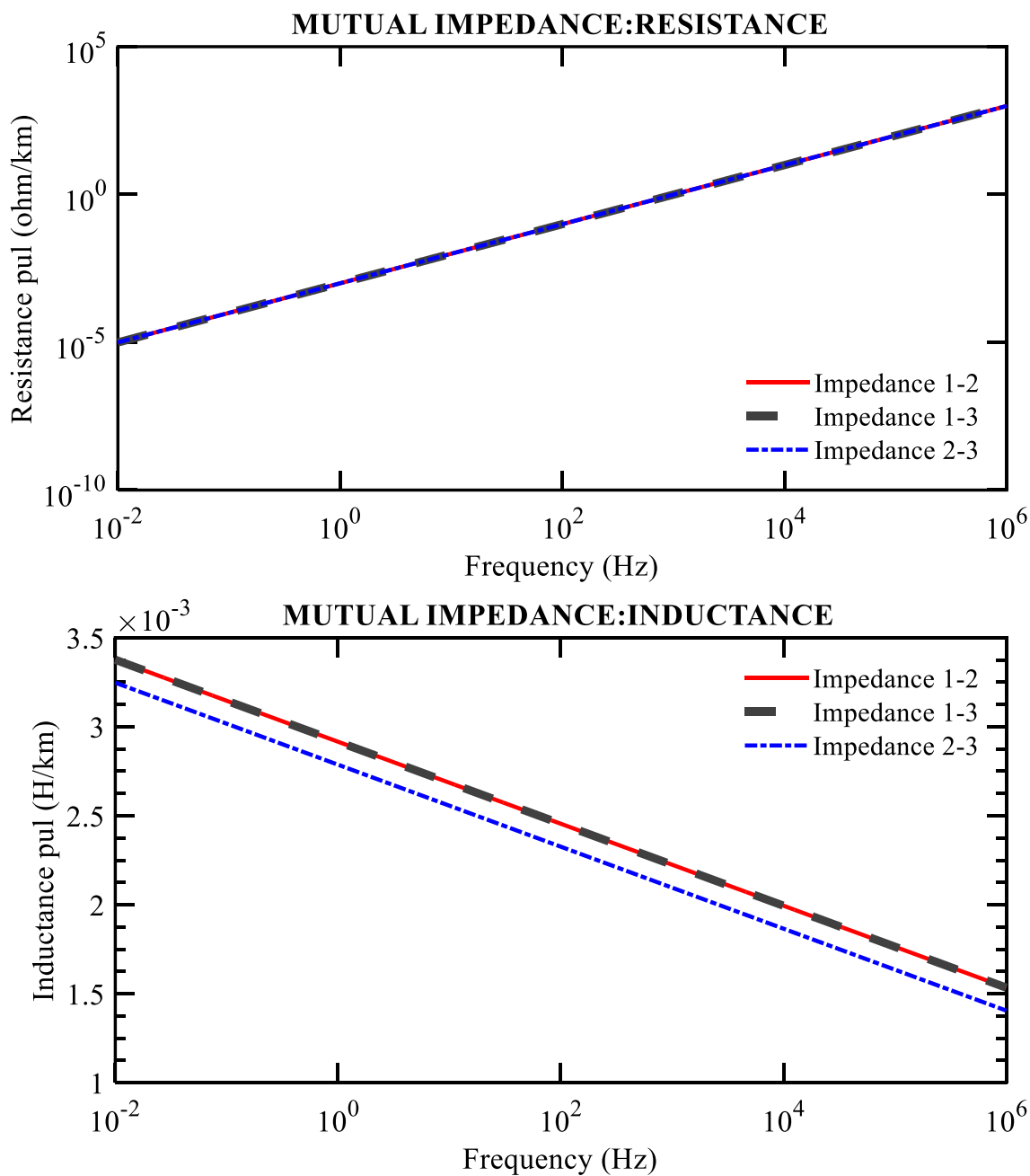
Figure 18 – Phase 1's self-impedance



Source: Compiled by author

Due to the vertical symmetry on the transmission line, mutual impedances from phase 1 (central phase) with phase 2 and 3 (side phases) are the same as shown in Figure 19. As self-impedances, mutual resistances are strongly frequency dependent.

Figure 19 – Mutual impedances



Source: Compiled by author

The transversal capacitance matrix \mathbf{C} obtained in nodal form is

$$\mathbf{C} = \begin{bmatrix} 0.1134 & -0.0285 & -0.0285 \\ -0.0285 & 0.1094 & -0.0114 \\ -0.0285 & -0.0114 & 0.1094 \end{bmatrix} 10^{-7} \left[\frac{F}{km} \right] \quad (81)$$

As expected, due to line symmetry, mutual capacitances from phase 1 to phase 2 and 3 are similar and in consequence mutual admittances are also equal.

With all parameters computed, we can assemble the differential equations needed to model and simulate the transmission line as will be developed in the next chapter.

2.9 CONCLUSION

In this chapter, all equations needed to compute the p.u.l. longitudinal impedance matrix \mathbf{Z} and p.u.l. transversal admittance matrix \mathbf{Y} for aerial transmission lines were discussed. We showed that longitudinal impedance is strongly frequency-dependent and has three components: external impedance, inner impedance and earth-return impedance.

Longitudinal impedance and transversal admittance are necessary to assemble the transmission line's differential equations as will be showed in the next chapter.

3 FREQUENCY DOMAIN MODEL OF A MULTICONDUCTOR TRANSMISSION LINE

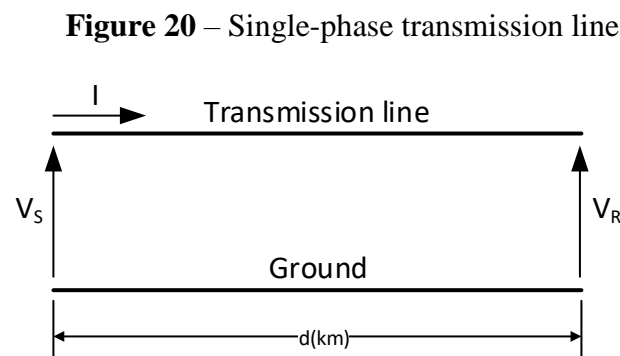
3.1 INTRODUCTION

In the previous chapter, the equations that describe the parameters of the multiphase transmission line in the frequency domain were presented. These parameters describe the behavior of an overhead transmission line.

In this chapter, the classic equations that describe an MTL in the frequency domain will be presented as well as its solution.

3.2 SINGLE PHASE TRANSMISSION LINE DIFFERENTIAL EQUATIONS

Let us consider a single phase transmission line length d , constituted by two isolated rectilinear conductors, far enough from any type of interference as shown in Figure 20^{76,69}.



Source: Compiled by author

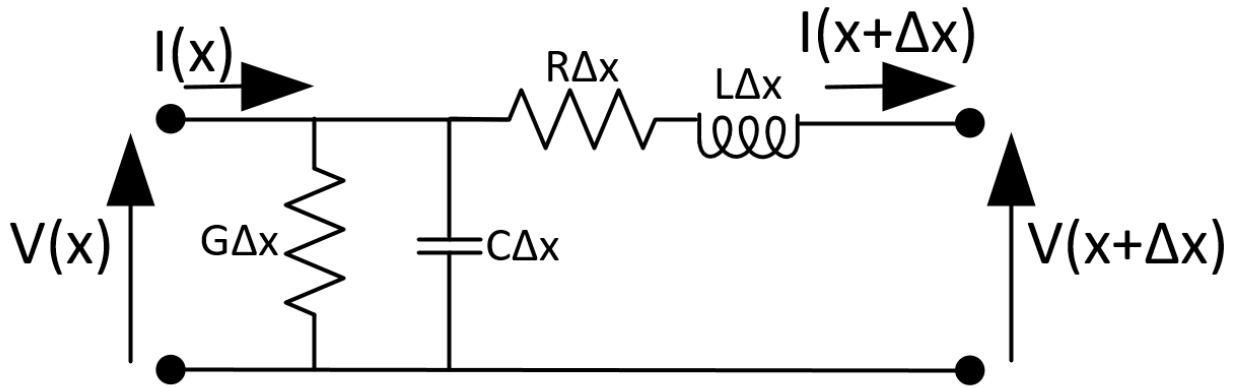
In Figure 20, subscripts S and R denote the sending and receiving terminals respectively, and the return path of the current is through ground.

Oliver Heaviside developed the first transmission line model in the 1880s. Telegrapher's equations describe the voltages and currents of that transmission line model as a function of

position and time. Like all other equations describing electrical phenomena, Telegrapher's equations result from Maxwell equations. The model demonstrates that the electromagnetic waves can be reflected on the wire and that wave patterns appear along the line.

The transmission line shown in Figure 20 is decomposed into an infinite series of two port elementary circuits, each representing an infinitesimally short segment of length Δx . Each segment, shown in Figure 21, is composed by the conductor losses $R\Delta x$, the lumped inductance $L\Delta x$ (due to magnetic fields around the wire, self-inductance, etc.), lumped capacitance $C\Delta x$ (capacitance between the two conductors) and losses in the dielectric $G\Delta x$.

Figure 21 – Transmission line's infinitesimal segment



Source: Compiled by author

All currents and voltages are in the frequency-domain. The equations that describe the circuit of Figure 21 are

$$V(x + \Delta x) - V(x) = \Delta V = -R \Delta x I(x + \Delta x) - j\omega L \Delta x I(x + \Delta x) \quad (82)$$

$$I(x + \Delta x) - I(x) = \Delta I = -G \Delta x V(x + \Delta x) - j\omega C \Delta x V(x + \Delta x) \quad (83)$$

Dividing both sides of the prior equations by Δx and applying the limit when $\Delta x \rightarrow 0$ results in the following differential equations

$$\frac{dV(x)}{dx} = -(R + j\omega L)I(x) \quad (84)$$

$$\frac{dI(x)}{dx} = -(G + j\omega C)V(x) \quad (85)$$

where currents and voltages are not written as partial derivatives because voltage V and current I are only function of the position x .

Equations (84) and (85) are the frequency-domain differential equations of a generic single-phase transmission line. The first one describes the rate of change of voltage V as a function of the series impedance multiplied by the phase current in that point. The second one describes the rate of change of current I as the product of the shunt admittance multiplied by the phase voltage in that point ⁷⁶.

3.3 GENERAL SOLUTION OF THE TRANSMISSION LINE EQUATIONS

Consider the frequency domain differential equations (84) and (85) that describe the voltages and currents of a single phase transmission line. For convenience, we drop the position notation x as follows

$$\frac{dV}{dx} = -ZI \quad (86)$$

$$\frac{dI}{dx} = -YV \quad (87)$$

where the longitudinal impedance Z and the transversal admittance Y are, respectively

$$Z = (R + j\omega L) \quad (88)$$

$$Y = (G + j\omega C) \quad (89)$$

At first sight, the negative signs of equations (86) and (87) may suggest that voltages and currents diminish constantly along the distance over time, but that is not true ⁷⁶. Thus, conclusions cannot be made just by simple inspection ⁷².

Equations (86) and (87) differentiated with respect to x become

$$\frac{d^2V}{dx^2} = -Z \frac{dI}{dx} \quad (90)$$

$$\frac{d^2I}{dx^2} = -Y \frac{dV}{dx} \quad (91)$$

And substituting (87) in (90), and (86) in (91) leads to

$$\frac{d^2V}{dx^2} = Z Y V \quad (92)$$

$$\frac{d^2I}{dx^2} = Y Z I \quad (93)$$

Equation (92) now depends only on the voltage V , and (93) depends only on the current I . This suggest an exponential solution.

Let equation (94) be an admissible solution for (92). Differentiating it twice with respect to x leads to (95), which confirms that the proposed solution was correct.

$$V = A_1 e^{\sqrt{YZ}x} + A_2 e^{-\sqrt{YZ}x} \quad (94)$$

$$\frac{d^2V}{dx^2} = YZ \left[A_1 e^{\sqrt{YZ}x} + A_2 e^{-\sqrt{YZ}x} \right] \quad (95)$$

Therefore equation (94) is the solution of (92).

Substitution of (94) in (86) allows us to find the current in the frequency domain as follows

$$I = \frac{1}{\sqrt{Z}} A_1 e^{\sqrt{YZ}x} - \frac{1}{\sqrt{Z}} A_2 e^{-\sqrt{YZ}x} \quad (96)$$

The constants A_1 and A_2 can be obtained by defining the boundary conditions of the transmission line. At the receiving terminal $x = 0$, $V = V_R$ and $I = I_R$. By substituting the aforementioned conditions, (94) and (96) become

$$V = \frac{V_R + I_R Z_c}{2} e^{\Gamma x} + \frac{V_R - I_R Z_c}{2} e^{-\Gamma x} \quad (97)$$

$$I = \frac{\frac{V_R}{Z_c} + I_R}{2} e^{\Gamma x} - \frac{\frac{V_R}{Z_c} - I_R}{2} e^{-\Gamma x} \quad (98)$$

where the propagation constant Γ and characteristic impedance Z_c are, respectively

$$\Gamma = \sqrt{YZ} \quad (99)$$

$$Z_c = \sqrt{\frac{Z}{Y}} \quad (100)$$

By using the following hyperbolic functions

$$\sinh \theta = \frac{e^\theta - e^{-\theta}}{2} \quad (101)$$

$$\cosh \theta = \frac{e^\theta + e^{-\theta}}{2} \quad (102)$$

and setting the other boundary conditions at the sending terminal as $x = d$, $V = V_s$ e $I = I_s$, (97) and (98) become, respectively

$$V_s = V_R \cosh(\Gamma d) + I_R Z_c \sinh(\Gamma d) \quad (103)$$

$$I_s = I_R \cosh(\Gamma d) + \frac{V_R}{Z_c} \sinh(\Gamma d) \quad (104)$$

and can be written in matrix form as follows

$$\begin{bmatrix} V_s \\ I_s \end{bmatrix} = \begin{bmatrix} \cosh(\Gamma d) & Z_c \sinh(\Gamma d) \\ \frac{1}{Z_c} \sinh(\Gamma d) & \cosh(\Gamma d) \end{bmatrix} \begin{bmatrix} V_R \\ I_R \end{bmatrix} \equiv \begin{bmatrix} A & B \\ C & D \end{bmatrix} \begin{bmatrix} V_R \\ I_R \end{bmatrix} \quad (105)$$

Equation (105) is known as the ABCD-parameters representation of a transmission line, and it is written so that currents I_S and I_R have the same sense. Another representation of (105), where the receiving terminal is defined as a function of the sending terminal, is

$$\begin{bmatrix} V_R \\ I_R \end{bmatrix} = \begin{bmatrix} \cosh(\Gamma d) & -Z_c \sinh(\Gamma d) \\ -\frac{1}{Z_c} \sinh(\Gamma d) & \cosh(\Gamma d) \end{bmatrix} \begin{bmatrix} V_S \\ I_S \end{bmatrix} \quad (106)$$

Equations (105) and (106) are in the frequency-domain. The time domain representation of a transmission line can only be obtained by using the Numeric Laplace Transform ^{52,53}.

The frequency-domain solution of a transmission line is very useful for validating new line models and simulating certain scenarios because its accuracy is undisputed ⁷⁷. However, it has very technical limitations due to frequency-representation of non-linear elements, e.g., surge arresters. Because of those limitations, time-domain models are preferred for practical purposes.

In general, frequency-domain techniques are limited to time-invariant systems. Furthermore, they are particularly limited multivariable systems because of the input-output emphasis of the transfer functions. In return, time-domain techniques are readily available for nonlinear, multivariable and time-variant systems ⁷⁸.

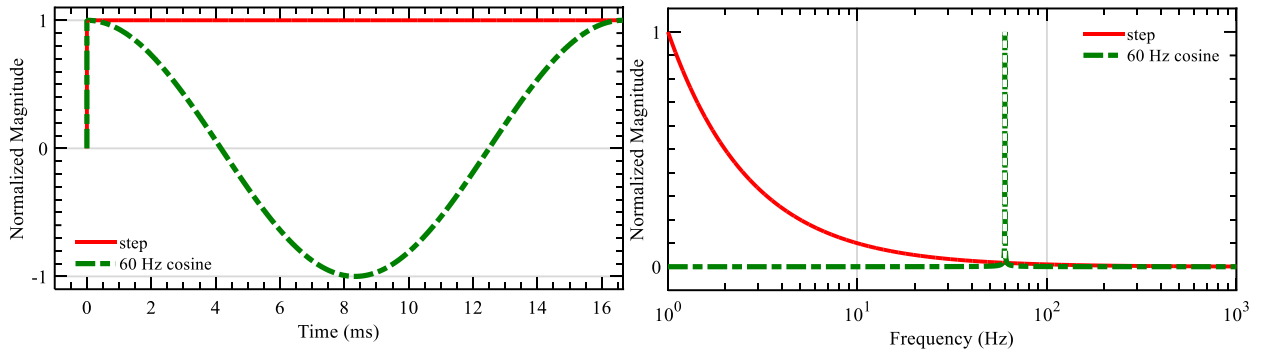
3.4 FREQUENCIES INVOLVED IN PRACTICAL CASES

The ABCD-parameters of a single-phase transmission line in (105) are defined by the transmission line parameters $Z(\omega)$, $Y(\omega)$ and its length d . They relate the voltages and currents in one terminal to the voltages and currents in the other terminal: low frequency inputs will produce low frequency outputs and high frequency inputs will produce high frequency outputs.

Typical frequency spectrum for transient analysis in power systems range up to $1MHz$. In order to show this, we present in Figure 22 and Figure 23 the most common waveforms used in power systems analysis, both in time-domain and frequency-domain. Figure 22 shows two common low frequency waveforms: cosine and step(Heaviside) waveforms, and Figure 23 shows two common high frequency waveforms: $1.2/50\mu s$ surge⁷⁹ and Gaussian waveform with a Full

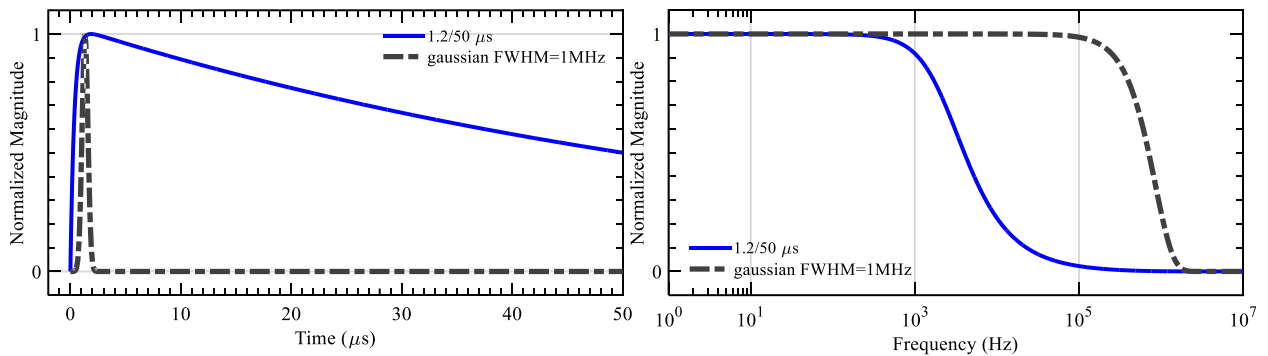
Width at Half Maximum FWHM of 1MHz . All waveforms are normalized so that the maximum amplitude doesn't exceed 1 for comparison purposes.

Figure 22 – Common low frequency waveforms used in transient analysis



Source: Compiled by author

Figure 23 – Common high frequency waveforms used in transient analysis



Source: Compiled by author

3.5 MODAL TRANSFORMATION OF MULTICONDUCTOR TRANSMISSION LINES

The analysis of the single-phase line presented in section 3.3 can be extended for multiconductor transmission lines. For this, let us consider a $(n + 1)$ -conductor (*i.e.* n conductors plus ground) transmission line that is described by the following equations in the frequency domain

$$\frac{dV}{dx} = -Z I \quad (107)$$

$$\frac{d\mathbf{I}}{dx} = -\mathbf{Y} \mathbf{V} \quad (108)$$

where $[\mathbf{Z}]$ and $[\mathbf{Y}]$ are the longitudinal impedance and transversal admittance, respectively. Voltages $[\mathbf{V}]$ and currents $[\mathbf{I}]$ are vectors that contain the voltages and currents of each of the n conductors. The major issue for solving these equations is the coupling between conductors, *i.e.*, the off-diagonal elements in the matrices $[\mathbf{Z}]$ and $[\mathbf{Y}]$.

One powerful tool in multiphase power systems is modal analysis, which decouples the phases of the line. That way, a system that has n coupled phases can be represented by n single-phase systems that are mathematically identical to the original system.

Equations (107) and (108) differentiated with respect to x become

$$\frac{d^2\mathbf{V}}{dx^2} = -\mathbf{Z} \frac{d\mathbf{I}}{dx} \quad (109)$$

$$\frac{d^2\mathbf{I}}{dx^2} = -\mathbf{Y} \frac{d\mathbf{V}}{dx} \quad (110)$$

Substitution of (108) in (109), and (107) in (110) gives

$$\frac{d^2\mathbf{V}}{dx^2} = \mathbf{Z} \mathbf{Y} \mathbf{V} \equiv \mathbf{S}_V \mathbf{V} \quad (111)$$

$$\frac{d^2\mathbf{I}}{dx^2} = \mathbf{Y} \mathbf{Z} \mathbf{I} \equiv \mathbf{S}_I \mathbf{I} \quad (112)$$

Since the matrices \mathbf{Z} and \mathbf{Y} are symmetrical, then their products \mathbf{S}_V and \mathbf{S}_I are related as one being the transposed of the other as given by

$$\mathbf{S}_V = \mathbf{S}_I^T \quad (113)$$

However \mathbf{S}_V and \mathbf{S}_I are not necessarily symmetrical.

Due to relationship (113), \mathbf{S}_V and \mathbf{S}_I share the same characteristic polynomial and in consequence have the same eigenvalues λ_i , which can be expressed in matrix form as $\boldsymbol{\lambda}$, where

each component of the diagonal is one of the eigenvalues λ_i . Nonetheless, a matrix and its transpose do not have the same eigenvectors. Thus, assuming eigenvectors to be independent of position x , the matrix of eigenvalues λ is related to \mathbf{S}_V and \mathbf{S}_I through the eigenvectors \mathbf{T}_V and \mathbf{T}_I as follows

$$\lambda = \mathbf{T}_V^{-1} \mathbf{S}_V \mathbf{T}_V = \mathbf{T}_V^{-1} \mathbf{Z} \mathbf{Y} \mathbf{T}_V \quad (114)$$

$$\lambda = \mathbf{T}_I^{-1} \mathbf{S}_I \mathbf{T}_I = \mathbf{T}_I^{-1} \mathbf{Y} \mathbf{Z} \mathbf{T}_I \quad (115)$$

Isolating the products $\mathbf{Z} \mathbf{Y}$ and $\mathbf{Y} \mathbf{Z}$ from equations (114) and (115) results in

$$\mathbf{S}_V = \mathbf{Z} \mathbf{Y} = \mathbf{T}_V \lambda \mathbf{T}_V^{-1} \quad (116)$$

$$\mathbf{S}_I = \mathbf{Y} \mathbf{Z} = \mathbf{T}_I \lambda \mathbf{T}_I^{-1} \quad (117)$$

Substitution of (116) in (111), and (117) in (112) gives

$$\frac{d^2 \mathbf{V}}{dx^2} = \mathbf{T}_V \lambda \mathbf{T}_V^{-1} \mathbf{V} \quad (118)$$

$$\frac{d^2 \mathbf{I}}{dx^2} = \mathbf{T}_I \lambda \mathbf{T}_I^{-1} \mathbf{I} \quad (119)$$

Equations (118) and (119) can be rewritten as

$$\frac{d^2 \mathbf{V}_m}{dz^2} = \lambda \mathbf{V}_m \quad (120)$$

$$\frac{d^2 \mathbf{I}_m}{dz^2} = \lambda \mathbf{I}_m \quad (121)$$

where modal voltages \mathbf{V}_m and modal currents \mathbf{I}_m are, respectively

$$\mathbf{V}_m = \mathbf{T}_V^{-1} \mathbf{V} \leftrightarrow \mathbf{V} = \mathbf{T}_V \mathbf{V}_m \quad (122)$$

$$\mathbf{I}_m = \mathbf{T}_I^{-1} \mathbf{I} \leftrightarrow \mathbf{I} = \mathbf{T}_I \mathbf{I}_m \quad (123)$$

and the modal impedance \mathbf{Z}_m and modal shunt admittance \mathbf{Y}_m are defined as

$$\mathbf{Z}_m = \mathbf{T}_V^{-1} \mathbf{Z} \mathbf{T}_I \quad (124)$$

$$\mathbf{Y}_m = \mathbf{T}_I^{-1} \mathbf{Y} \mathbf{T}_V \quad (125)$$

Substitution of (122)-(125) in (107) and (108) leads to

$$\frac{d\mathbf{V}_m}{dx} = -\mathbf{T}_V^{-1} \mathbf{Z} \mathbf{T}_I \mathbf{I}_m \equiv \frac{d\mathbf{V}_m}{dx} = -\mathbf{Z}_m \mathbf{I}_m \quad (126)$$

$$\frac{d\mathbf{I}_m}{dx} = -\mathbf{T}_I^{-1} \mathbf{Y} \mathbf{T}_V \mathbf{V}_m \equiv \frac{d\mathbf{I}_m}{dx} = -\mathbf{Y}_m \mathbf{V}_m \quad (127)$$

Equations (126) and (127) describe the behavior of n single-phase transmission lines. Diagonal matrices \mathbf{Z}_m and \mathbf{Y}_m contain the series impedance and shunt admittance of each decoupled mode.

3.6 TRANSFORMATION MATRICES

As stated before, the eigenvalues λ of \mathbf{S}_V and \mathbf{S}_I in (116)-(117) are the same. But the transformation matrices \mathbf{T}_V and \mathbf{T}_I are not equal nor unique. Any matrix of the form $\mathbf{D} \mathbf{T}_I$ is also a modal transformation matrix, where $\mathbf{D} = d \mathbf{U}$, \mathbf{U} being the identity matrix and d a constant. However, the transformation matrices can be related since they lead to the same eigenvalues. Equation (113) can be rewritten as

$$\mathbf{S}_V = \mathbf{S}_I^T = (\mathbf{T}_I \lambda \mathbf{T}_I^{-1})^T \quad (128)$$

Note that the transpose of a product of matrices equals the product of their transposes in reverse order as follows

$$(\mathbf{A} \mathbf{B})^T = \mathbf{B}^T \mathbf{A}^T \quad (129)$$

Therefore, the transpose of the product of three matrices is

$$((\mathbf{A} \mathbf{B}) \mathbf{C})^T = \mathbf{C}^T (\mathbf{A} \mathbf{B})^T = \mathbf{C}^T \mathbf{B}^T \mathbf{A}^T \quad (130)$$

As a result of (130), (128) becomes

$$\mathbf{S}_V = \mathbf{T}_I^{-T} \boldsymbol{\lambda}^T \mathbf{T}_I^T \quad (131)$$

Where the transpose of a diagonal matrix is the matrix itself $\boldsymbol{\lambda}^T = \boldsymbol{\lambda}$. Thus,

$$\mathbf{S}_V = \mathbf{T}_I^{-T} \boldsymbol{\lambda} \mathbf{T}_I^T \quad (132)$$

\mathbf{S}_V in equation (132) is also defined as $\mathbf{S}_V = \mathbf{T}_V \boldsymbol{\lambda} \mathbf{T}_V^{-1}$. Hence, \mathbf{T}_I^{-T} and \mathbf{T}_V are modal transformation matrices of \mathbf{S}_V , and thus they are related as follows

$$\mathbf{T}_I^{-T} = \mathbf{T}_V \mathbf{D}^{-1} \quad (133)$$

$$\mathbf{T}_I^T = \mathbf{D} \mathbf{T}_V^{-1} \quad (134)$$

Where $\mathbf{D} = d\mathbf{U}$, \mathbf{U} being the identity matrix and d is a constant. If $d = 1$ ⁸⁰, then

$$\mathbf{T}_V^{-1} = \mathbf{T}_I^T \quad (135)$$

Modal series impedance \mathbf{Z}_m and modal shunt admittance \mathbf{Y}_m , defined in (124) and (125), are diagonal because of the following relationship

$$\boldsymbol{\lambda} = \mathbf{T}_V^{-1} \mathbf{Z} \mathbf{Y} \mathbf{T}_V = (\mathbf{T}_V^{-1} \mathbf{Z} \mathbf{T}_I) (\mathbf{T}_I^{-1} \mathbf{Y} \mathbf{T}_V) = \mathbf{Z}_m \mathbf{Y}_m \quad (136)$$

$$\boldsymbol{\lambda} = \mathbf{T}_I^{-1} \mathbf{Y} \mathbf{Z} \mathbf{T}_I = (\mathbf{T}_I^{-1} \mathbf{Y} \mathbf{T}_V) (\mathbf{T}_V^{-1} \mathbf{Z} \mathbf{T}_I) = \mathbf{Y}_m \mathbf{Z}_m \quad (137)$$

which suggests that $\boldsymbol{\lambda} = \mathbf{Z}_m \mathbf{Y}_m = \mathbf{Y}_m \mathbf{Z}_m$. The aforementioned implies that \mathbf{Y}_m and \mathbf{Z}_m are both diagonal. This holds for both transposed and untransposed MTL.

The above analysis can be simplified if the transmission line is considered uniformly transposed (see section 2.7 for more details about transposition). In that case:

$$\mathbf{S}_V = \mathbf{S}_I = \mathbf{Z} \mathbf{Y} = \mathbf{Y} \mathbf{Z} \quad (138)$$

As a consequence, for transposed lines, the modal transformation matrices $[\mathbf{T}_V]$ and $[\mathbf{T}_I]$, defined in equations (114)-(115), are related by

$$\mathbf{T}_V = \mathbf{T}_I \quad (139)$$

\mathbf{T}_V and \mathbf{T}_I contain in each column an eigenvector associated to their corresponding eigenvalues in λ . Since both \mathbf{T}_V and \mathbf{T}_I are a set of eigenvectors, then both \mathbf{T}_V and \mathbf{T}_I have infinite number of solutions. There are many methods for numerically obtaining \mathbf{T}_V and \mathbf{T}_I , which will be further discussed in this section. For untransposed lines, equation (135) allows us to calculate the \mathbf{T}_V from \mathbf{T}_I , whereas for transposed lines equation (139) relates \mathbf{T}_V to \mathbf{T}_I .

3.6.1 Frequency-Dependent Transformation Matrices

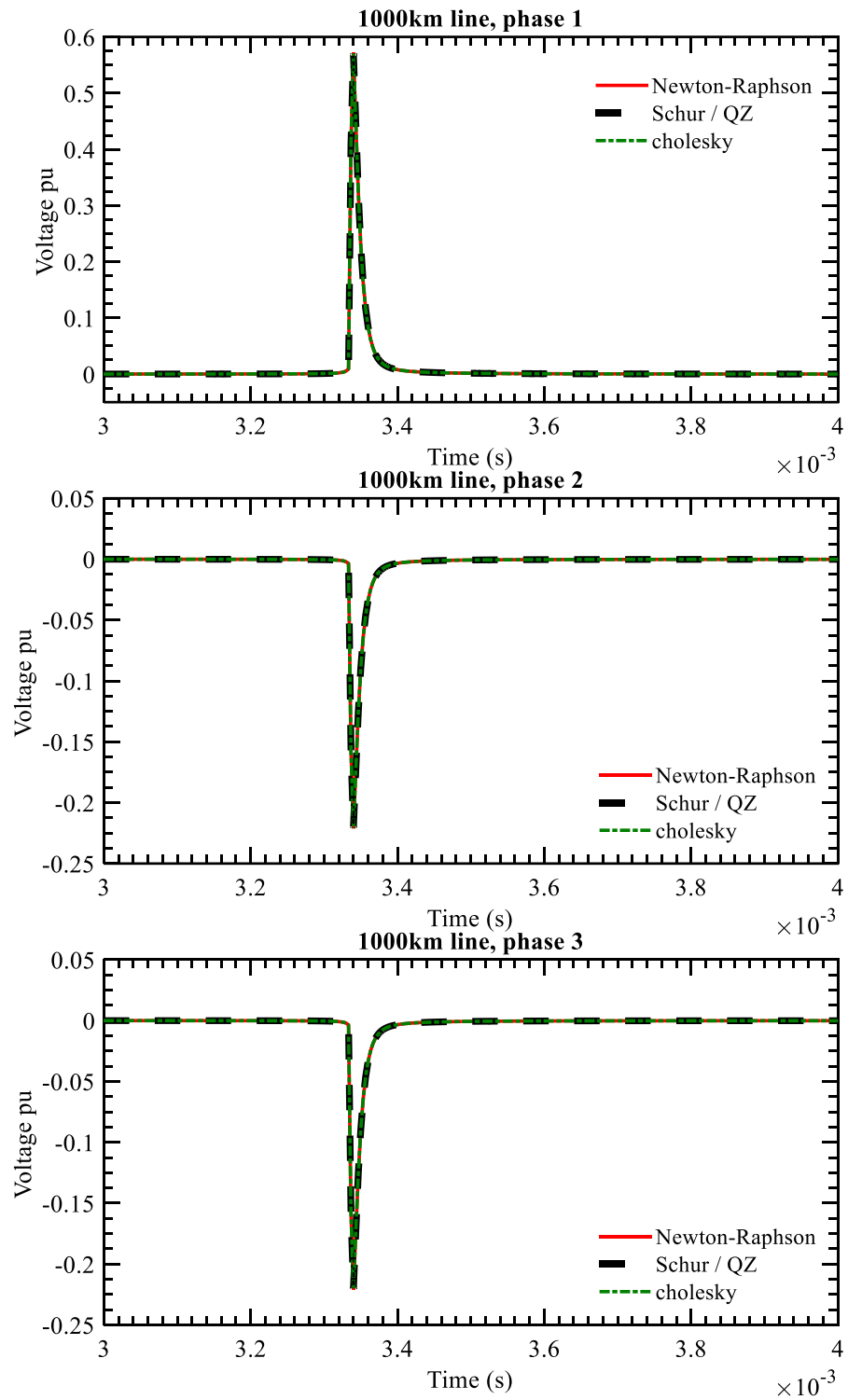
The modal transformation discussed in section 3.5 is valid to decouple any geometrical arrangement of conductors in a MTL: vertical or horizontal conductor arrangements, multicircuit parallel lines, etcetera⁸¹. Modal analysis equations (122)-(127) are in the frequency domain. As a consequence, modal impedances and admittances are considered to be frequency dependent and thus, modal transformation matrices are also frequency dependent.

There are several computational routines available to compute the eigenvectors associated to the transformation matrices \mathbf{T}_V and \mathbf{T}_I for each frequency, among which it may be worth of mentioning⁸²:

- Newton-Raphson method in association with one additional constraint equation to provide consistency for the solution: sums of the squares of the elements of the eigenvectors must be one. This method is widely described in reference⁸³.
- Cholesky decomposition^{84,85}.
- The generalized Schur decomposition, sometimes called QZ decomposition⁸⁶.

All the aforementioned methods compute \mathbf{T}_V and \mathbf{T}_I from \mathbf{S}_V and \mathbf{S}_I for each frequency point. There are several methods for solving the eigenvalues-eigenvectors problem, however they are not discussed in this document. For comparison purposes, the three aforementioned methods were implemented to compute \mathbf{T}_V and \mathbf{T}_I of a 1000 km long non-transposed three-phase transmission line. A fast transient (1.2/50 μ s waveform) was simulated when all other terminals are open-circuited. The time-domain voltages are shown in Figure 24.

Figure 24 – Frequency dependent transformation matrices response



Source: Compiled by author

As seen in Figure 24, all three methods have the same accuracy even though they produce different sets of eigenvectors. Therefore, all three are interchangeable. For our research, the Newton-Raphson method ⁸³ will be considered as the reference routine for obtaining the transformation matrix \mathbf{T}_I for each frequency point, and \mathbf{T}_V will be obtained from \mathbf{T}_I using (135). It is important to point out that the Newton-Raphson method ⁸³ in practice presented some conflicts while decoupling perfectly transposed lines due to the symmetry of the matrices involved. In those cases, the other numerical methods can be used to find the transformation matrices \mathbf{T}_V and \mathbf{T}_I .

3.6.2 Constant Transformation Matrices

The methods for obtaining modal transformation matrices discussed in the previous section are valid to decouple any geometrical arrangement of conductors in a transmission line *e.g.* multicircuit parallel lines. It is common in practice, conversely, to minimize losses and to transpose the conductors of transmission lines so all conductors occupy all possible geometrical positions. The general modal analysis theory is equally valid for this particular case (perfectly transposed lines). Frequency-dependent transformation matrices can still be found using the numerical techniques mentioned in the previous section. However, when solving the eigenvalue/eigenvector problem for balanced matrices, the conditions for the solution are more relaxed because of the symmetry of the problem. As a result, there are multiple sets of eigenvectors that decouple these balanced systems ⁸¹. Many authors proposed sets of eigenvectors with constant values to decouple perfectly transposed MTL as follows.

3.6.3 Two-Phase Constant Transformation Matrices

For balanced two-phase transmission lines, the following transformation matrix \mathbf{T}_I can be used to decouple the line into its modes ^{74,83}.

$$\mathbf{T}_I = \frac{1}{2} \begin{bmatrix} 1 & 1 \\ 1 & -1 \end{bmatrix} \quad (140)$$

Since the transmission line is assumed to be transposed, then \mathbf{T}_V is obtained from (139) as follows

$$\mathbf{T}_V = \mathbf{T}_I = \frac{1}{2} \begin{bmatrix} 1 & 1 \\ 1 & -1 \end{bmatrix} \quad (141)$$

The modal impedance matrix \mathbf{Z}_m , defined in (124), obtained using (140)-(141) is

$$\mathbf{Z}_m = \frac{1}{4} \begin{bmatrix} 1 & 1 \\ 1 & -1 \end{bmatrix} \begin{bmatrix} Z_{11} & Z_{12} \\ Z_{12} & Z_{22} \end{bmatrix} \begin{bmatrix} 1 & 1 \\ 1 & -1 \end{bmatrix} = \frac{1}{4} \begin{bmatrix} Z_{11} + 2Z_{12} + Z_{22} & Z_{11} - Z_{22} \\ Z_{11} - Z_{22} & Z_{11} - 2Z_{12} + Z_{22} \end{bmatrix} \quad (142)$$

Since the transmission line was assumed to be ideally transposed, then Z_{11} is equal to Z_{22} . Therefore, all the off-diagonal elements are zero and the line is decoupled into its exact modes.

3.6.4 Three-phase Constant Transformation Matrices

For the particular, and most common case, of three-phase transmission lines, the following transformation matrices have been widely used:

- a) Clarke's transformation (alpha-beta-zero transformation) ^{87,56,88}

The most used transformation matrix for transposed lines or non-transposed lines with vertical symmetry is Clarke's, defined by ^{87,88}

$$\mathbf{T}_I = \begin{bmatrix} 2/\sqrt{6} & 0 & 1/\sqrt{3} \\ -1/\sqrt{6} & 1/\sqrt{2} & 1/\sqrt{3} \\ -1/\sqrt{6} & -1/\sqrt{2} & 1/\sqrt{3} \end{bmatrix} \quad (143)$$

$$\mathbf{T}_V = \mathbf{T}_I^{-T} = \begin{bmatrix} 2/\sqrt{6} & 0 & 1/\sqrt{3} \\ -1/\sqrt{6} & 1/\sqrt{2} & 1/\sqrt{3} \\ -1/\sqrt{6} & -1/\sqrt{2} & 1/\sqrt{3} \end{bmatrix} \quad (144)$$

The modal impedance \mathbf{Z}_m obtained using transformation matrices (143)-(144) is

$$\mathbf{Z}_m = \begin{bmatrix} Z_\alpha & Z_{\alpha\beta} & Z_{\alpha 0} \\ Z_{\alpha\beta} & Z_\beta & Z_{\beta 0} \\ Z_{\alpha 0} & Z_{\beta 0} & Z_0 \end{bmatrix} \quad (145)$$

where

$$Z_{\alpha} = \frac{2}{3}Z_{11} - \frac{2}{3}Z_{12} - \frac{2}{3}Z_{13} + \frac{1}{6}Z_{22} + \frac{1}{3}Z_{23} + \frac{1}{6}Z_{33} \quad (146)$$

$$Z_{\alpha\beta} = \frac{1}{\sqrt{3}}Z_{12} - \frac{1}{\sqrt{3}}Z_{13} - \frac{1}{2\sqrt{3}}Z_{22} + \frac{1}{3\sqrt{2}}Z_{33} \quad (147)$$

$$Z_{\alpha 0} = \frac{\sqrt{2}}{3}Z_{11} + \frac{1}{3\sqrt{2}}Z_{12} + \frac{1}{3\sqrt{2}}Z_{13} - \frac{1}{3\sqrt{2}}Z_{22} - \frac{\sqrt{2}}{3}Z_{23} - \frac{1}{3\sqrt{2}}Z_{33} \quad (148)$$

$$Z_{\beta} = \frac{1}{2}Z_{22} - Z_{23} + \frac{1}{2}Z_{33} \quad (149)$$

$$Z_{\beta 0} = \frac{1}{\sqrt{6}}Z_{12} - \frac{1}{\sqrt{6}}Z_{13} + \frac{1}{\sqrt{6}}Z_{22} - \frac{1}{\sqrt{6}}Z_{33} \quad (150)$$

$$Z_0 = \frac{1}{3}Z_{11} + \frac{2}{3}Z_{12} + \frac{2}{3}Z_{13} + \frac{1}{3}Z_{22} + \frac{2}{3}Z_{23} + \frac{1}{3}Z_{33} \quad (151)$$

For the specific case of lines with vertical symmetry, where conductors referred as 2 and 3 are in symmetry with respect to conductor 1, , $Z_{12} = Z_{13}$ and $Z_{22} = Z_{33}$. In consequence, modal couplings $Z_{\alpha\beta}$ and $Z_{\beta 0}$ become 0 and $[Z]$ in (145) becomes

$$[Z] = \begin{bmatrix} Z_{\alpha} & 0 & Z_{\alpha 0} \\ 0 & Z_{\beta} & 0 \\ Z_{\alpha 0} & 0 & Z_0 \end{bmatrix} \quad (152)$$

where

$$Z_{\alpha} = \frac{2}{3}Z_{11} - \frac{4}{3}Z_{12} + \frac{1}{3}Z_{22} + \frac{1}{3}Z_{23} \quad (153)$$

$$Z_{\alpha 0} = \frac{\sqrt{2}}{3}Z_{11} + \frac{\sqrt{2}}{3}Z_{12} - \frac{\sqrt{2}}{3}Z_{22} - \frac{\sqrt{2}}{3}Z_{23} \quad (154)$$

$$Z_{\beta} = Z_{22} - Z_{23} \quad (155)$$

$$Z_0 = \frac{1}{3}Z_{11} + \frac{4}{3}Z_{12} + \frac{2}{3}Z_{22} + \frac{2}{3}Z_{23} \quad (156)$$

Furthermore, if the transmission line with vertical symmetry is perfectly transposed, $Z_{11} = Z_{22}$ and $Z_{12} = Z_{23}$. Thus for perfectly transposed transmission lines with vertical symmetry, $Z_{\alpha 0} = 0$ and Clarke's decomposition gives the exact modes.

b) Karrenbauer's transformation ^{89,90}

$$\mathbf{T}_V = \mathbf{T}_I = \frac{1}{2} \begin{bmatrix} 1 & 1 & 1 \\ 1 & -2 & 1 \\ 1 & 1 & -2 \end{bmatrix} \quad (157)$$

c) Traveling-wave transformation ⁸⁰

$$\mathbf{T}_I = \frac{1}{\sqrt{3}} \begin{bmatrix} 1 & 1 & 1 \\ 1 & 0 & -2 \\ 1 & -1 & 1 \end{bmatrix} \quad (158)$$

$$\mathbf{T}_V = \mathbf{T}_I^{-T} = \frac{1}{6} \begin{bmatrix} 2 & 2 & 2 \\ 3 & 0 & -3 \\ 1 & -2 & 1 \end{bmatrix} \quad (159)$$

d) K transformation ⁹¹

$$\mathbf{T}_V = \mathbf{T}_I = \frac{1}{2} \begin{bmatrix} 1/\sqrt{3} & -1/\sqrt{2} & 0 \\ 1/\sqrt{3} & 1/\sqrt{2} & 1/\sqrt{2} \\ 1/\sqrt{3} & 0 & -1/\sqrt{2} \end{bmatrix} \quad (160)$$

e) Wedepohl's transformation ^{92,90}

$$\mathbf{T}_V = \mathbf{T}_I = \begin{bmatrix} 1 & 1 & 1 \\ 1 & 0 & -2 \\ 1 & -1 & 1 \end{bmatrix} \quad (161)$$

f) Symmetrical components (Fortescue's transformation) ⁸¹

$$\mathbf{T}_V = \mathbf{T}_I = \begin{bmatrix} 1 & 1 & 1 \\ 1 & a^2 & a \\ 1 & a & a^2 \end{bmatrix} \quad (162)$$

where $a = e^{\frac{2}{3}\pi j}$.

From the transformations presented above, those that consider $\mathbf{T}_V = \mathbf{T}_I$ were obtained under the assumption that the transmission line is perfectly transposed and the transformation itself gives its best result when this condition is met. In order to show this, we simulated a 1000 km long perfectly transposed three-phase transmission line. A fast transient (1.2/50 μ s waveform) was applied to one of the phases in one terminal while all other phases were short-circuited. The other terminal was open-circuited. Figure 25 shows the voltage simulated at the receiving end of the transmission line.

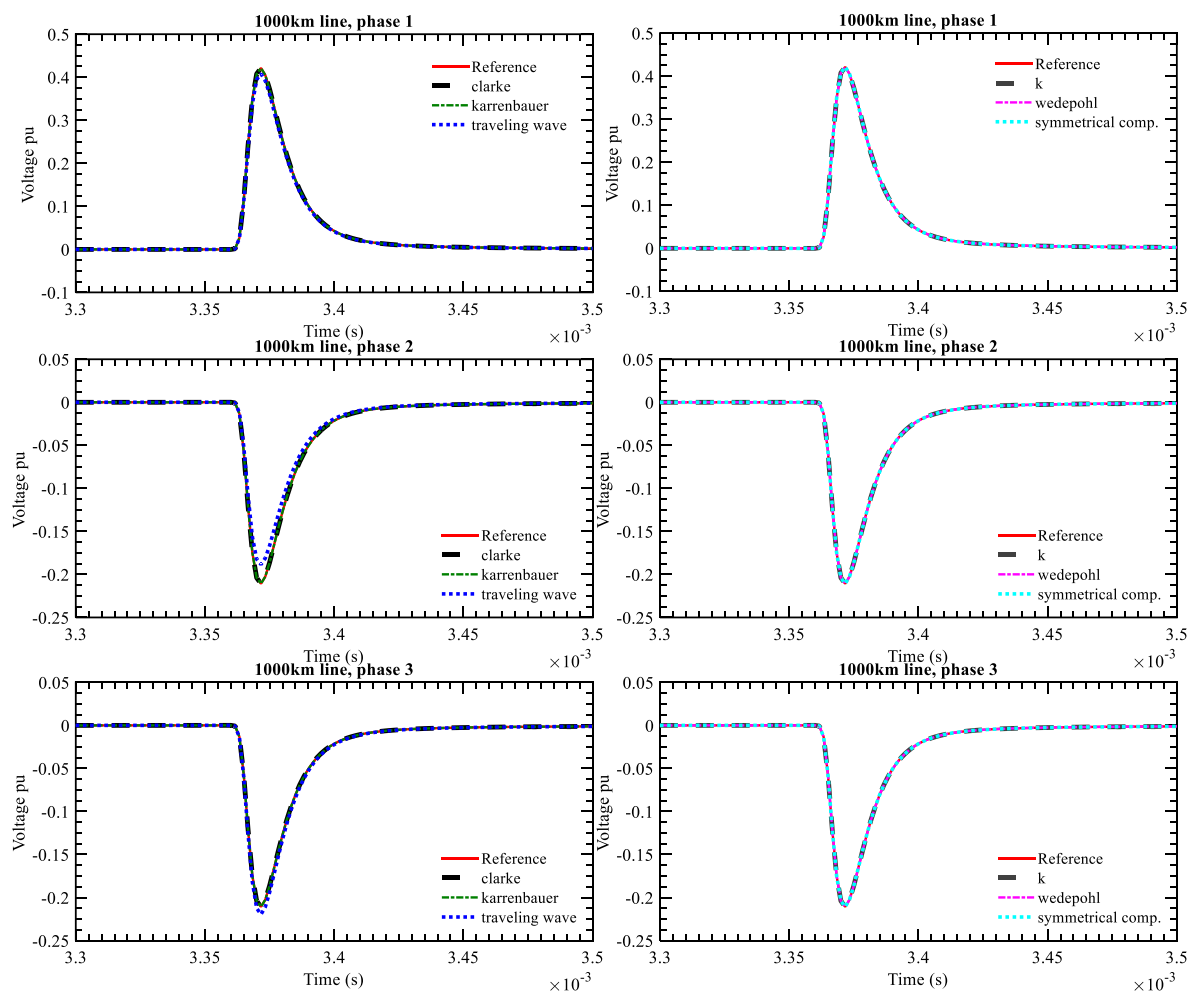
As it can be seen in Figure 25, all constant transformations matrices discussed in this section have approximately the same response when compared to the frequency-dependent transformation matrices discussed in section 3.6.1 of this document.

The assumption of balanced matrices is primarily helpful for two- and three-phase circuits. Nevertheless, for untransposed lines, acceptable results can be often obtained with balanced matrices⁸⁹. In order to show this, the same scenario as in Figure 25 was simulated but with the line untransposed. The results are shown in Figure 26.

From the results shown in Figure 26, Clarke's decomposition is more accurate than all other constant transformation matrices.

All constant transformations matrices discussed in this section are real except for the symmetrical components matrices. This is important because these matrices are usually used to realize time-domain operations and therefore do not require inverse Laplace transforms. This does not apply to symmetrical components, which cannot be used in time-domain operations due to the existence of complex numbers within its elements.

Figure 25 – Constant transformation matrices response in a transposed line



Source: Compiled by author

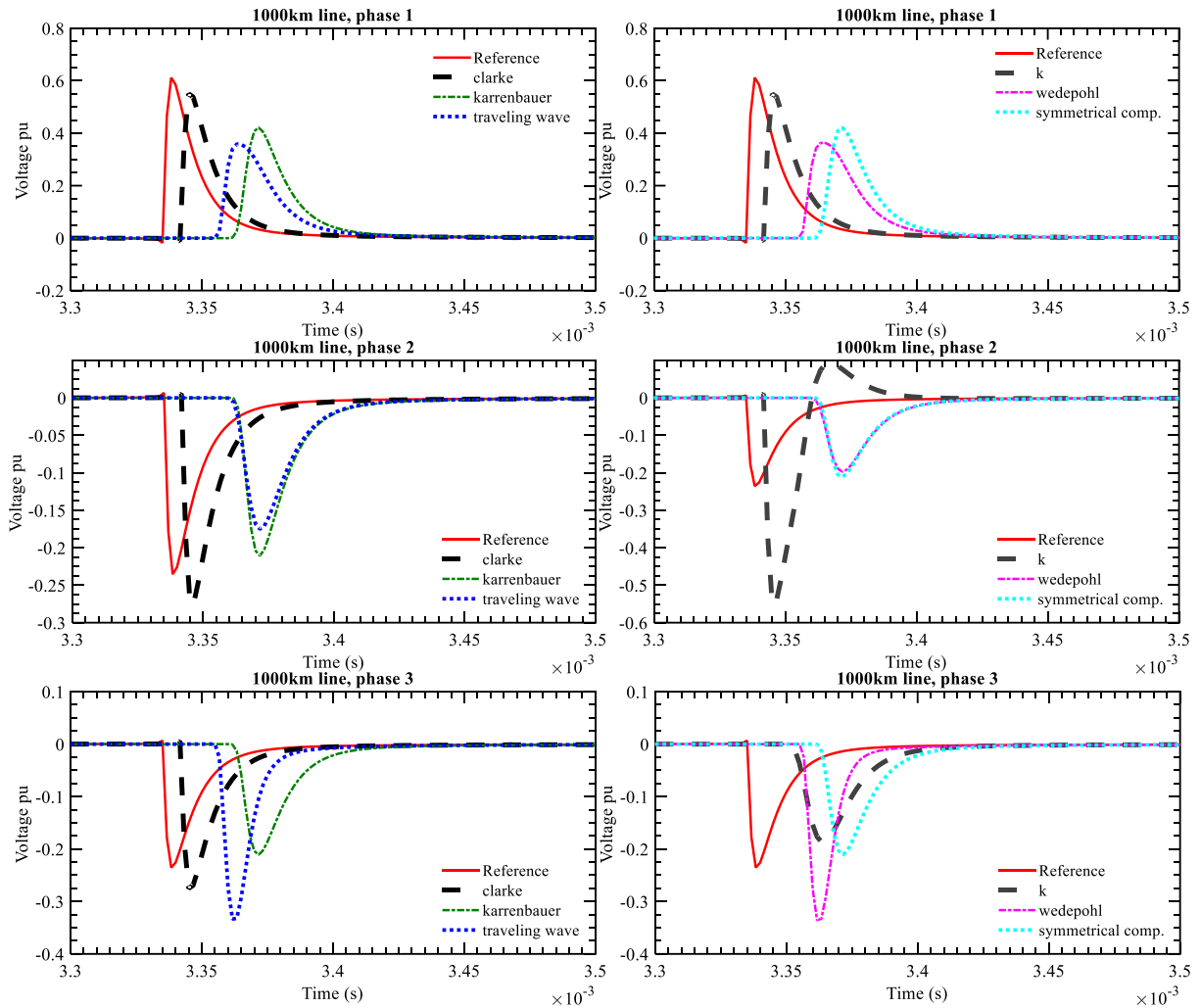
Due to its relative precision, Clarke's matrix is preferred over all other three-phase constant transformation matrices.

3.6.5 Multi-phase constant transformation matrices

For completely balanced (transposed) multi-phase transmission lines, there are a few constant and real transformation matrices which decouples the line into its modes. One of them is the Karrenbauer transformation, that can be used for any number of phases. For a transmission line with M phases, the transformation matrices are ⁸⁹

$$\mathbf{T}_V = \mathbf{T}_I = \begin{bmatrix} 1 & 1 & 1 & \dots & 1 \\ 1 & 1-M & 1 & \dots & 1 \\ 1 & 1 & 1-M & \dots & 1 \\ \vdots & \vdots & \vdots & \ddots & \vdots \\ 1 & 1 & 1 & \dots & 1-M \end{bmatrix} \quad (163)$$

Figure 26 – Constant transformation matrices response in an untransposed line



Source: Compiled by author

3.7 PHASE-DOMAIN SOLUTION OF A TRANSMISSION LINE IN THE FREQUENCY DOMAIN

The ABCD-parameters solution of a transmission line (105) can be rewritten to relate input (subscript *in*) and output (subscript *out*) currents having the same sense, to input and output voltages as follows

$$\begin{bmatrix} I_{out} \\ I_{in} \end{bmatrix} = \begin{bmatrix} \frac{\operatorname{csch}(\Gamma d)}{Z_c} & \frac{\operatorname{coth}(\Gamma d)}{Z_c} \\ -\frac{\operatorname{coth}(\Gamma d)}{Z_c} & -\frac{\sinh(\Gamma d)}{Z_c} + \frac{\cosh(\Gamma d) \operatorname{coth}(\Gamma d)}{Z_c} \end{bmatrix} \begin{bmatrix} V_{in} \\ V_{out} \end{bmatrix} \quad (164)$$

Equation (164) is the frequency domain solution of a single phase transmission line. When a MTL is decomposed into n modes, the solution of a single mode k is given by

$$\begin{bmatrix} I_{outm}^k \\ I_{inm}^k \end{bmatrix} = \begin{bmatrix} A^k & B^k \\ C^k & D^k \end{bmatrix} \begin{bmatrix} V_{inm}^k \\ V_{outm}^k \end{bmatrix} \quad (165)$$

where currents and voltages are in the mode domain (subscript m), and

$$A^k = \frac{\operatorname{csch}(\Gamma^k d)}{Z_c^k} \quad (166)$$

$$B^k = \frac{\operatorname{coth}(\Gamma^k d)}{Z_c^k} \quad (167)$$

$$C^k = -\frac{\operatorname{coth}(\Gamma^k d)}{Z_c^k} \quad (168)$$

$$D^k = -\frac{\sinh(\Gamma^k d)}{Z_c^k} + \frac{\cosh(\Gamma^k d) \operatorname{coth}(\Gamma^k d)}{Z_c^k}. \quad (169)$$

Propagation constant Γ^k and characteristic impedance Z_c^k of the k -th mode (superscript k) are given by

$$\Gamma^k = \sqrt{Y_m^k Z_m^k} \quad (170)$$

$$Z_c^k = \sqrt{\frac{Z_m^k}{Y_m^k}}, \quad (171)$$

and are calculated using mode impedance Z_m^k and mode admittance Y_m^k of the k -th mode. Both parameters are the diagonal elements of the impedance matrix \mathbf{Z}_m and the admittance matrix \mathbf{Y}_m in (122)-(125).

The global solution of a MTL decomposed in n modes using (165) is given by

$$\begin{bmatrix} I_{outm}^1 \\ I_{inm}^1 \\ I_{outm}^2 \\ I_{inm}^2 \\ \vdots \\ I_{outm}^n \\ I_{inm}^n \end{bmatrix} = \begin{bmatrix} A^1 & B^1 & & & & \\ C^1 & D^1 & & & & \\ & & A^2 & B^2 & & \\ & & C^2 & D^2 & & \\ & & & & \ddots & \\ & & & & & A^n & B^n \\ & & & & & C^n & D^n \end{bmatrix} \begin{bmatrix} V_{inm}^1 \\ V_{outm}^1 \\ V_{inm}^2 \\ V_{outm}^2 \\ \vdots \\ V_{inm}^n \\ V_{outm}^n \end{bmatrix}. \quad (172)$$

Equation (172), rearranged to separate inputs (subscript *in*) from outputs (subscript *out*), becomes

$$\begin{bmatrix} I_{outm}^1 \\ I_{outm}^2 \\ \vdots \\ I_{outm}^n \\ I_{inm}^1 \\ I_{inm}^2 \\ \vdots \\ I_{inm}^n \end{bmatrix} = \begin{bmatrix} A^1 & & & B^1 & & & & \\ & A^2 & & & B^2 & & & \\ & & \ddots & & & & & \\ & & & A^n & & & B^n & \\ C^1 & & & & D^1 & & & \\ & C^2 & & & & D^2 & & \\ & & \ddots & & & & \ddots & \\ & & & C^n & & & & D^n \end{bmatrix} \begin{bmatrix} V_{inm}^1 \\ V_{inm}^2 \\ \vdots \\ V_{inm}^n \\ V_{outm}^1 \\ V_{outm}^2 \\ \vdots \\ V_{outm}^n \end{bmatrix}. \quad (173)$$

Modal voltages and currents in (173) are in the modal domain and are transformed to the phase domain using transformation matrices \mathbf{T}_i and \mathbf{T}_v from (122)-(123) as follows

$$\begin{bmatrix} \mathbf{T}_i^{-1} \\ \mathbf{T}_i^{-1} \end{bmatrix} \begin{bmatrix} I_{out1} \\ I_{out2} \\ \vdots \\ I_{outn} \\ I_{in1} \\ I_{in2} \\ \vdots \\ I_{inn} \end{bmatrix} = \begin{bmatrix} A^1 & & & B^1 & & & \\ & A^2 & & & B^2 & & \\ & & \ddots & & & \ddots & \\ & & & A^n & & & B^n \\ C^1 & & & & D^1 & & \\ & C^2 & & & & D^2 & \\ & & \ddots & & & & \ddots \\ & & & C^n & & & D^n \end{bmatrix} \begin{bmatrix} \mathbf{T}_v^{-1} \\ \mathbf{T}_v^{-1} \end{bmatrix} \begin{bmatrix} V_{in1} \\ V_{in2} \\ \vdots \\ V_{inn} \\ V_{out1} \\ V_{out2} \\ \vdots \\ V_{outn} \end{bmatrix}. \quad (174)$$

Thus currents and voltages in the phase domain are directly related by a transfer matrix as follows

$$\begin{bmatrix} \mathbf{I}_{out} \\ \mathbf{I}_{in} \end{bmatrix} = \begin{bmatrix} \mathbf{H}_1 & \mathbf{H}_2 \\ \mathbf{H}_3 & \mathbf{H}_4 \end{bmatrix} \begin{bmatrix} \mathbf{V}_{in} \\ \mathbf{V}_{out} \end{bmatrix} \quad (175)$$

where

$$\mathbf{I}_{out} = [I_{out1} \ I_{out2} \ \cdots \ I_{outn}]^T \quad (176)$$

$$\mathbf{I}_{in} = [I_{in1} \ I_{in2} \ \cdots \ I_{inn}]^T \quad (177)$$

$$\mathbf{V}_{out} = [V_{out1} \ V_{out2} \ \cdots \ V_{outn}]^T \quad (178)$$

$$\mathbf{V}_{in} = [V_{in1} \ V_{in2} \ \cdots \ V_{inn}]^T \quad (179)$$

and the transfer matrix elements are calculated as follows

$$\mathbf{H}_1 = \mathbf{T}_i \begin{bmatrix} A^1 & & \\ & A^2 & \\ & & \ddots \\ & & & A^n \end{bmatrix} \mathbf{T}_v^{-1} \quad (180)$$

$$\mathbf{H}_2 = \mathbf{T}_i \begin{bmatrix} B^1 & & \\ & B^2 & \\ & & \ddots \\ & & & B^n \end{bmatrix} \mathbf{T}_v^{-1} \quad (181)$$

$$\mathbf{H}_3 = \mathbf{T}_i \begin{bmatrix} C^1 & & \\ & C^2 & \\ & & \ddots \\ & & & C^n \end{bmatrix} \mathbf{T}_v^{-1} \quad (182)$$

$$\mathbf{H}_4 = \mathbf{T}_i \begin{bmatrix} D^1 & & & \\ & D^2 & & \\ & & \ddots & \\ & & & D^n \end{bmatrix} \mathbf{T}_v^{-1}. \quad (183)$$

A load with an admittance matrix \mathbf{Y}_{load} , connected to the terminal labeled as *out* in (175), relates voltage vector \mathbf{V}_{out} and current vector \mathbf{I}_{out} as follows

$$\mathbf{I}_{out} = \mathbf{Y}_{load} \mathbf{V}_{out}. \quad (184)$$

Equation (184) applied to (175) gives

$$\begin{bmatrix} \mathbf{0} & \mathbf{Y}_{load} \\ \mathbf{0} & \mathbf{0} \end{bmatrix} \begin{bmatrix} \mathbf{V}_{in} \\ \mathbf{V}_{out} \end{bmatrix} + \begin{bmatrix} \mathbf{0} \\ \mathbf{I}_{in} \end{bmatrix} = \begin{bmatrix} \mathbf{H}_1 & \mathbf{H}_2 \\ \mathbf{H}_3 & \mathbf{H}_4 \end{bmatrix} \begin{bmatrix} \mathbf{V}_{in} \\ \mathbf{V}_{out} \end{bmatrix} \quad (185)$$

$$\begin{bmatrix} \mathbf{0} \\ \mathbf{I}_{in} \end{bmatrix} = \begin{bmatrix} \mathbf{H}_1 & \mathbf{H}_2 - \mathbf{Y}_{load} \\ \mathbf{H}_3 & \mathbf{H}_4 \end{bmatrix} \begin{bmatrix} \mathbf{V}_{in} \\ \mathbf{V}_{out} \end{bmatrix} \quad (186)$$

where $\mathbf{0}$ are matrices filled with zeros. The solution of (186) is

$$\mathbf{V}_{out} = (\mathbf{Y}_{load} - \mathbf{H}_2)^{-1} \mathbf{H}_1 \mathbf{V}_{in} \quad (187)$$

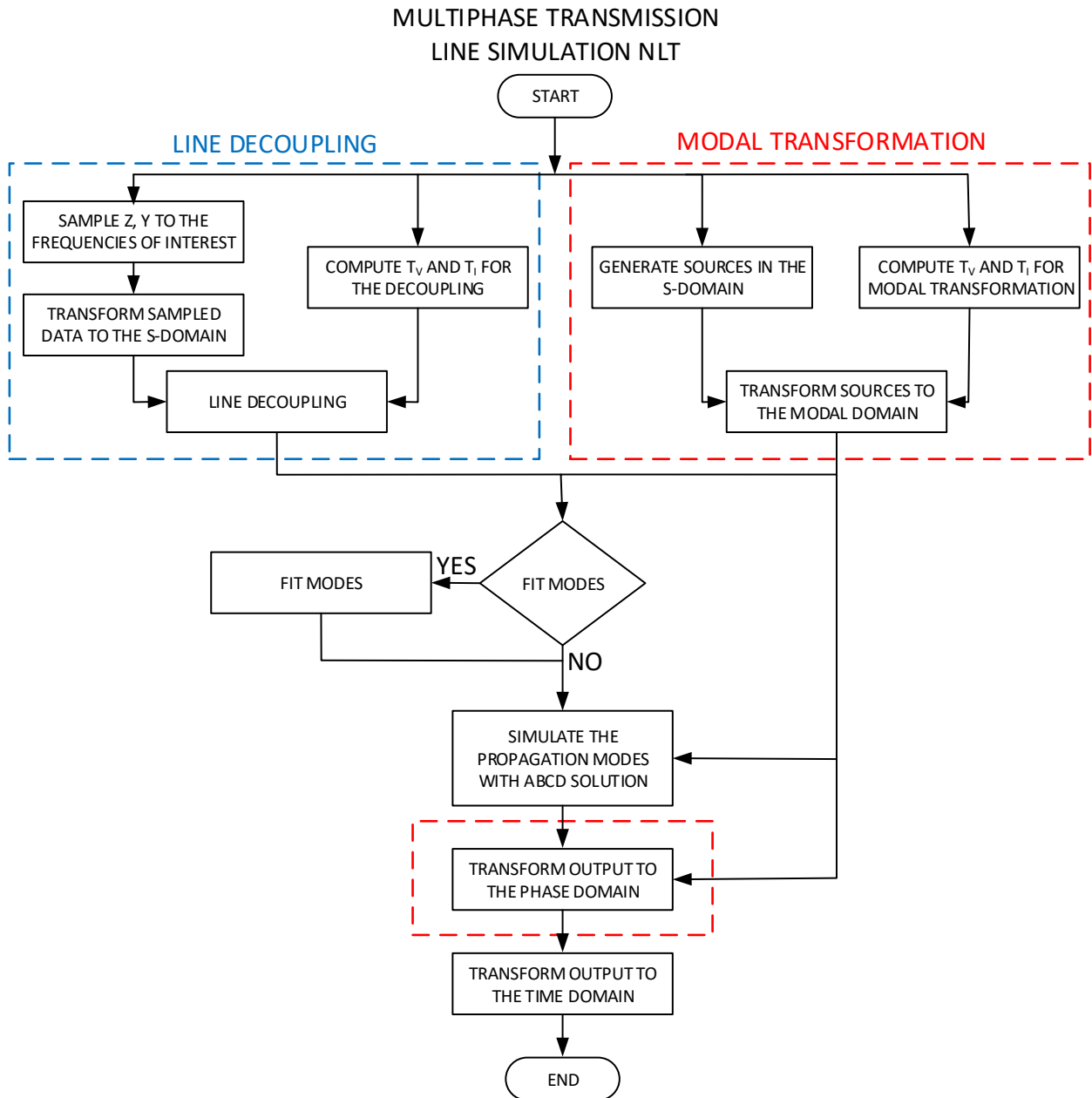
$$\mathbf{I}_{in} = \mathbf{H}_3 \mathbf{V}_{in} + \mathbf{H}_4 \mathbf{V}_{out} \quad (188)$$

All phase-voltages and phase-currents obtained in (184), (187)-(188) are in the frequency-domain and may be transformed to the time-domain by numerical techniques e.g. the Numerical Laplace Transform ^{52,53}.

3.8 IMPLEMENTATION

The basic flowchart for simulating a multiphase transmission line using modal transformation in the frequency-domain explained in this chapter is shown in Figure 27.

Figure 27 – Frequency domain solution flowchart



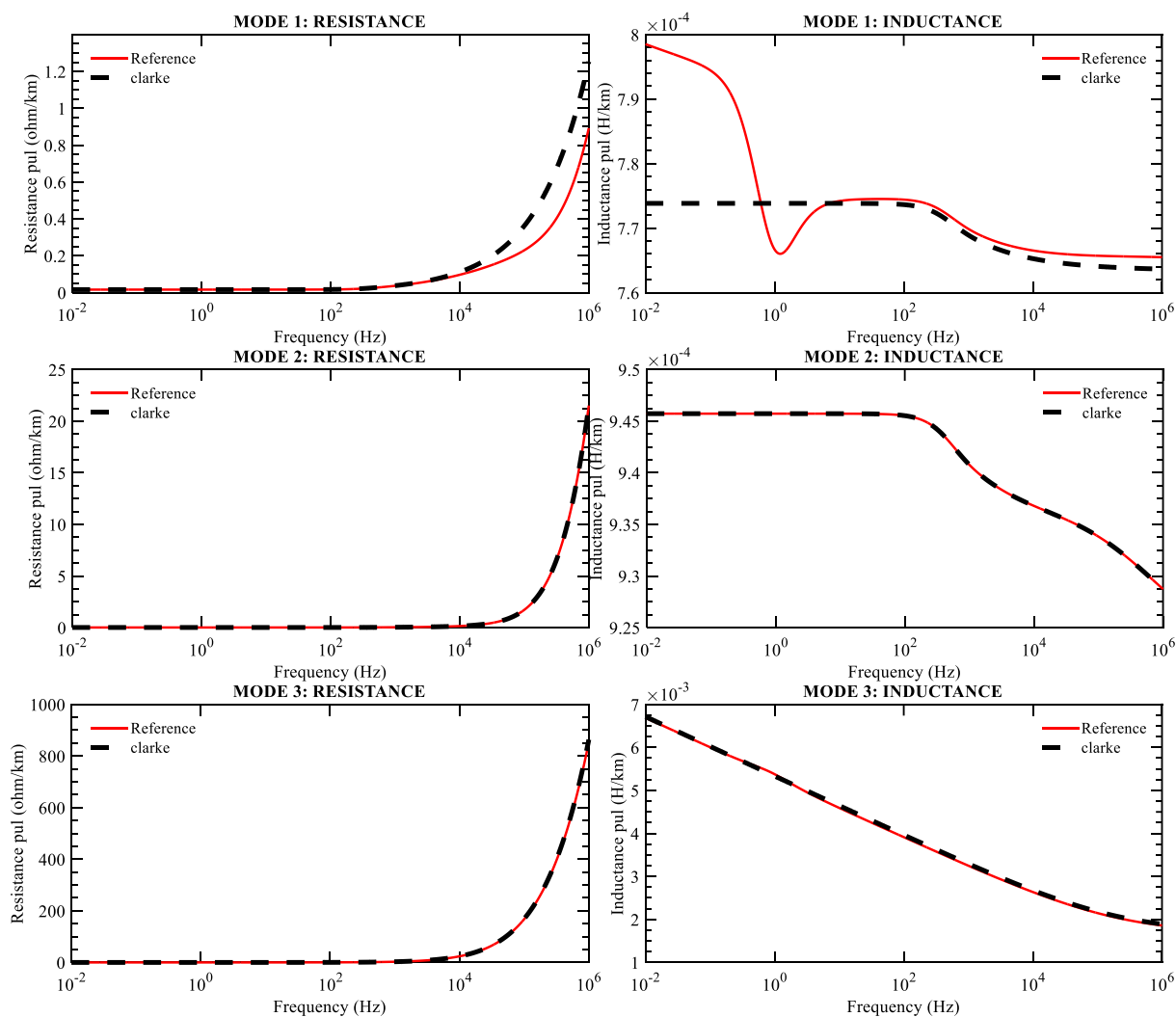
Source: Compiled by author

3.9 CONSIDERATIONS ON MODAL TRANSFORMATION

We applied the modal transformation developed in this chapter to the CESP line presented in section 2.8 of this document. The “exact” modes were obtained using the Newton-Raphson

method for untransposed transmission lines ⁸³ (reference model) described in section 3.6.1. Additionally, for comparison purposes, we obtained the quasi-modes (approximate modes) using Clarke's matrix described in section 3.6.4. The p.u.l. longitudinal resistance and inductance for all 3 modes, using both methods for decoupling the MTL, are shown in Figure 28 and the transversal capacitance for all 3 modes are presented in Table 1.

Figure 28 – CESP's Transmission line modes



Source: Compiled by author

Figure 28 shows that Clarke's transformation (alpha-beta-zero transformation) decouples the exact mode β , an accurate quasi-mode 0 and a reasonably accurate quasi-mode α for most frequencies as described in section 3.6.4 for MTL with vertical symmetry.

Table 1 – a Capacitance associated to each mode

	Capacitance [F/km] Reference Model	Capacitance [F/km] Clarke's transformation
Mode 1 (α)	1.4591e-08	1.4633e-08
Mode 2 (β)	1.2073e-08	1.2073e-08
Mode 3 (0)	6.5509e-09	6.5086e-09

Source: Compiled by author

It is important to remark that Clarke's transformation and the transformation produced by the matrices obtained with the Newton-Raphson method are similar. However, due to the eigenvector problem's nature, there are an infinite combinations of transformation matrices. Therefore, there are an infinite number of transformations matrices that produce different mode impedance matrices \mathbf{Z}_m and mode admittance matrices \mathbf{Y}_m . In consequence, the modes obtained using other methods for obtaining the transformation matrices \mathbf{T}_i and \mathbf{T}_v may be different without being wrong or inaccurate.

3.10 CONCLUSION

In this chapter we presented the frequency-domain differential equations of a single-phase transmission line. The differential equations were solved considering infinitesimal portions of the MTL. The solution of the MTL in the frequency domain was obtained using ABCD parameters.

We also presented the modal transformation, that can be used to decouple a multiphase line into its modes, each one independent from the other (no coupled parameters). That way, each mode can be modeled individually as a single-phase transmission line using the ABCD solution. There are several methods for obtaining frequency-dependent and constant transformation matrices.

The ABCD solution of a MTL is known to be one of the most accurate models for a generic transmission line. However, it has many disadvantages: it needs the Numeric Laplace Transform to transform voltages and currents to the time-domain, non-linear elements need convolution

integrals, time dependent elements most of the time cannot be modeled in the frequency domain. In consequence, time-domain models are preferred for simulating transmission lines.

In the next chapter, we show a transmission line model directly developed in the time-domain, the Bergeron model.

4 TIME DOMAIN TRANSMISSION LINE MODELS

4.1 INTRODUCTION

For this research, we will confine our analysis to classic transmission lines, i.e., physical connections between a source and a consumer. A rigorous study of this matter would require a direct application of Maxwell's equations. Nonetheless, under certain circumstances, much simpler approximations can be used.

In most practical cases, electromagnetic transient phenomena and devices connected to power systems are modeled in the time domain because frequency domain models are complex and impractical.

With that consideration, we show in this chapter a time domain model available in technical literature developed entirely in time domain, free of inverse transforms or convolution integrals.

4.2 TRANSMISSION LINE DIFFERENTIAL EQUATIONS IN THE TIME DOMAIN

Let us consider a single-phase transmission line of any length, formed by two rectilinear metallic completely isolated conductors, sufficiently distant from structures or another transmission lines so it is not influenced by any external agents⁶⁹. For this system, we consider the infinitesimal portion of the transmission line Δx where p.u.l. losses R in the conductors and p.u.l. losses G in the dielectric are uniformly distributed as shown in Figure 29. Kirchhoff's current and voltage laws of the circuit of Figure 29 are, respectively, given by

$$i(x + \Delta x, t) = i(x, t) - G \Delta x V(x, t) - C \Delta x \frac{\partial V(x, t)}{\partial t} \quad (189)$$

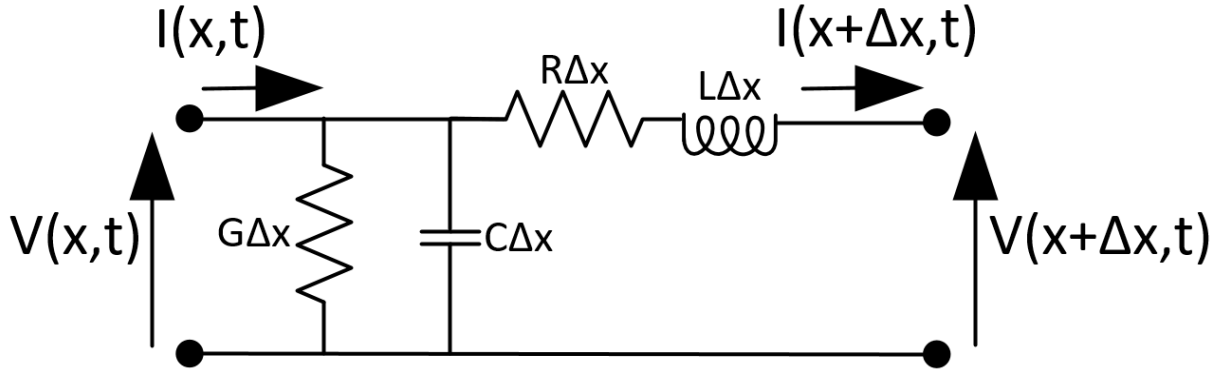
$$V(x + \Delta x, t) = V(x, t) - L \Delta x \frac{\partial i(x + \Delta x, t)}{\partial t} - R \Delta x i(x + \Delta x, t), \quad (190)$$

and can be approximated by Taylor series as follows⁹³

$$i(x + \Delta x, t) \approx i(x, t) + \Delta x \frac{\partial i(x, t)}{\partial x} + \dots \quad (191)$$

$$V(x + \Delta x, t) \approx V(x, t) + \Delta x \frac{\partial V(x, t)}{\partial x} + \dots \quad (192)$$

Figure 29 – Infinitesimal portion of the transmission line



Source: Compiled by author

Voltages and currents approximated by Taylor series (191)-(192) differentiated with respect to time are given by

$$\frac{\partial i(x + \Delta x, t)}{\partial t} = \frac{\partial i(x, t)}{\partial t} + \Delta x \frac{\partial^2 i(x, t)}{\partial t \partial x} + \dots \quad (193)$$

$$\frac{\partial V(x + \Delta x, t)}{\partial t} = \frac{\partial V(x, t)}{\partial t} + \Delta x \frac{\partial^2 V(x, t)}{\partial t \partial x} + \dots \quad (194)$$

Considering only the first two terms in (191)-(194) and substituting them in equations (189)-(190) leads to

$$i(x + \Delta x, t) = i(x, t) - G \Delta x \left[V(x + \Delta x, t) - \Delta x * \frac{\partial V(x, t)}{\partial x} \right] - C \Delta x \left[\frac{\partial V(x + \Delta x, t)}{\partial t} - \Delta x \frac{\partial^2 V(x, t)}{\partial t \partial x} \right] \quad (195)$$

$$V(x + \Delta x, t) = V(x, t) - L \Delta x \left[\frac{\partial i(x, t)}{\partial t} + \Delta x \frac{\partial^2 i(x, t)}{\partial t \partial x} \right] - R \Delta x \left[i(x, t) + \Delta x \frac{\partial i(x, t)}{\partial x} \right] \quad (196)$$

that can be rearranged for convenience as follows

$$\frac{i(x + \Delta x, t) - i(x, t)}{\Delta x} = -G \left[V(x + \Delta x, t) - \Delta x \frac{\partial V(x, t)}{\partial x} \right] - C \left[\frac{\partial V(x + \Delta x, t)}{\partial t} - \Delta x \frac{\partial^2 V(x, t)}{\partial t \partial x} \right] \quad (197)$$

$$\frac{V(x + \Delta x, t) - V(x, t)}{\Delta x} = -L \left[\frac{\partial i(x, t)}{\partial t} + \Delta x \frac{\partial^2 i(x, t)}{\partial t \partial x} \right] - R \left[i(x, t) + \Delta x \frac{\partial i(x, t)}{\partial x} \right] \quad (198)$$

The limit of currents and voltages in (197)-(198) when x approaches 0 are given by⁹³

$$\lim_{\Delta x \rightarrow 0} \frac{i(x + \Delta x, t) - i(x, t)}{\Delta x} = \frac{\partial i(x, t)}{\partial x} \quad (199)$$

$$\lim_{\Delta x \rightarrow 0} \frac{V(x + \Delta x, t) - V(x, t)}{\Delta x} = \frac{\partial V(x, t)}{\partial x} \quad (200)$$

and can be substituted in (197)-(198) as follows⁹⁴

$$\frac{\partial i(x, t)}{\partial x} = -G V(x, t) - C \frac{\partial V(x, t)}{\partial t} \quad (201)$$

$$\frac{\partial V(x, t)}{\partial x} = -L \frac{\partial i(x, t)}{\partial t} - R i(x, t) \quad (202)$$

First order differential equations (201)-(202) describe a single-phase transmission line in the time domain when R , L , G and C are assumed to be constant i.e. frequency-independent.

4.3 BERGERON'S LINE MODEL

Due to the benefits of time domain simulations, we discuss one solution found for the first order differential equations (201)-(202), the Bergeron's line model. One of the advantages of time domain models is that they can be solved numerically in conventional computers, with whom is possible to develop reliable, powerful and versatile network simulators⁹⁵.

A computational digital solution is a procedure where the solution is developed step by step through time with a fixed or variable time step Δt . Due to computational limitations, digital solutions do not produce a continuous response of the system, they produce a discrete sequence of points. This time discretization leads to truncation errors and can even cause a numerical instability in the response of the system.

Bergeron's model uses a portion of the "line's history" to solve line's equations. This model can be solved using numerical integration such as the trapezoidal rule of integration, which is known to be very stable and reliable when compared to other methods ³.

Although Bergeron's model can be applied to lossy lines, the resulting differential equations are not directly integrable ². Therefore, the method of characteristics, also known as Bergeron's method, assumes that distributed parameters are lossless ³.

Let us consider a lossless line with a p.u.l. inductance L and p.u.l. capacitance C . Under this assumption, differential equations (201)-(202) become

$$\frac{\partial i(x, t)}{\partial x} = -C \frac{\partial V(x, t)}{\partial t} \quad (203)$$

$$\frac{\partial V(x, t)}{\partial x} = -L \frac{\partial i(x, t)}{\partial t}, \quad (204)$$

which has a general solution, found by d'Alembert, that is given by

$$i(x, t) = f_1(x - vt) + f_2(x + vt) \quad (205)$$

$$V(x, t) = Zf_1(x - vt) - Zf_2(x + vt) \quad (206)$$

where characteristic impedance Z and propagation velocity v are calculated as follows

$$Z = \sqrt{\frac{L}{C}} \quad (207)$$

$$v = \frac{1}{\sqrt{LC}} \quad (208)$$

Multiplying (205) by Z and adding it to (206) results in (209). Similarly, multiplying (205) by Z and subtracting it from (206) results in (210).

$$V(x, t) + Z i(x, t) = 2Zf_1(x - vt) \quad (209)$$

$$V(x, t) - Z i(x, t) = -2Zf_2(x + vt) \quad (210)$$

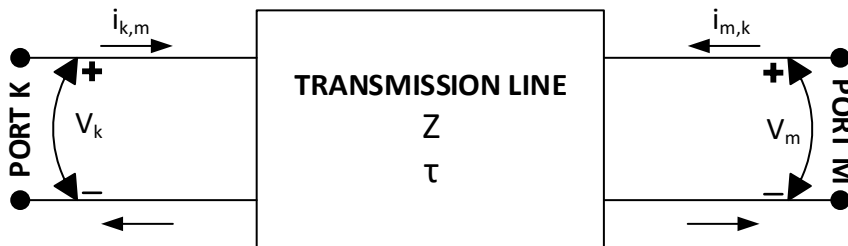
In (209)-(210), $V(x, t) + Z i(x, t)$ is constant when $(x - vt)$ is constant, and $V(x, t) - Z i(x, t)$ is constant when $(x + vt)$ is constant. $(x - vt) = \text{constant}$ and $(x + vt) = \text{constant}$ are the differential equation characteristics³. The propagation time τ that takes to cover the line's length d at propagation velocity v is given by

$$\tau = \frac{d}{v} = d\sqrt{LC}. \quad (211)$$

Considering that points k and m are the line ends, $(V + Zi)$ at k and instant $t - \tau$ should have the same value at the line's end point m at instant t . This can be written using a two port network topology (Figure 30) as follows^{3,13}

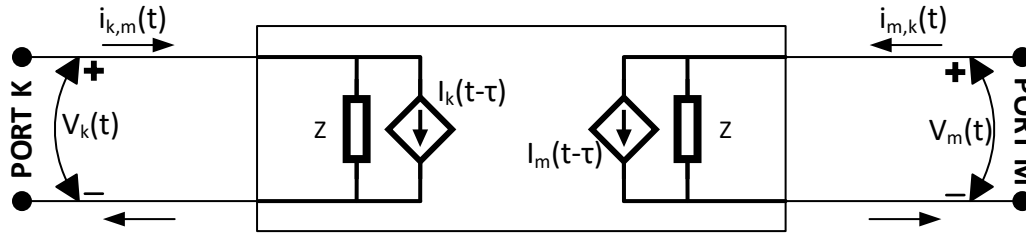
$$V_m(t - \tau) + Z i_{m,k}(t - \tau) = V_k(t) + Z (-i_{k,m}(t)). \quad (212)$$

Figure 30 – Line's two port network



Source: Compiled by author

Figure 31 – Equivalent impedances network



Source: Compiled by author

The two-port network shown in Figure 30's has the equivalent impedances shown in Figure 31. Current sources I_k and I_m use the "line's history" and are given by

$$I_k(t - \tau) = -\frac{1}{Z} V_m(t - \tau) - i_{m,k}(t - \tau) \quad (213)$$

$$I_m(t - \tau) = -\frac{1}{Z} V_k(t - \tau) - i_{k,m}(t - \tau) \quad (214)$$

Simplicity of this method rely on the assumption that losses can be neglected. This simplicity is also sustained in distortion-less lines, i.e., lines where $R/L = G/C$. This lines are called distortion-less because they transmit any type of signal without losing its form^{3,76}.

Unfortunately, transmission lines have distortion if conductance G cannot be neglected (or a very complex voltage function appears if corona effect is to be considered).

Distributed p.u.l. resistance R' , assuming negligible p.u.l. conductance G , can be approximated by treating the line as lossless and adding the losses as concentrated resistances in the line terminals. The concentrated resistance are defined as follows

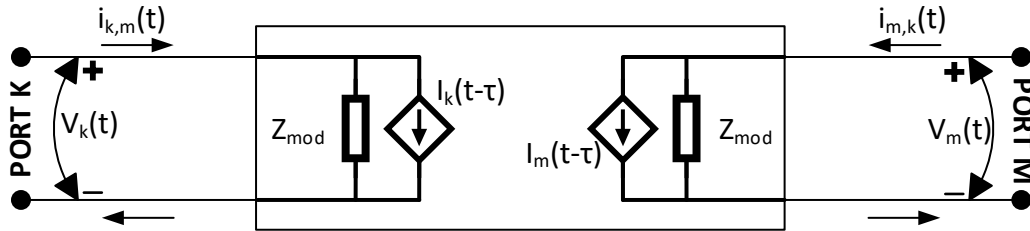
$$R = R' * \frac{\text{total length}}{\text{number of sections}} \quad (215)$$

$R' = \text{p. u. l. resistance}$

This concentrated resistances can be damped in many places along the line when the line's length d is divided in segments and connected in cascade ³.

For n line sections, each having half of its concentrated resistance R connected to the entry point and half connected to the exit point of the network, we expect to have the equivalent modified quadrupole shown in Figure 32.

Figure 32 – Modified quadrupole



Source: Compiled by author

The equations that describe the modified quadrupole network shown in Figure 32 are

$$i_{k,m}(t) = \frac{1}{Z_{modified}} V_k(t) + I_k(t - \tau) \quad (216)$$

$$i_{m,k}(t) = \frac{1}{Z_{modified}} V_m(t) + I_m(t - \tau) \quad (217)$$

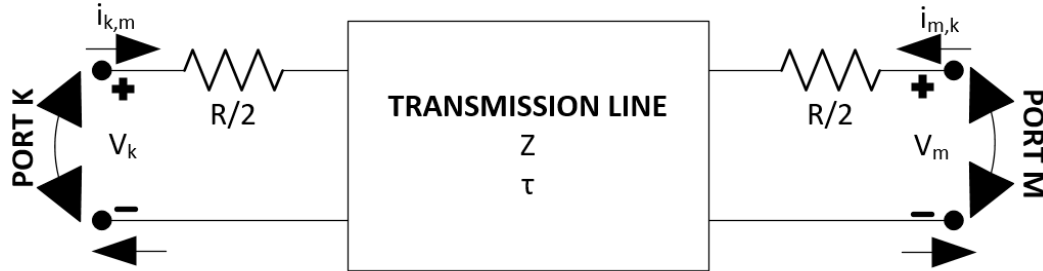
For the simplest case, where the line is not divided into segments and the losses are concentrated in both terminals of the line as shown in Figure 33, the modified impedance Z_{mod} and the historic currents I_k and I_m are given by

$$Z_{mod} = Z + \frac{R}{2} \quad (218)$$

$$I_k(t - \tau) = -\frac{1}{Z_{mod}} \left[V_m(t - \tau) + \left(Z - \frac{R}{2} \right) i_{m,k}(t - \tau) \right] \quad (219)$$

$$I_m(t - \tau) = -\frac{1}{Z_{mod}} \left[V_k(t - \tau) + \left(Z - \frac{R}{2} \right) i_{k,m}(t - \tau) \right] \quad (220)$$

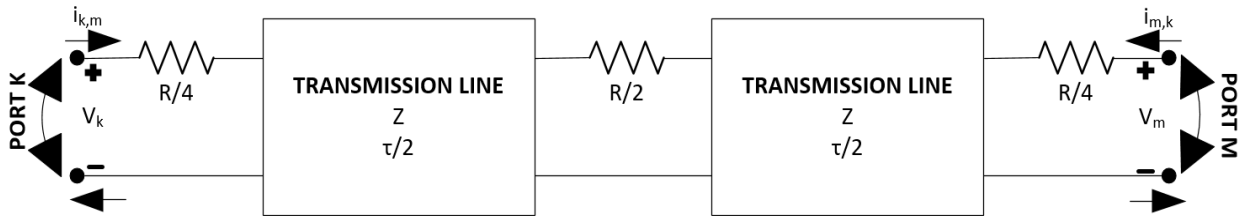
Figure 33 – Bergeron's model with losses concentrated on both terminals



Source: Compiled by author

General equations (216)-(217) describe a transmission line where the losses are lumped in three points as shown in Figure 34. The modified impedance Z_{mod} and the historic currents I_k and I_m are given by

Figure 34 – Bergeron's model with losses lumped in three points



Source: Compiled by author

$$Z_{mod} = Z + \frac{R}{4} \quad (221)$$

$$I_k(t - \tau) = -\frac{Z}{\left(Z + \frac{R}{4} \right)^2} \left[V_m(t - \tau) + \left(Z - \frac{R}{4} \right) i_{m,k}(t - \tau) \right] - \frac{\frac{R}{4}}{\left(Z + \frac{R}{4} \right)^2} \left[V_k(t - \tau) + \left(Z - \frac{R}{4} \right) i_{k,m}(t - \tau) \right] \quad (222)$$

$$\begin{aligned}
I_m(t - \tau) = & -\frac{Z}{\left(Z + \frac{R}{4}\right)^2} \left[V_k(t - \tau) + \left(Z - \frac{R}{4}\right) i_{k,m}(t - \tau) \right] \\
& - \frac{\frac{R}{4}}{\left(Z + \frac{R}{4}\right)^2} \left[V_m(t - \tau) + \left(Z - \frac{R}{4}\right) i_{m,k}(t - \tau) \right]
\end{aligned} \tag{223}$$

Dommel's scheme combined Bergeron's method and the trapezoidal rule of integration in an algorithm able to solve transients in multiphase transmission lines. This model has an acceptable error as long as $R \ll z_o$ ⁴⁰.

Bergeron's model is accurate enough for lossless, distortion-less lines. However, the parameters used in Bergeron's model are constant while transmission line's real parameters are frequency-dependent ⁹⁶.

4.4 CONCLUSION

In this chapter we showed the time domain differential equations of a transmission line. We introduced the Bergeron's model for lossless lines and Dommel's scheme to include losses in Bergeron's model. As any other model, Bergeron's model has advantages and disadvantages and based on the assumptions made, it is very limited to frequency-independent lines.

In the next chapter we will show the techniques available for including the frequency dependence directly in the time-domain.

5 PARAMETER REPRESENTATION USING RATIONAL FUNCTIONS

5.1 INTRODUCTION

One of the difficulties in power systems modeling is the inclusion of frequency dependent effects on time-domain simulations. Such effects arise from many factors as eddy currents, relaxation phenomena in dielectrics, skin effect, earth-return effect and others. These effects concretize as frequency-dependent variations in the parameters of the model: resistance, inductance and capacitance for transmission lines case.

Frequency dependence in time-domain models usually leads to convolutions, which require strong computational effort and compromise the efficiency of the computational procedure. Analytical expressions can be derived only for very particular configurations and closed-form expressions are not available. Another important issue of the convolution products is the numerical implementation of the solution, requiring the storage of all solutions at previous time-steps, thus resulting in exponential growth of the computation time and error buildup⁹⁷.

Most of the issues related to the convolution products resulting from the inverse Fourier transform can be treated efficiently by means of fitting models.

5.2 FITTING MODELS

Consider a function $f(s)$ that represents a frequency-dependent parameter of a system, e.g., the series impedance of a transmission line. We assume that $f(s)$ can be approximated by a rational function $f_{fit}(s)$ having D poles a_n and N zeros z_n as follows

$$f_{fit}(s) = \frac{\sum_{n=0}^N N_n s^n}{\sum_{n=0}^D D_n s^n} = \frac{N_N \prod_{n=1}^N (s - z_n)}{D_D \prod_{n=1}^D (s - a_n)} \approx f(s) \quad (224)$$

The rational function $f_{fit}(s)$ is fitted to $f(s)$ using fitting methods. If $D = N$, the pole-residue form of $f_{fit}(s)$ is given by

$$f_{fit}(s) = \sum_{n=1}^N \frac{c_n}{s - a_n} + d + se \approx f(s) \quad (225)$$

where a_n is the n -th pole, c_n is the n -th residue, d is the high-frequency asymptotic constant and e is the linear term.

A critical aspect is the stability of the fitting model. Dynamic stability of a model is assured if all its poles are characterized by a negative real part. If a fitting model is applied to a transfer function, then input-output stability should be also enforced. Dynamic stability can be enforced as a constraint in the calculation of the terms in the rational function $f_{fit}(s)$ whereas input-output stability can be achieved applying a correction procedure after the fitting model is defined.

In the following, we present three fitting procedures, their advantages, limitations and specific applications.

5.2.1 The Model-Based Parameter Estimation (MBPE)

The MBPE method represents the extension of Prony's approach to the treatment of frequency-domain data. The fitting model expressed in equation (224) is defined by evaluating the unknown poles a_n and zeros z_n .

The following constraints are enforced on the fitting model ⁹⁷:

1. Set $D_d = 1$
2. All poles a_n are assumed to be real or complex conjugated pairs, so that $f(t)$ is a real-value function.
3. The unknown coefficients are assumed to be real numbers.
4. The function $f_{fit}(s)$ is assumed to be strictly proper with $D = N + 1$ (the order of the denominator in equation (224) less than the order of the numerator) in order to assure causality. If $\lim_{\omega \rightarrow \infty} f(s) = d$, the fitting model is applied to the modified function $\hat{f}(s) = f(s) - d$.

The $2d$ unknown coefficients are computed by applying a point-matching algorithm, which consists in enforcing $f_{fit}(s) = \hat{f}(s)$ for only d values of the s -variable s_i . The following $2d$ linear equations with real coefficients are then obtained:

$$f_{fit}(s) = \sum_{h=1}^{d/2} (-1)^h \omega^{d-2h} [\hat{f}_i^R D_{d-2h} - N_{d-2h} - s_i \hat{f}_i^I D_{d+1-2h}] = -s_i^d \hat{f}_i^R \quad (226)$$

$$f_{fit}(s) = \sum_{h=1}^{d/2} (-1)^h \omega^{d-2h} [\hat{f}_i^I D_{d-2h} + s_i N_{d+1-2h} - s_i \hat{f}_i^R D_{d+1-2h}] = s_i^d \hat{f}_i^R \quad (227)$$

In which $i = 1 \dots d$ and $\hat{f}(s_i) = \hat{f}_i^R + j\hat{f}_i^I$.

This method is very simple and easy to implement. However, special care should be taken into account due to computer overflow problems for high values of the complex frequency s .

MBPE is suitable for transfer functions of complex electromagnetic systems with multiple resonances and smooth functions without resonance peaks.

5.2.2 The Vector Fitting VF

The objective is to approximate a frequency function $f(s)$ (generally a vector, hence the designation Vector Fitting) with a rational function in pole-residue form that is given by

$$f_{fit}(s) = \sum_{n=1}^N \frac{c_n}{s - a_n} + d + se \approx f(s). \quad (228)$$

Within this model, terms d and e in are optional.

The method first identifies the poles of $f(s)$ by solving in the least-squares sense, the linear problem ⁵⁴

$$\sigma(s)f(s) = p(s) \quad (229)$$

where

$$\sigma(s) = \sum_{k=1}^m \frac{\tilde{r}_k}{s - q_k} + 1 \quad (230)$$

$$p(s) = \sum_{k=1}^m \frac{r_k}{s - q_k} + d + se \quad (231)$$

All poles and residues in (230)-(231) are real or come in complex conjugate pairs, terms d and e are real, $\sigma(s)$ is a scalar while $p(s)$ is generally a vector, and $\{q_k\}$ is a set of initial poles. The poles of $f(s)$ must be equal to the zeros of $\sigma(s)$, and are calculated as follows

$$\{a_k\} = eig(A - b \cdot c^T) \quad (232)$$

where A is a diagonal matrix holding the initial poles $\{q_k\}$, b is a column vector containing 1 and c^T is a row vector holding the residues $\{\tilde{r}_k\}$.

This procedure can be applied in an iterative manner where (229)-(232) are solved repeatedly with the new poles $\{a_k\}$ replacing the previous poles $\{q_k\}$. This usually converges in 2-3 iterations. After the poles had been identified, the residues are calculated by solving the corresponding Least-Square problem with the known poles ⁵⁴.

A critical aspect is the choice of initial poles. Normally the initial poles for VF would be selected as complex conjugate pairs that are linearly distributed over the full frequency range. However, the initial poles can be selected as real and logarithmically spaced over the fitting range for smooth functions, which is the “recommended” choice for transmission line modeling.

5.2.3 The Debye's type Fitting DF

A simplified formulation of the fitting model can be obtained when fitting smooth functions. In such cases it is assumed that $f_{fit}(s)$ has only real negative poles and residues as follows

$$f_{fit}(s) = \sum_{n=1}^N \frac{K_n}{1 + j\omega Q_n} + d. \quad (233)$$

In which K_n and Q_n are real positive quantities given by

$$K_n = -\frac{c_n}{a_n} \quad (234)$$

$$Q_n = -\frac{1}{a_n} \quad (235)$$

and terms c_n and a_n are the residues and poles, respectively, of $f_{fit}(s)$.

The main advantages of the DF are: it satisfies the Kramers-Kronig dispersion relation in the frequency-domain because it only admits real poles, causality in time-domain is guaranteed because poles are considered negative, it has an easy circuit representation and the calculation of the unknown parameters can be easily performed by applying any commercial software based on the Least-Squared algorithm.

Nonetheless, one critical aspect of the DF model consists in the proper choice of the order of the rational approximation and the set of initial values of K_n and Q_n . There are some procedures available in technical literature for choosing number and initial poles as described in ⁵⁴.

5.2.4 Modified Vector Fitting MVF

By replacing the high-frequency asymptotic requirement of the VF's scaling function with a more relaxed condition, it is possible to improve the VF convergence performance and reduce the importance of the initial pole set specification ⁵⁴.

The modified Vector Fitting removes the asymptotic requirement of the Least Square problem by replacing (230) with

$$\sigma(s) = \sum_{k=1}^m \frac{\tilde{r}_k}{s - q_k} + \tilde{d} \quad (236)$$

where term \tilde{d} is real.

In order to avoid the trivial (null) solution, the following equation is added to the problem

$$\text{Re} \left\{ \sum_{h=1}^{N_s} \left(\sum_{k=1}^m \frac{\tilde{r}_k}{s_h - q_k} + \tilde{d} \right) \right\} = N_s \quad (237)$$

which enforces that the sum of the real part of $\sigma(s)$ over a given frequency samples equals some nonzero value, without fixing any of the free variables, i.e., does not impose any constraint in the LS problem other than preventing $\sigma(s)$ from becoming zero.

Equation (237) should be weighted in relation to the size of $f(s)$ in the LS problem as follows

$$\text{weight} = \frac{\|w(s) \cdot f(s)\|_2}{N_s} \quad (238)$$

where $w(s)$ is the specified weight for the fitting of $f(s)$.

MVF gives a much faster convergence and high accuracy for the end result despite any noise mixed with $f(s)$. Additionally, it reduces the importance of the initial poles selection, giving more flexibility to the method ⁵⁴.

Higher convergence in an already very fast algorithm (low-order fitting) might be negligible for some scenarios. However, some procedures rely in a large number of calls to the fitting procedure, making a faster convergence advantageous by any means.

5.2.5 Fast Vector Fitting FVF

Another enhancement to the VF was done in reference ⁵⁵. By exploiting the sparsity of the LS equations that are solved during the pole-identification step, QR decomposition was mixed with the VF originating the FVF.

By introducing QR decomposition to the single-element LS equations, simplified sets of equations were found which translates into less memory requirements and smaller processing times. Results shown that the memory needed to compute an accurate macromodel for a 60-port PCB with standard VF is 54 GB of RAM, infeasible on most computers. By using Matlab's sparse

library, it is possible to reduce the memory needed to 88MB of RAM and process the data in 1 hour and 22 minutes. By implementing the FVF the same accurate macromodel needed 1.46MB of RAM and was processed in 44 seconds ⁵⁵.

5.2.6 Fast Relaxed Vector Fitting FRVF

By mixing the enhancements made in the MVF and FVF, we obtain the Fast Relaxed Vector Fitting FRVF, which is available free in the internet ⁵⁵.

Comparing the FRVF, that mixes all the advantages of the MVF and the FVF, with the MBPE and the DF. We can see that is by far more flexible than the other two: MBPE is more restricted and has numerical limitations while DF is only a specific case of the fitting function that constraints the coefficients to be real.

Due to the limitations of the other two (MBPE and DF) and the computational advantages and flexibility of the FRVF, we choose to use FRVF to represent the frequency dependence of the parameters in this dissertation.

5.3 EQUIVALENT CIRCUIT TOPOLOGIES

One of the most appealing aspects of representing frequency-dependent parameters using rational functions is that they can be associated with equivalent circuit representations that behave similarly to the function represented.

In particular, equivalent circuit models with passive elements can be easily associated with rational functions characterized by only negative real poles ⁵⁴.

We find in technical literature circuit topologies whose equivalent admittance (parallel branches) or equivalent impedance (series branches) are associated to elements of a rational function ⁹⁶. Those circuit topologies are obtained by

- fitting a rational function to $f(s)$ (direct), or
- fitting a rational function to a function derived from $f(s)$ (indirect).

5.3.1 Direct-Circuit Topology

Let $f(s)$ be approximated by a rational function $f_{fit}(s)$ that is given by

$$f(s) \approx f_{fit}(s) = d + se + \sum_{k=1}^{N_R} \frac{c_k}{s - a_k} + \sum_{p=1}^{N_C} \left(\frac{c_p}{s - a_p} + \frac{c_p^*}{s - a_p^*} \right) \quad (239)$$

The rational function $f_{fit}(s)$ has three parts

1. a constant term d and a constant in the linear term e ,
2. a sum of N_R partial fractions containing real residues and poles, and
3. a sum of N_C partial fractions containing complex conjugate pairs of residues and poles.

Antonini ⁹⁸ proposes the following circuit topologies for representing a rational function that fits a frequency-dependent admittance or impedance:

a) Admittance-type topology

If $f(s)$ is an admittance, then $f_{fit}(s)$ in (239) can be associated with the circuit topology shown in Figure 35. Each circuit branch represents an element of $f_{fit}(s)$.

The elements in the first branch are calculated using constants e and d as follows

$$C = e \quad (240)$$

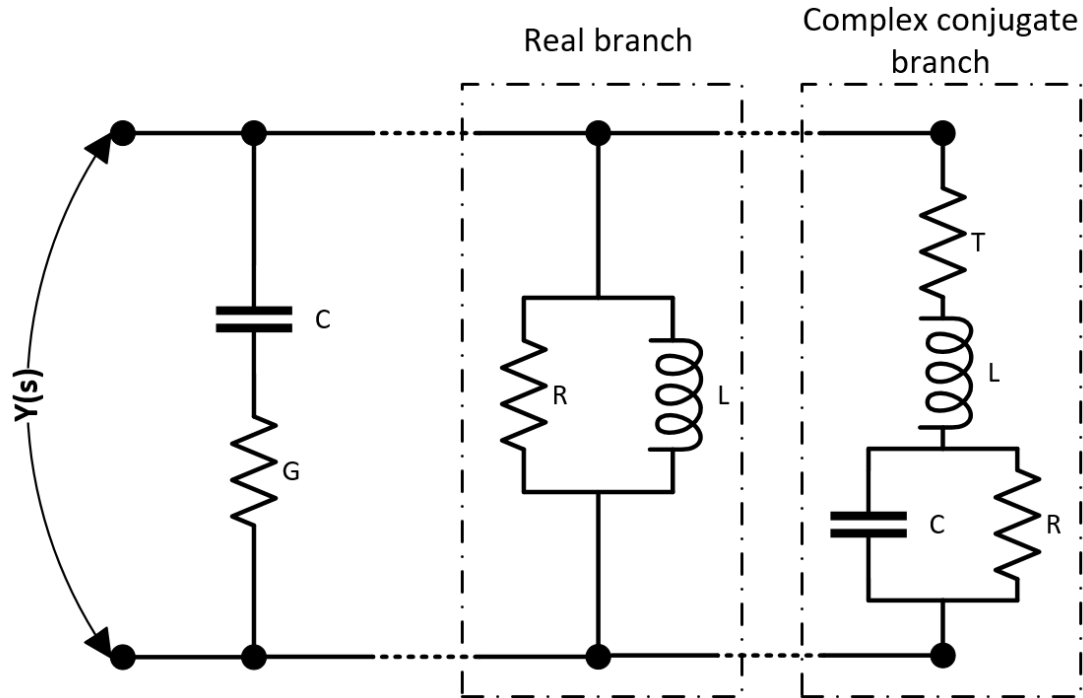
$$G = \frac{1}{d} \quad (241)$$

For each one of the N_R real pole-residues, a “real branch” is added in parallel to the circuit. The elements of the k -th “real branch” associated to the k -th pole a_k and residue c_k are given by

$$L = \frac{1}{c_k} \quad (242)$$

$$R = -\frac{a_k}{c_k} \quad (243)$$

Figure 35 – Admittance-type direct circuit topology.



Source: Compiled by author

For each one of the N_c pairs of complex conjugate poles-residues, a “complex conjugate branch” is added in parallel to the circuit. The elements of the p -th “complex conjugate branch” associated to the p -th pair of complex conjugate poles a_p and a_p^* and their respective residues c_p and c_p^* are given by

$$L = \frac{1}{c_p + c_p^*} \quad (244)$$

$$T = \frac{1}{c_p + c_p^*} \left[-(a_p + a_p^*) + \frac{1}{c_p + c_p^*} (c_p a_p^* + c_p^* a_p) \right] \quad (245)$$

$$C = \frac{(c_p + c_p^*)}{a_p a_p^* + \left[-(a_p + a_p^*) + \frac{1}{c_p + c_p^*} (c_p a_p^* + c_p^* a_p) \right]} \frac{1}{\frac{c_p a_p^* + c_p^* a_p}{c_p + c_p^*}} \quad (246)$$

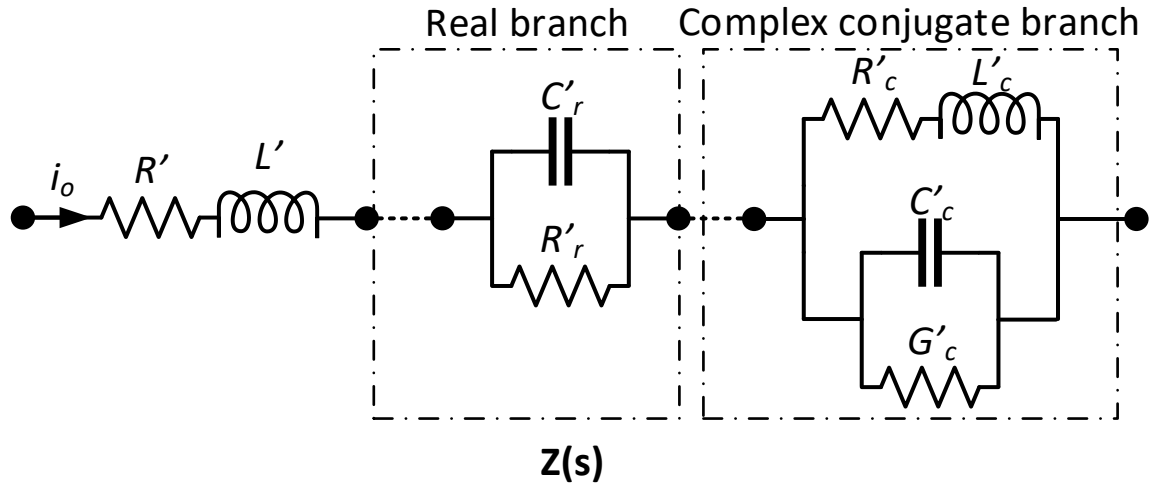
$$R = -\frac{1}{C} \frac{c_p + c_p^*}{c_p a_p^* + c_p^* a_p} \quad (247)$$

The elements G , R and T in Figure 35 are all resistances.

b) Impedance-type equivalent circuit

If $f(s)$ is a p.u.l. impedance $Z(s)$, then $f_{fit}(s)$ in (239) can be associated with the circuit topology shown in Figure 36. Each series circuit branch represents an element of $f_{fit}(s)$.

Figure 36 – Impedance-type direct circuit topology.



Source: Compiled by author

The elements in the first branch are calculated using constants e and d as follows

$$R' = d \quad (248)$$

$$L' = e \quad (249)$$

For each one of the N_R real pole-residues, a “real branch” is added in series to the circuit. The elements of the k -th “real branch” associated to the k -th pole a_k and residue c_k are given by

$$R'_r = -\frac{c_k}{a_k} \quad (250)$$

$$C'_r = \frac{1}{c_k} \quad (251)$$

For each one of the N_C pairs of complex conjugate poles-residues, a “complex conjugate branch” is added in series to the circuit. The elements of the p -th “complex conjugate branch” associated to the p -th pair of complex conjugate poles a_p and a'_p , and their respective residues c_p and c'_p are given by

$$C'_c = \frac{1}{c_p + c'_p} \quad (252)$$

$$G'_c = -C'^2_c (c_p a_p + c'_p a'_p) \quad (253)$$

$$L'_c = \frac{-\frac{1}{c_p c'_p C'^3_c}}{(a_p - a'_p)^2} \quad (254)$$

$$R'_c = -(c_p a'_p + c'_p a_p) L'_c C'_c \quad (255)$$

Another equivalent circuits can be found in technical literature involving dependent sources or additional circuit elements^{98,99}. However, in computational terms, each source would add an input to the state equations of the total system. The more inputs the system have stored the more times the integration algorithm would need to read that data. Since reading data from memory is one of the most delayed tasks in modern computing, more inputs usually translates into longer computation times.

5.3.2 Indirect-Circuit Topology

Vector Fitting can also be applied to approximate improper functions, such as the p.u.l. impedance of a lossy line. For this purpose, a rational function can be indirectly fitted to $f(s)$. This is achieved by fitting $f'(s)$, which is calculated from $f(s)$ as follows

$$f'(s) = \frac{f(s) - \Re\{f(s=0)\}}{s} \quad (256)$$

where $\Re\{f(s=0)\}$ represents the asymptotic real value of $f(s)$ next to the zero axis.

Let $f'(s)$ be approximated by a rational function $f_{fit}(s)$ that is given by

$$f'(s) \approx f_{fit}(s) = d + \sum_{k=1}^{N_R} \frac{c_k}{s - a_k} + \sum_{p=1}^{N_C} \left(\frac{c_p}{s - a_p} + \frac{c_p^*}{s - a_p^*} \right) \quad (257)$$

The rational function $f_{fit}(s)$ has three parts

1. a constant term d ,
2. a sum of N_R partial fractions containing real residues and poles, and
3. a sum of N_C partial fractions containing complex conjugate pairs of residues and poles.

The function $f_{fit}(s)$ is fitted to $f'(s)$ and is indirectly related to $f(s)$ as follows

$$f(s) = \Re\{f(s=0)\} + s \left[d + \sum_{k=1}^{N_R} \frac{c_k}{s - a_k} + \sum_{p=1}^{N_C} \left(\frac{c_p}{s - a_p} + \frac{c_p^*}{s - a_p^*} \right) \right] \quad (258)$$

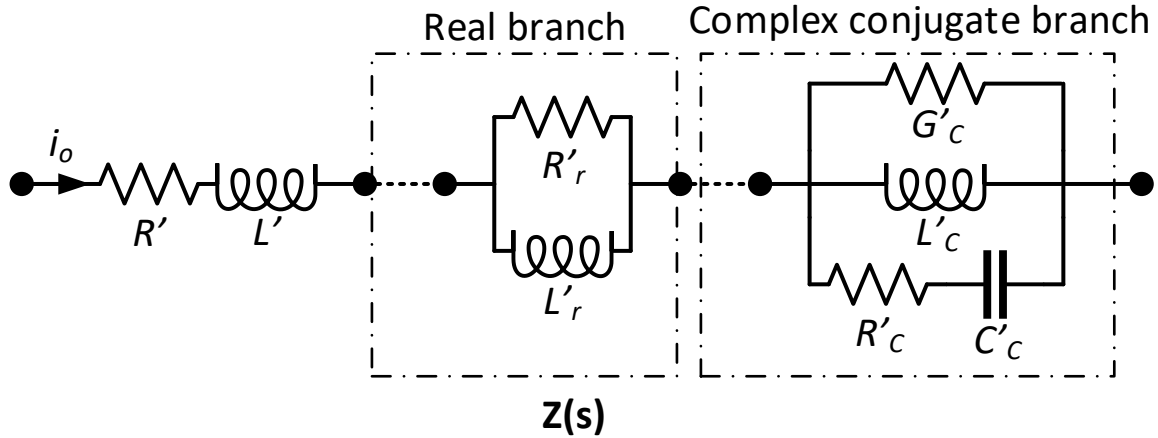
Comparison between the direct method (239) and indirect method (258) shows that the constant term d in (258) is equivalent to the constant in the linear term e in (239). And the constant term $\Re\{f(s=0)\}$ in (258) is equivalent to the constant term d in (239). Thus, the constant in the linear term e in (257) does not need to be fitted.

Usually, smooth functions are characterized by negative real poles a_k but depending on the sampling of $f(s)$, complex conjugate poles-residues may appear.

The function $f(s)$ could be an impedance or an admittance. However, because of its use in fitting overhead transmission line's impedance, only the impedance-type topology had been discussed in technical literature. Some authors^{47,97}, neglecting the existence of complex conjugate poles-residues, presented the impedance-type circuit topology associated to (258).

For this research, we admit the possibility of the existence of complex conjugate pairs of poles-residues. In consequence, we propose a branch that represents the partial functions corresponding to the complex conjugate pairs of poles-residues. Altogether with the branches found in technical literature, the circuit topology that represents (258) is shown in Figure 37

Figure 37 – Impedance-type modified-fitting equivalent circuit



Source: Compiled by author

The elements in the first branch are calculated using constants e and d as follows

$$R' = \Re\{f(s = 0)\} \quad (259)$$

$$L' = d \quad (260)$$

For each one of the N_R real pole-residues, a “real branch” is added in series to the circuit. The elements of the k -th “real branch” associated to the k -th pole a_k and residue c_k are given by

$$R'_k = c_k \quad (261)$$

$$L'_k = -\frac{c_k}{a_k} \quad (262)$$

For each one of the N_C pairs of complex conjugate poles-residues, a “complex conjugate branch” is added in series to the circuit. The elements of the p -th “complex conjugate branch” associated to the p -th pair of complex conjugate poles a_p and a'_p , and their respective residues c_p and c'_p are given by

$$L'_c = \frac{c_p a_p^* + c_p^* a_p}{a_p a_p^*} \quad (263)$$

$$G'_c = -\frac{\frac{c_p^* a_p}{a_p^*} + \frac{c_p a_p^*}{a_p}}{L'_c (c_p a_p^* + c_p^* a_p)} \quad (264)$$

$$R'_c = \frac{1}{\frac{1}{c_p + c_p^*} - G'_c} \quad (265)$$

$$C'_c = -\frac{c_p + c_p^*}{R'_c (c_p a_p^* + c_p^* a_p)} \quad (266)$$

5.3.3 Equivalent Circuit for longitudinal impedance in transmission lines

The parameters of a MTL are calculated using numerical series as shown in chapter 2 and have no specific order. Thus condition (229) of the VF algorithm may not be satisfied. In this case, the FRVF technique gives the fit with the lowest LS error.

Between the direct and indirect circuit topologies, there is no exact way of telling which of the aforementioned is better. By doing some tests fitting the modes presented in section 2.8, we found that the constant in the linear term of both circuit topologies are similar as shown in Table 2, which indicates certain resemblance in both types of fitting procedures. However, the constant term appears to be different in both types of circuit fitting as seen in Table 3.

Table 2 – Constant in the linear term for direct and indirect circuit topologies

	Mode 1	Mode 2	Mode 3
Direct circuit	0.00076292	0.00093565	0.0051
Indirect circuit	0.00076293	0.00093565	0.0051

Source: Compiled by author

Table 3 – Constant term obtained for different types of circuit fitting

	Mode 1	Mode 2	Mode 3
Direct circuit	1.2690	0.8528	3200.4
Indirect circuit	0.165	0.165	0.166

Source: Compiled by author

By enforcing the constant term to be $\Re\{f(s=0)\}$, the indirect circuit topology guarantees that the series inductor has a positive and real value. The direct circuit topology, instead, assigns the constant term a value that gives the lowest LS error, which can be positive or negative. In order for the circuit elements to have a physical meaning, real and positive values are desired. But since FRVF is a mathematical procedure, those cannot be guaranteed in the direct circuit topology.

In terms of the error of the fitting, both circuit topologies show similar, almost negligible, errors if computed appropriately. Therefore, indirect-circuit topology is preferred over direct-circuit topology because it enforces real and positive values for the circuit elements.

5.4 NUMBER OF POLES-RESIDUES

The accuracy of the fitting depends on the fitting circuit topology, the number of poles-residues used and the algorithm used to obtain the best fit possible.

In order to compare the quality of a fitting procedure, we define the Normalized Root-Mean Square Error NRMSE of a fitted function $f_{fit}(s)$ as follows

$$NRMSE = \frac{\sqrt{\frac{\sum_{i=1}^{samples} (|f_{fit}(s) - f(s)|)^2}{samples}}}{|f(s)|_{max} - |f(s)|_{min}}. \quad (267)$$

The RMSE (Root Mean Square Error) measures the error of a fit and by normalizing it we facilitate the comparison between datasets or models with different scales. In general, the most complex datasets require more poles-residues. Therefore, not all data sets (e.g. transmission line modes) should have the same number of poles-residues.

As the number of terms increases, the accuracy gain of the fit is less significant. Which means that any additional terms unnecessarily increase the complexity of the system (overfitting), making it computationally expensive and without any significant gains. In order to show this, Table 4 shows the NRMSE (before refination) obtained by fitting the transmission line modes presented in section 2.8 **Error! Reference source not found.** for various numbers of poles-residues.

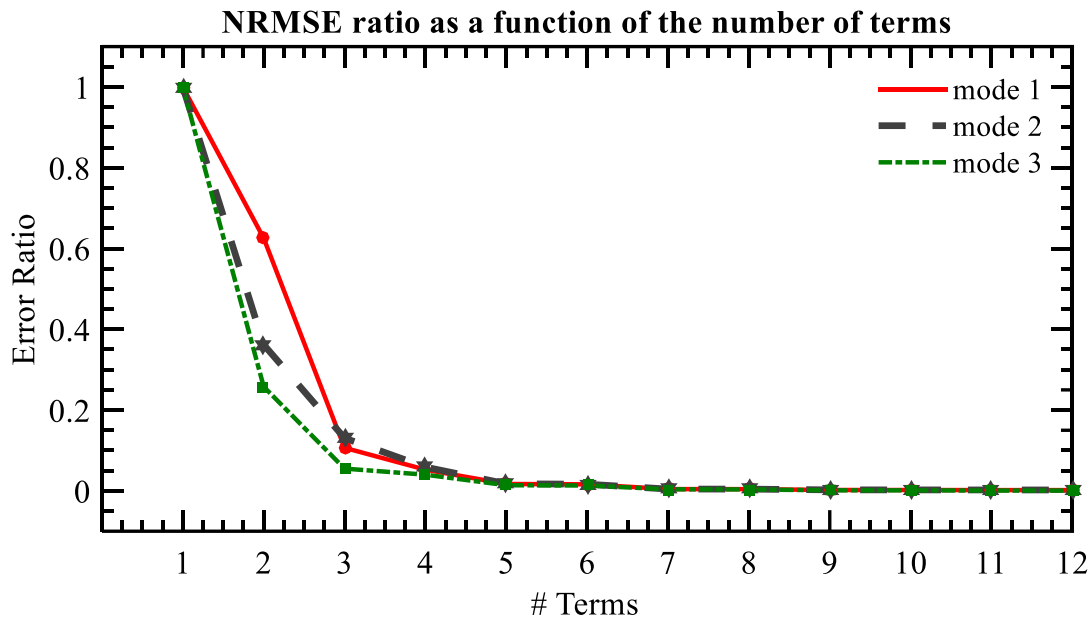
Table 4 – Fitting raw-NRMSE for various numbers of terms

	Mode 1 Fitting's NRMSE	Mode 2 Fitting's NRMSE	Mode 3 Fitting's NRMSE
# poles-residues =1	7.3020E-05	4.8081E-05	7.5394E-03
# poles-residues =2	4.5675E-05	1.7399E-05	1.9438E-03
# poles-residues =3	7.7770E-06	6.2827E-06	4.1491E-04
# poles-residues =4	3.8269E-06	2.8269E-06	3.0152E-04
# poles-residues =5	1.2405E-06	8.4410E-07	1.0448E-04
# poles-residues =6	1.1747E-06	7.9134E-07	9.9812E-05
# poles-residues =7	3.1534E-07	2.1364E-07	2.8631E-05
# poles-residues =8	3.0678E-07	2.0616E-07	2.6231E-05
# poles-residues =9	1.5332E-07	1.1710E-07	9.7012E-06
# poles-residues =10	1.4846E-07	1.1337E-07	9.0782E-06
# poles-residues =11	1.3267E-07	1.0590E-07	5.3582E-06
# poles-residues =12	1.3288E-07	1.0607E-07	5.2810E-06

Source: Compiled by author

Additionally, Figure 38 shows graphically the ratio between the NRMSE for each number of poles-residues to only one pole-residue.

It can be concluded from the previous analysis that the number of poles-residues must be high enough to have a significant accuracy without making the system unnecessarily complex.

Figure 38 – Error reduction as a function of the number of terms

Source: Compiled by author

5.5 INITIAL POLES

Another critical aspect of the fitting algorithms is allocating the initial (starting) poles. Gustavsen²⁵ differentiates three types of starting poles positions

- real spaced poles: real poles are logarithmically or linearly spaced as function of frequency. Normally used for fitting smooth functions.
- complex conjugate linearly spaced poles: Complex conjugate poles with imaginary parts linearly distributed over the frequency range of interest. Each pole is constituted by its imaginary part and a negative real part sufficiently small to avoid the ill-conditioning problem in the fit. The real part can be defined as the imaginary part of the pole divided by 100.
- complex conjugate logarithmically spaced poles: Complex conjugate poles with imaginary parts logarithmically spaced over the frequency range of interest. Each pole is constituted by its imaginary part and a negative real part sufficiently small

to avoid the ill-conditioning problem in the fit. The real part can be defined as the imaginary part of the pole divided by 100.

In the original VF, the allocation of initial poles selection was important but after all the enhancements made to the VF, the procedure became less sensitive to the initial poles⁵⁴.

By using the FRVF, most of the time, if a fit has real spaced poles and the data can't be fitted with real poles, the poles will reallocate to complex conjugate pairs without having the ill-conditioning issue. Similarly, if the data has complex conjugate poles and the initial poles were real spaced poles, most of the time, they will reallocate to complex conjugate positions to avoid the ill-conditioning issue. Therefore, the initial pole selection may have impact in the raw NRMSE but the method will still work.

Admitting the existence of complex conjugate pairs of poles-residues, for this work, we chose all initial poles as complex conjugate logarithmically spaced poles by default.

5.6 POLE REFINEMENT

After the initial poles were reallocated to new positions for the first time, they can be further reallocated to new positions to reduce the NRMSE of the fit. This can be done in a recursive manner to produce new generations of poles. This procedure is known as pole refinement.

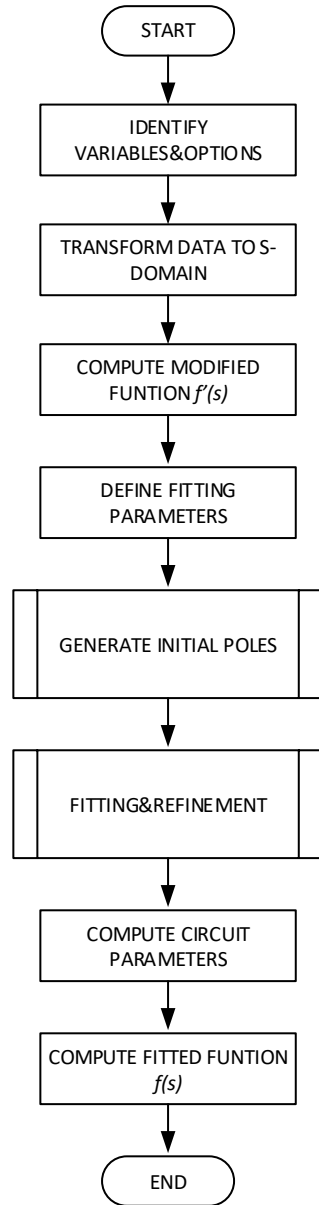
After each iteration, the NRMSE is reduced up to a point. After this point, the NRMSE will either remain equal or increase slightly. Here is where the refining process should be stopped.

5.7 IMPLEMENTATION

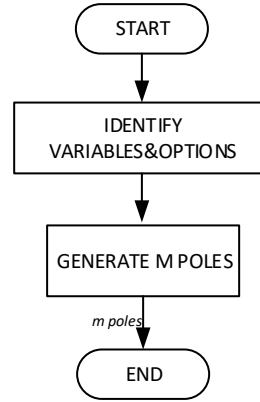
With all the information presented in this chapter, the algorithm shown in the flowchart of Figure 39 was developed. This procedure fits any type of data into an electric circuit whose impedance or admittance has the same behavior as the data.

Figure 39 – Modified Circuit Fitting flowchart

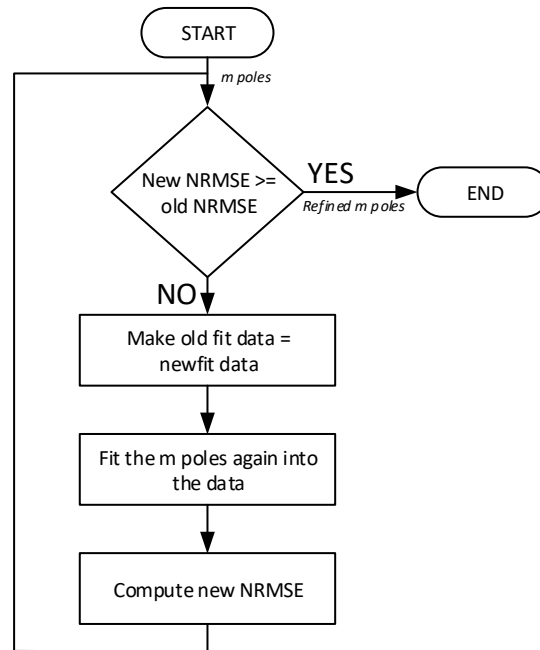
MODIFIED CIRCUIT FITTING PROCEDURE



GENERATE INITIAL POLES



FITTING & REFINEMENT

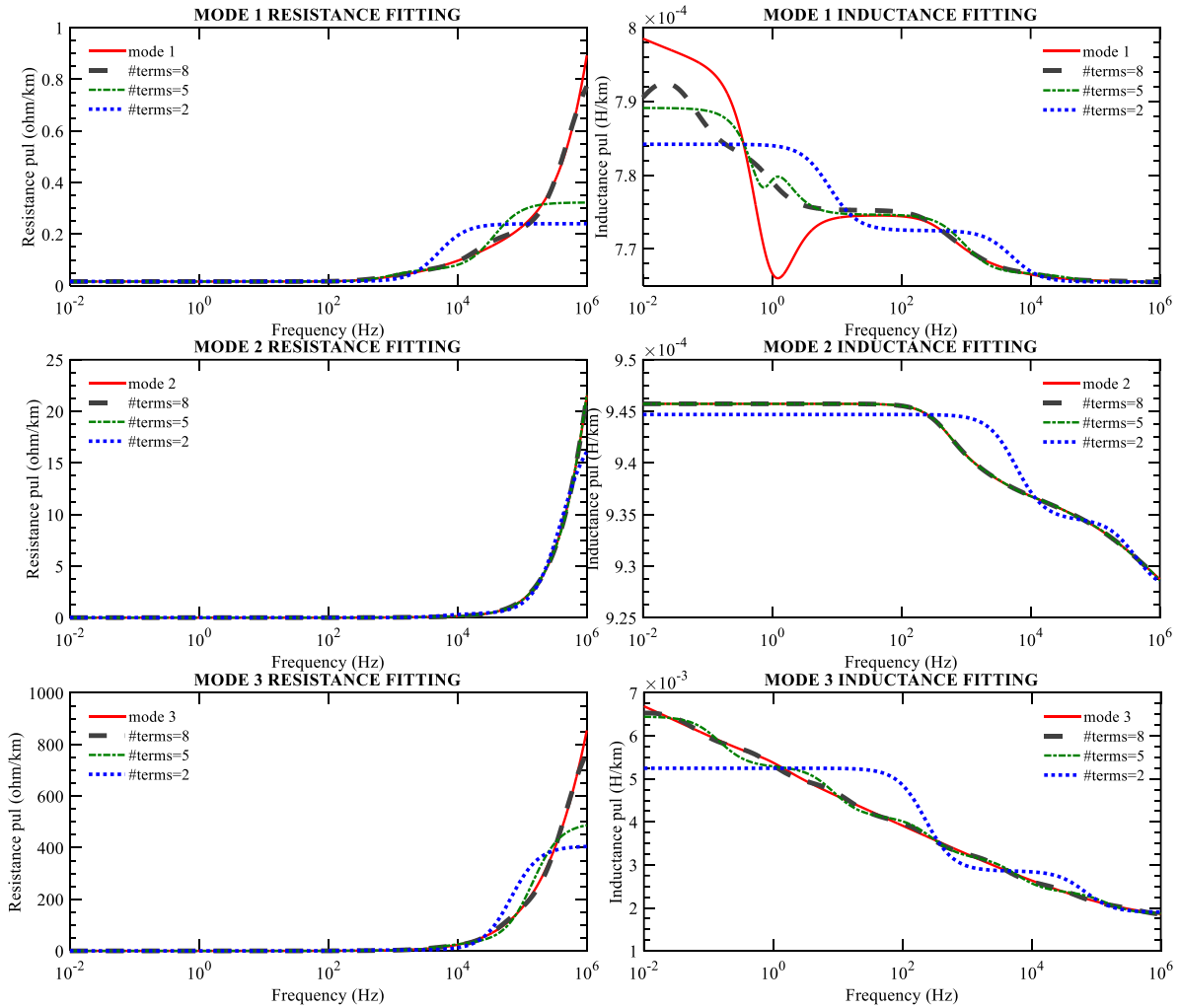


Source: Compiled by author

5.8 APPLICATION

With the procedure developed in this chapter, we fitted an electrical circuit to the three modes shown in section 2.8 for various number of poles-residues. The curves obtained are shown in in Figure 40.

Figure 40 – Modified Circuit Fitting

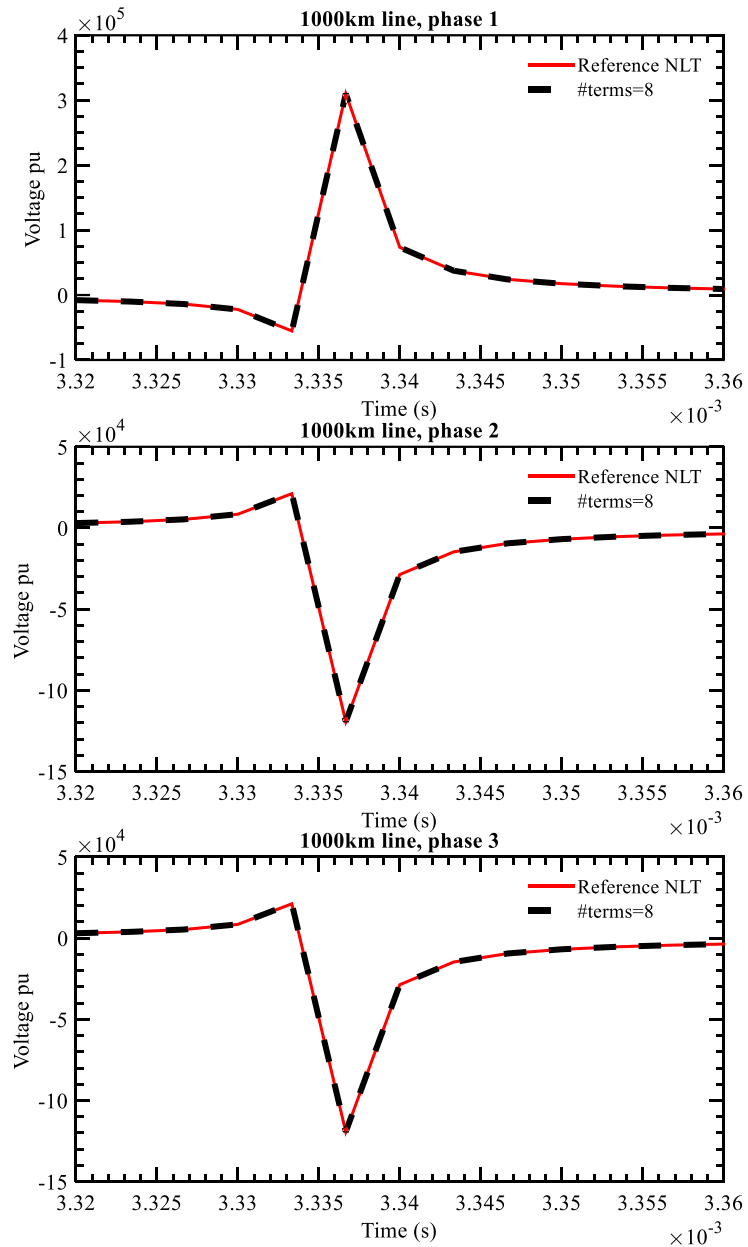


Source: Compiled by author

Figure 40 shows that the more poles-residues are used, the more accurate the fitting is. 8 poles-residues give an accurate fit for typical frequency spectrum in power system transient

analysis. We show in Figure 41 the voltages obtained by applying a $2.5/50 \mu\text{s}$ to one of the ends of the MTL of section 2.8 using the procedure described in section 3.8.

Figure 41 – Accuracy of the Modified Circuit Fitting.



Source: Compiled by author

The peak error of the fitted model in the most extreme case has a maximum error of 0.06%.

5.9 CONCLUSION

In this chapter, a review of the fitting procedures available in technical literature was presented as well as the equivalent circuits associated to the rational functions fitted. We chose the FRVF as the main fitting procedure for our research.

MTL modes are smooth functions that can usually be fitted with real poles-residues. However, complex pairs of poles-residues may appear.

We introduced the direct-circuit topology and indirect-circuit topology that can be used to represent rational functions. Nonetheless, the indirect-circuit topology is more suitable for fitting MTL modes since it guarantees positive real values for its electrical components without compromising accuracy.

Other fitting issues such as initial poles and pole refinement were discussed in this chapter and a computation routine was implemented. The fitted circuit allows our research to include the frequency effect in the MTL series impedance.

6 OUR APPROACH: INCLUSION OF THE FREQUENCY EFFECT IN THE METHOD OF CHARACTERISTICS FOR MULTICONDUCTOR TRANSMISSION LINES

6.1 INTRODUCTION

From the Bergeron lossless line model presented in section 4.3 of this document and following the train of thought of Dommel ³, we included in our previous research the frequency-dependence effect in the longitudinal parameters in the Bergeron line model ^{100,101}, which will be now expanded for more generic cases, i.e., MTL.

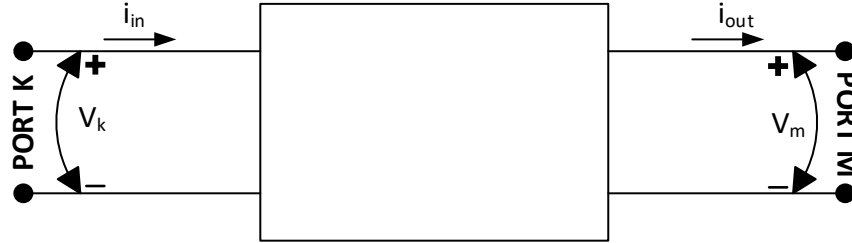
First, we will modify the two-port representation of the lossless method of characteristics in order to increase its computational efficiency. Then, we will present the equations that describe the longitudinal impedance of the transmission line through the circuit topologies presented chapter 5. The resulting state equations will be incorporated to the modified method of characteristics and the resulting Ordinary Differential Equations ODEs will be presented, and solved through numerical methods.

6.2 MODIFIED METHOD OF CHARACTERISTICS

The conventional method of characteristics, also known as lossless Bergeron Line model, is a two port network that meets the port condition: the electric current flowing through one terminal is equal to the current emerging from the other terminal on the same port. The ports constitute interfaces where the network connects to other networks.

Conventional (symmetrical) two-port networks have their port currents facing each other. However, for cascaded networks, it is more efficient if both currents have the same sense as shown in Figure 42. Mathematically, there is no difference from changing the sense of the currents or voltages. However, in computational terms, each unnecessary sign inversion adds flops to the solution of the network. Therefore, keeping the network as simple and direct as possible will make the model more efficient.

Figure 42 – Modified Two-port network



Source: Compiled by author

The solution of a lossless transmission line of length d using d'Alembert's formula is

$$V(x, t) + Z_c I(x, t) = 2Z_c [i^+(x - vt)] \quad (268)$$

$$V(x, t) - Z_c I(x, t) = -2Z_c [i^-(x + vt)] \quad (269)$$

where $Z_c = \sqrt{L/C}$ and $v = 1/\sqrt{LC}$. Term $i^+(x - vt)$ is an arbitrary waveform that maintains its shape and moves in the direction of the receiving end (port m), and $i^-(x + vt)$ is an arbitrary waveform that moves in the opposite direction. $i^+(x - vt)$ is referred to as a forward travelling wave and $i^-(x + vt)$ is referred to as a backward travelling wave.

The progressive wave i^+ evaluated at (k, t_k) and (m, t_m) are, respectively

$$V_k(t_k) + Z_c i_{in}(t_k) = 2Z_c [i^+(0 - vt_k)] \quad (270)$$

$$V_m(t_m) + Z_c i_{out}(t_m) = 2Z_c [i^+(d - vt_m)] \quad (271)$$

Similarly, the regressive wave i^- at (k, t_k) and (m, t_m) are, respectively

$$V_k(t_k) - Z_c i_{in}(t_k) = -2Z_c [i^-(0 + vt_k)] \quad (272)$$

$$V_m(t_m) - Z_c i_{out}(t_m) = -2Z_c [i^-(d + vt_m)] \quad (273)$$

where $(x + vt)$ is a constant that goes from (d, t_m) to $(0, t_k)$ at characteristic speed v . Thus

$$d + v t_m = 0 + v t_k \quad (274)$$

$$t_m = t_k - \frac{d}{v} = t_k - \tau \quad (275)$$

where $\tau = d/v$ and is known as the propagation time.

Equation (275) shows the relationship between the instant of a regressive wave passing through port m (273) and the instant of the same wave passing through port k (272) as follows

$$V_k(t) - Z_c i_{in}(t) = V_m(t - \tau) - Z_c i_{out}(t - \tau) \quad (276)$$

$$i_{in}(t) = \frac{V_k(t)}{Z_c} + I_k(t - \tau) \quad (277)$$

where the history current $I_k(t - \tau)$ source is given by

$$I_k(t - \tau) = -\frac{V_m(t - \tau)}{Z_c} + i_{out}(t - \tau). \quad (278)$$

Analogously, (270) is related to (271) as follows

$$i_{out}(t) = -\frac{V_m(t)}{Z_c} + I_m(t - \tau) \quad (279)$$

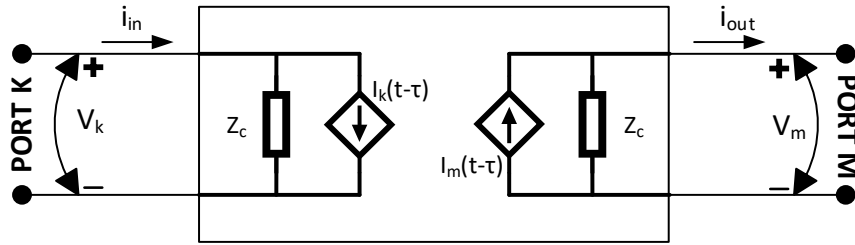
$$I_m(t - \tau) = \frac{V_k(t - \tau)}{Z_c} + i_{in}(t - \tau) \quad (280)$$

The circuit of Figure 43 is described by equations (277)-(280). The main improvement of the circuit of Figure 43 is changing the sense of the current at m . This reduces all the unnecessary negative and double negative signs from the conventional two-port network, making it more efficient.

6.3 STATE SPACE REPRESENTATION OF THE FITTED LONGITUDINAL IMPEDANCE

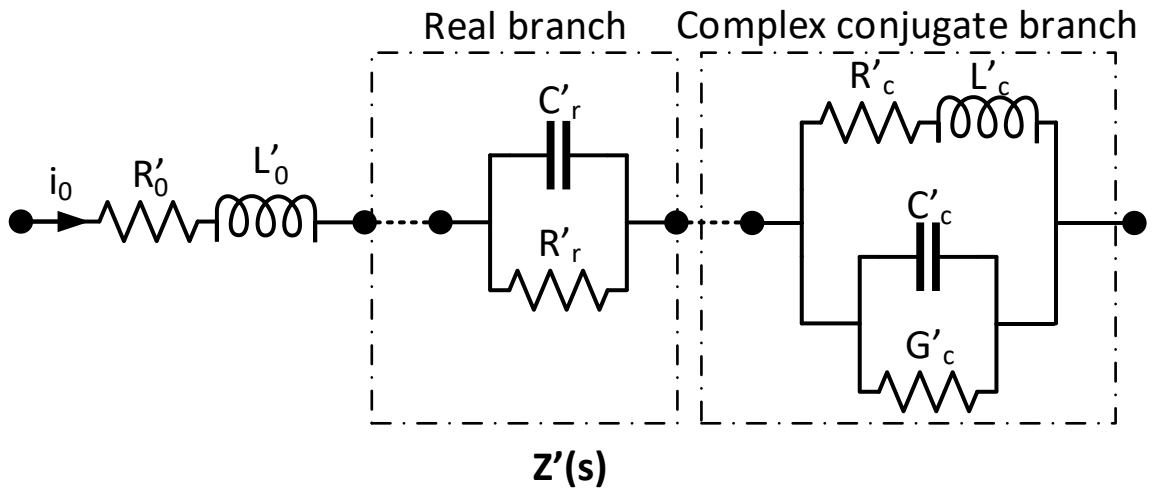
Circuit topologies described in chapter 5, that represent the fitted p.u.l. longitudinal impedance of a transmission line $Z'(s)$ are shown in Figure 44 and Figure 45.

Figure 43 – Modified Bergeron Circuit



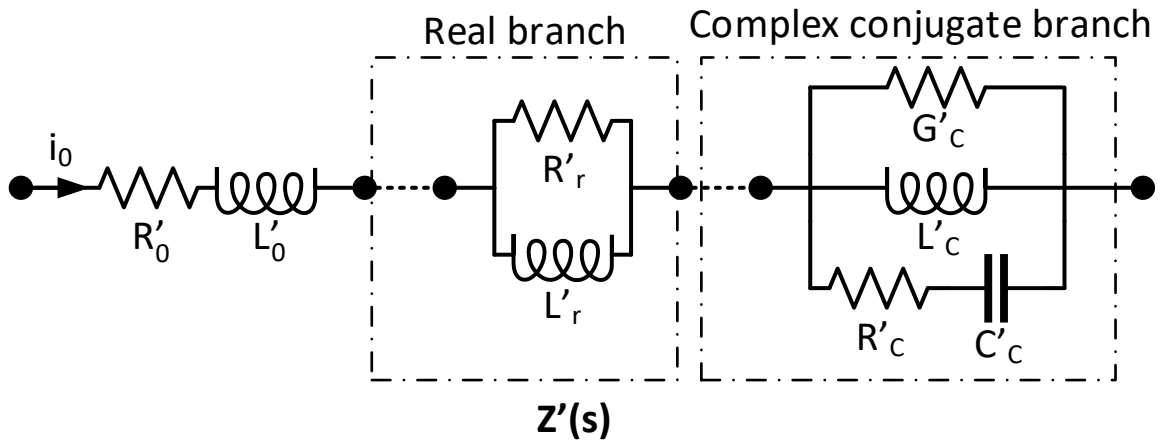
Source: Compiled by author

Figure 44 – Direct-circuit topology.



Source: Compiled by author

Figure 45 – Indirect circuit topology.



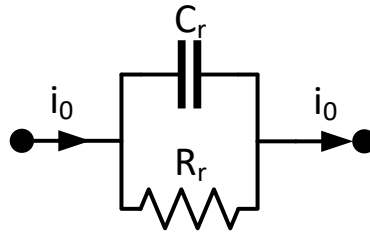
Source: Compiled by author

Both circuit topologies contain a series resistor R'_0 , a series inductor L'_0 , N_R first-order circuit branches that represent real poles-residues, and a N_C second-order circuit branches that represent complex conjugate poles-residues. The equations that describe first-order and second-order circuits for each circuit topology are presented in the following subsection.

6.3.1 First-Order Branch Circuit

a) *Direct-circuit topology* – The first-order branch for this topology is shown in Figure 46.

Figure 46 – First-order circuit of a direct fitting.



Source: Compiled by author

The current passing through the capacitor is

$$C_r \frac{dV_{C_r}}{dt} = -i_{R_r} + i_0 = -\frac{V_{C_r}}{R_r} + i_0 \quad (281)$$

and the derivative term isolated is

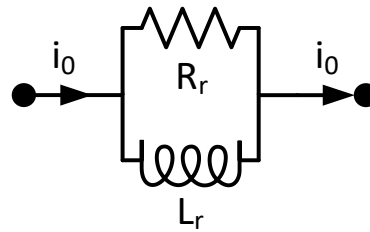
$$\frac{dV_{C_r}}{dt} = -\frac{1}{C_r R_r} V_{C_r} + \frac{1}{C_r} i_0 \quad (282)$$

b) *Indirect-circuit topology* – The first-order branch for this topology is shown in Figure 47.

The voltage across the inductor is

$$L_r \frac{di_{L_r}}{dt} = R_r (i_0 - i_{L_r}) \quad (283)$$

Figure 47 – First-order circuit of an indirect fitting.



Source: Compiled by author

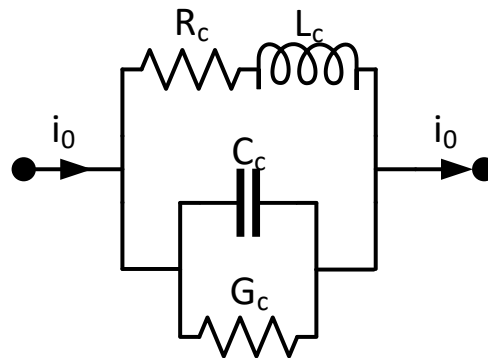
And the derivative term is

$$\frac{di_{L_r}}{dt} = -\frac{R_r}{L_r} i_{L_r} + \frac{R_r}{L_r} i_0 \quad (284)$$

6.3.2 Second-Order Circuit

- a) *Direct circuit topology*– The second-order circuit of the direct circuit topology is shown in Figure 48.

Figure 48 – Second-order circuit of a direct fitting.



Source: Compiled by author

The voltage drop across all three parallel connections, from upper to lower, is

$$R_c i_{L_c} + L_c \frac{di_{L_c}}{dt} = V_{C_c} = \frac{1}{G_c} \left(i_0 - C_c \frac{dV_{C_c}}{dt} - i_{L_c} \right). \quad (285)$$

The derivative term $\frac{dV_{C_c}}{dt}$ isolated from the middle and lower voltage drop equations is

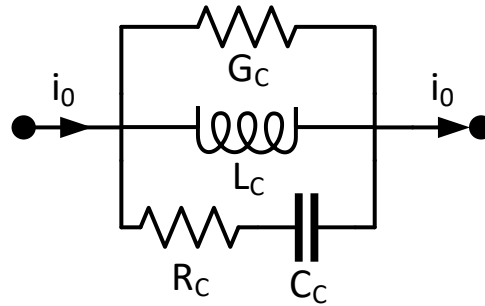
$$\frac{dV_{C_c}}{dt} = -\frac{G_c}{C_c} V_{C_c} - \frac{1}{C_c} i_{L_c} + \frac{1}{C_c} i_0 \quad (286)$$

And the derivative term $\frac{di_{L_c}}{dt}$ isolated from the middle and lower voltage drop equation is

$$\frac{di_{L_c}}{dt} = \frac{1}{L_c} V_{C_c} - \frac{R_c}{L_c} i_{L_c} \quad (287)$$

- b) *Indirect circuit topology* – The second-order circuit of this topology is shown in Figure 49.

Figure 49 – Second-order circuit of an indirect fitting.



Source: Compiled by author

The voltage drop across all three parallel connections, from lower to upper, is

$$R_c \left(C_c \frac{dV_{C_c}}{dt} \right) + V_{C_c} = L_c \frac{di_{L_c}}{dt} = \frac{1}{G_c} \left(i_0 - C_c \frac{dV_{C_c}}{dt} - i_{L_c} \right). \quad (288)$$

The derivative term $\frac{dV_{C_c}}{dt}$ isolated from the lower and upper voltage drop equation is

$$\frac{dV_{C_c}}{dt} = -\frac{G_c}{C_c(R_c G_c + 1)} V_{C_c} - \frac{1}{C_c(R_c G_c + 1)} i_{L_c} + \frac{1}{C_c(R_c G_c + 1)} i_0 \quad (289)$$

and the derivative term $\frac{di_{L_c}}{dt}$ isolated from the lower and middle voltage drop equation is

$$\frac{di_{L_c}}{dt} = \frac{R_c C_c}{L_c} \frac{dV_{C_c}}{dt} + \frac{1}{L_c} V_{C_c} \quad (290)$$

Substitution of (289) in (290) leads to

$$\frac{di_{L_c}}{dt} = \frac{1}{L_c(R_c G_c + 1)} V_{C_c} - \frac{R_c}{L_c(R_c G_c + 1)} i_{L_c} + \frac{R_c}{L_c(R_c G_c + 1)} i_0 \quad (291)$$

6.3.3 State Space Matrix Assembly

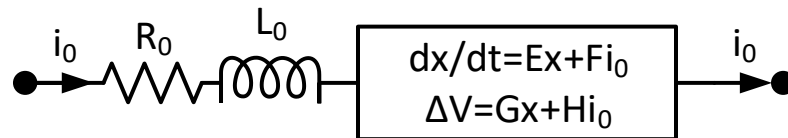
The state space equations that describe N_R first-order (real branch) and N_C second-order (complex conjugate branch) circuit branches are given by

$$\frac{d}{dt} \mathbf{x} = \mathbf{E} \mathbf{x} + \mathbf{F} i_0 \quad (292)$$

$$\Delta V = \mathbf{G} \mathbf{x} + \mathbf{H} i_0 \quad (293)$$

where matrix \mathbf{E} , vectors \mathbf{x} \mathbf{F} \mathbf{G} and constant \mathbf{H} are defined for each circuit topology and describe the relationship between input current i_0 and voltage drop ΔV across all first-order and second-order circuit branches as shown in Figure 50.

Figure 50 – Fitted circuit including state space equations.



Source: Compiled by author

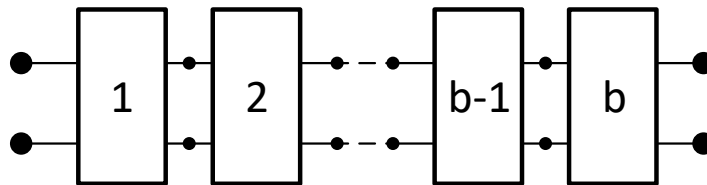
6.4 CASCADED FREQUENCY DEPENDENT METHOD OF CHARACTERISTICS

Experience has shown that a transmission line with negligible p.u.l. resistance R' and conductance G' can be modeled, with reasonable precision, as one or more lossless line sections connected to lumped resistances to represent losses⁴.

This lumped resistances can be included in several points along the line dividing it in several segments. Curiously, all cases tested by Dommel showed that there are no notable differences if the losses are lumped on a few or several points along the line. Dommel's simulations gave almost the same results for lumping the resistances in 3, 65 and 300 points. For this reason, Dommel proposed to divide the line in 2 segments and lump the resistances in 3 points³.

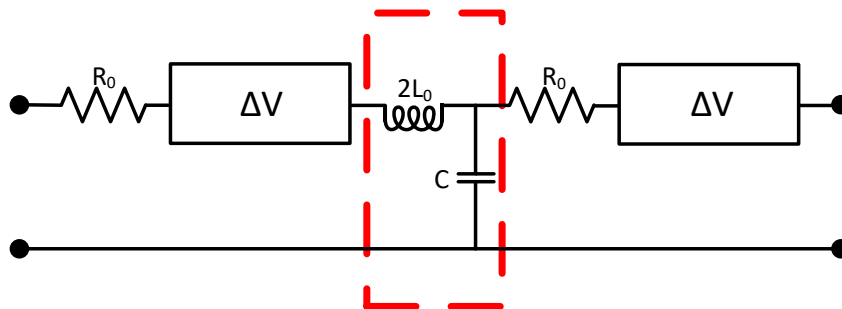
Following the same train of thought, a transmission line is divided in b sections (or so-called blocks) as shown in Figure 51. Each block contains two circuits of Figure 50 separated by a transversal capacitor and are assembled into a bridged T-network as shown in Figure 52. The circuits of Figure 50 represent the longitudinal parameters.

Figure 51 – Transmission line divided in b blocks



Source: Compiled by author

Figure 52 – Composition of each block



Source: Compiled by author

We propose to solve the red dashed area in Figure 52 using the modified method of characteristics developed in section 6.2. The resulting model is shown in Figure 53 and its circuit elements are calculated as follows

$$R_i = \frac{R'_i d}{2 b}, i = 0,1,2 \dots m \quad (294)$$

$$L_i = \frac{L'_i d}{2 b}, i = 1,2 \dots m \quad (295)$$

$$G_i = \frac{G'_i d}{2 b}, i = 1,2 \dots m \quad (296)$$

$$C_i = \frac{C'_i d}{2 b}, i = 1,2 \dots m \quad (297)$$

$$\tau = \frac{d}{b} \sqrt{L'_0 C'} \quad (298)$$

$$Z_c = \sqrt{\frac{L'_0}{C'}} \quad (299)$$

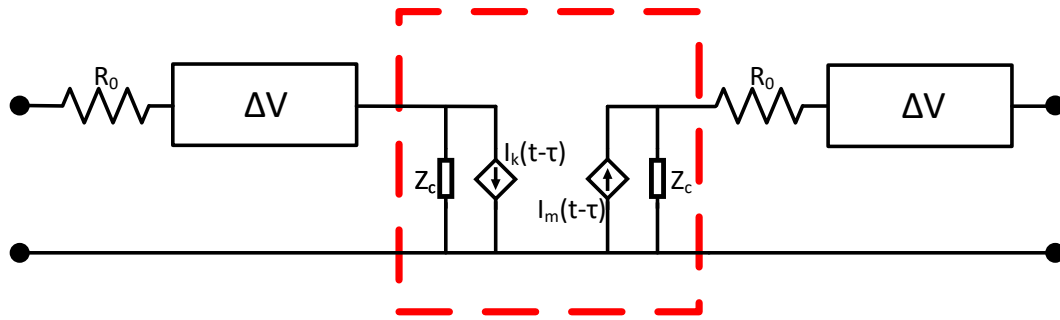
$$I_k(t - \tau) = -\frac{V_m(t - \tau)}{Z_c} + i_{out}(t - \tau) \quad (300)$$

$$I_m(t - \tau) = \frac{V_k(t - \tau)}{Z_c} + i_{in}(t - \tau) \quad (301)$$

where d is the length of the line, C' is the p.u.l. transversal capacitance, and b is the number of blocks. Voltages V_k and V_m , currents i_{in} and i_{out} are shown in Figure 43. All other p.u.l. resistances R'_i , inductances L'_i , conductances G'_i and capacitances C'_i are obtained by fitting the p.u.l. longitudinal impedance as described in section 6.3.

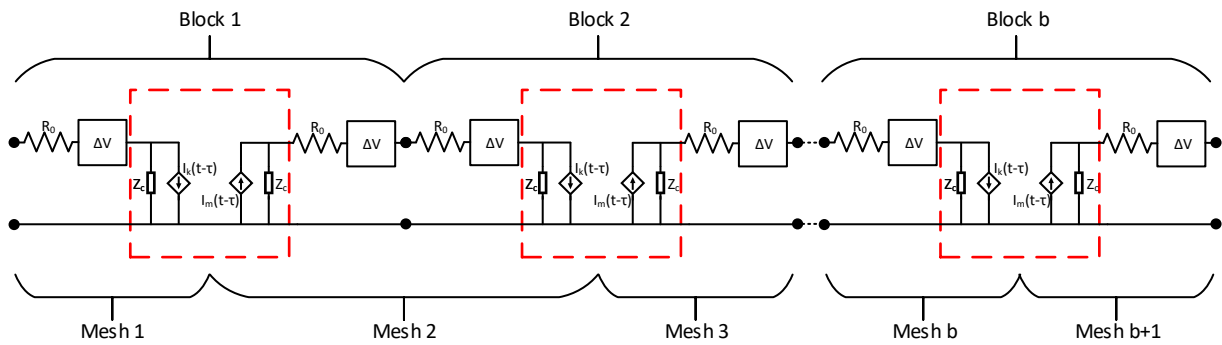
The cascade of b blocks of Figure 53 has $b + 1$ independent meshes as shown in Figure 54: an input mesh, $n - 1$ connection meshes and an output mesh.

Figure 53 – Single Frequency-Dependent Bergeron Model



Source: Compiled by author

Figure 54 – Cascaded Frequency Dependent Method of Characteristics



Source: Compiled by author

Each mesh is represented by the following state-space equations

$$\frac{d}{dt} \mathbf{x} = \mathbf{A} \mathbf{x} + \mathbf{B} \mathbf{u} \quad (302)$$

$$i_0 = \mathbf{C} \mathbf{x} + \mathbf{D} \mathbf{u} \quad (303)$$

where

$$\mathbf{A} = \mathbf{E} + \mathbf{F} \mathbf{C} \quad (304)$$

$$\mathbf{B} = \mathbf{F} \mathbf{D} \quad (305)$$

and $\mathbf{E} \mathbf{F} \mathbf{C} \mathbf{D}$ depend on the type of the mesh (input, output or connection)

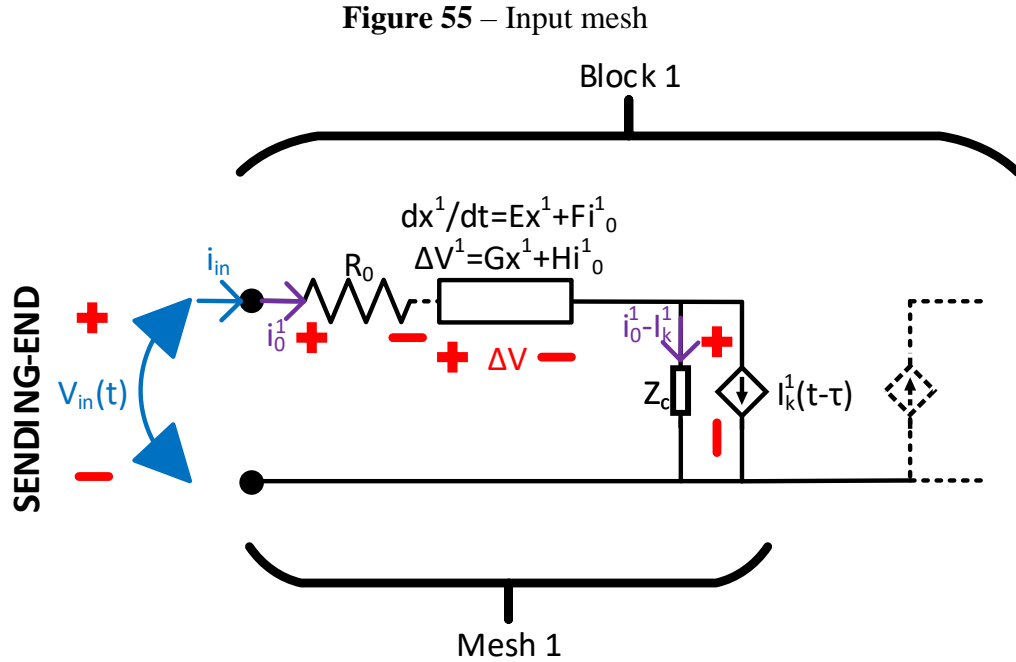
6.4.1 Input mesh

The first mesh, connected to one of the ends of the transmission line, is shown in Figure 55. The line's end has a voltage $V_{in}(t)$ and a current $i_{in}(t)$, which is equal to the current $i_0^1(t)$ of the first mesh (superscript 1). Kirchoff's voltage law for this mesh is given by

$$V_{in} - R_0 i_0^1 - \Delta V^1 - Z_c(i_0^1 - I_k^1) = 0 \quad (306)$$

and from (293), $\Delta V^1 = \mathbf{G} \mathbf{x}^1 + H i_0^1$ thus

$$(R_0 + Z_c) i_0^1 = [1 \quad Z_c] \begin{bmatrix} V_{in} \\ I_k^1 \end{bmatrix} - \mathbf{G} \mathbf{x}^1 - H i_0^1. \quad (307)$$



Source: Compiled by author

Substituting (307) in (292) results in the following values for the state-system (294)-(297)

$$\mathbf{E} = \mathbf{E}_1 \quad (308)$$

$$\mathbf{C} = \frac{-1}{R_0 + Z_c + H_1} \mathbf{G}_1 \quad (309)$$

$$\mathbf{F} = \mathbf{F}_1 \quad (310)$$

$$\mathbf{D} = \frac{1}{R_0 + Z_c + H_1} [1 \quad Z_c] \quad (311)$$

where \mathbf{E}_1 , \mathbf{F}_1 , \mathbf{G}_1 and H_1 are determined by the circuit topology of the fitting, and

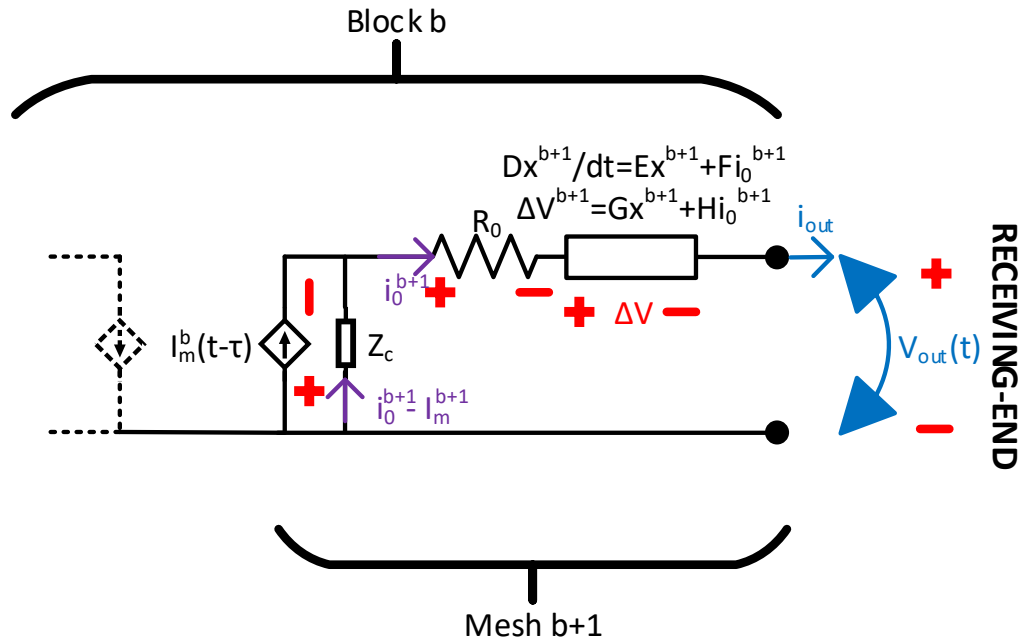
$$\mathbf{u}^1 = [V_{in} \quad I_k^1]^T \quad (312)$$

6.4.2 Output Mesh

The output mesh, connected to the other end of the transmission line, is shown in Figure 56. The line's end has a voltage $V_{out}(t)$ and a current $i_{out}(t)$, which is equal to the current $i_0^{b+1}(t)$ of the last mesh (superscript $b + 1$). Kirchoff's voltage law for this mesh is given by

$$-V_{out} - R_0 i_0^{b+1} - \Delta V^{b+1} - Z_c (i_0^{b+1} - I_m^{b+1}) = 0 \quad (313)$$

Figure 56 – Output mesh



Source: Compiled by author

and from (293), $\Delta V^{b+1} = \mathbf{G} \mathbf{x}^{b+1} + H i_0^{b+1}$ thus

$$(R_0 + Z_c) i_0^{b+1} = [Z_c \quad -1] \begin{bmatrix} I_m^b \\ V_{out} \end{bmatrix} - \mathbf{G} \mathbf{x}^{b+1} - H i_0^{b+1} \quad (314)$$

Substituting (314) in (292) results in the following values for the state-system (294)-(297)

$$\mathbf{E} = \mathbf{E}_1 \quad (315)$$

$$\mathbf{C} = \frac{-1}{R_0 + Z_c + H_2} \mathbf{G}_2 \quad (316)$$

$$\mathbf{F} = \mathbf{F}_1 \quad (317)$$

$$\mathbf{D} = \frac{-Z_c}{2R_0 + 2Z_c + H_2} [1 \quad 1] \quad (318)$$

where \mathbf{E}_1 , \mathbf{F}_1 , \mathbf{G}_2 and H_2 are determined by the circuit topology of the fitting, and

$$\mathbf{u}^{b+1} = [I_m^b \quad V_{out}]^T \quad (319)$$

6.4.3 Simplified Connection Mesh

The cascade of frequency-dependent method of characteristics has $b - 1$ connection meshes. Figure 57 shows the connection mesh that connects block k and block $k + 1$.

Considering that the ratio of the series impedance of block $k + 1$ to the series impedance of block k is a , it is possible to find an simplified circuit that represents the series impedance enclosed in the dashed area of Figure 57. This is achieved by using the equivalent circuits of Figure 58 and Figure 59 for first-order and second-order circuit branches, respectively. The resulting simplified circuit is shown in Figure 60, where $a = 1$ because the line is divided in b identical segments, thus the series impedance of blocks $k + 1$ and k are equal.

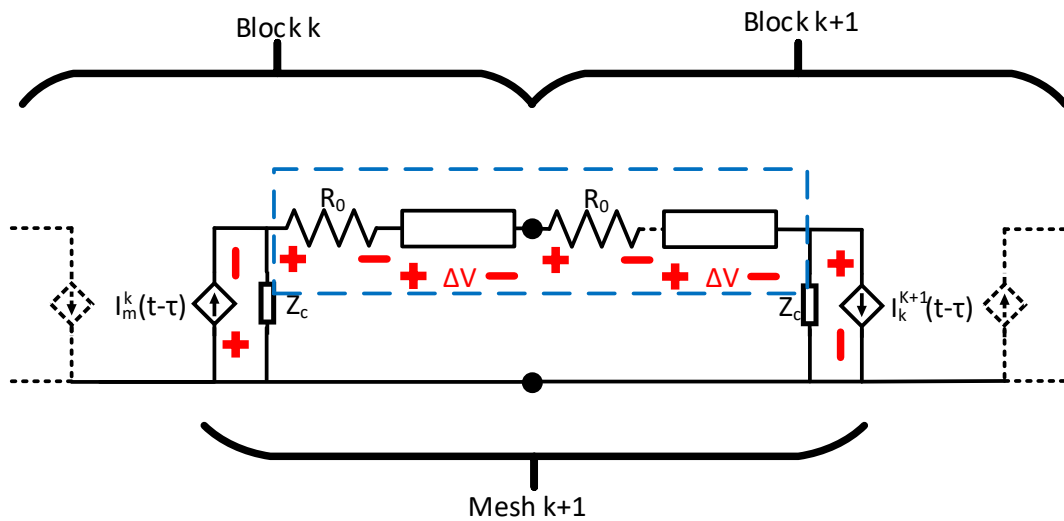
Kirchhoff's voltage law for the k -th simplified connection mesh is given by

$$Z_c(i_0^{k+1} - I_m^k) + 2R_0 i_0^{k+1} + \Delta V^{k+1} + Z_c(i_0^{k+1} - I_k^{k+1}) = 0 \tag{320}$$

and from (293), $\Delta V^{k+1} = \mathbf{G} \mathbf{x}^{k+1} + H i_0^{k+1}$ thus

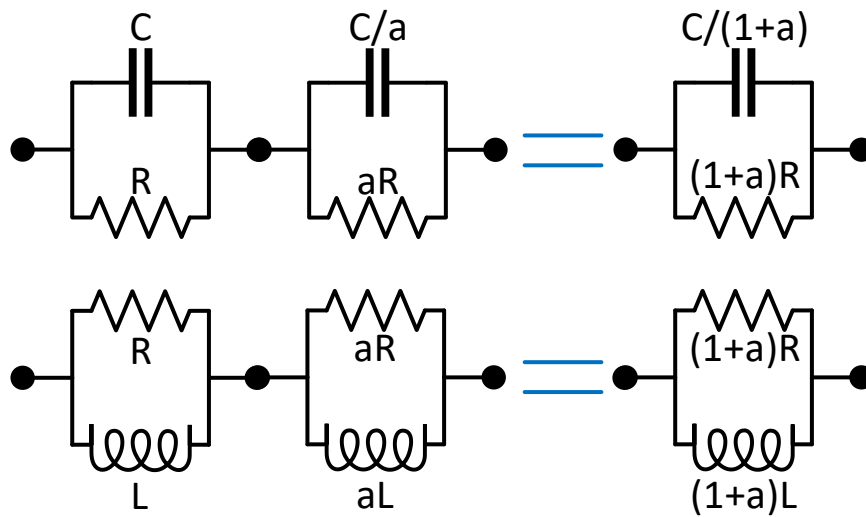
$$2(R_0 + Z_c)i_0^{k+1} = -Z_c[1 \quad 1] \begin{bmatrix} I_m^k \\ I_k^{k+1} \end{bmatrix} - \mathbf{G} \mathbf{x}^{k+1} - H i_0^{k+1} \tag{321}$$

Figure 57 – Connection mesh



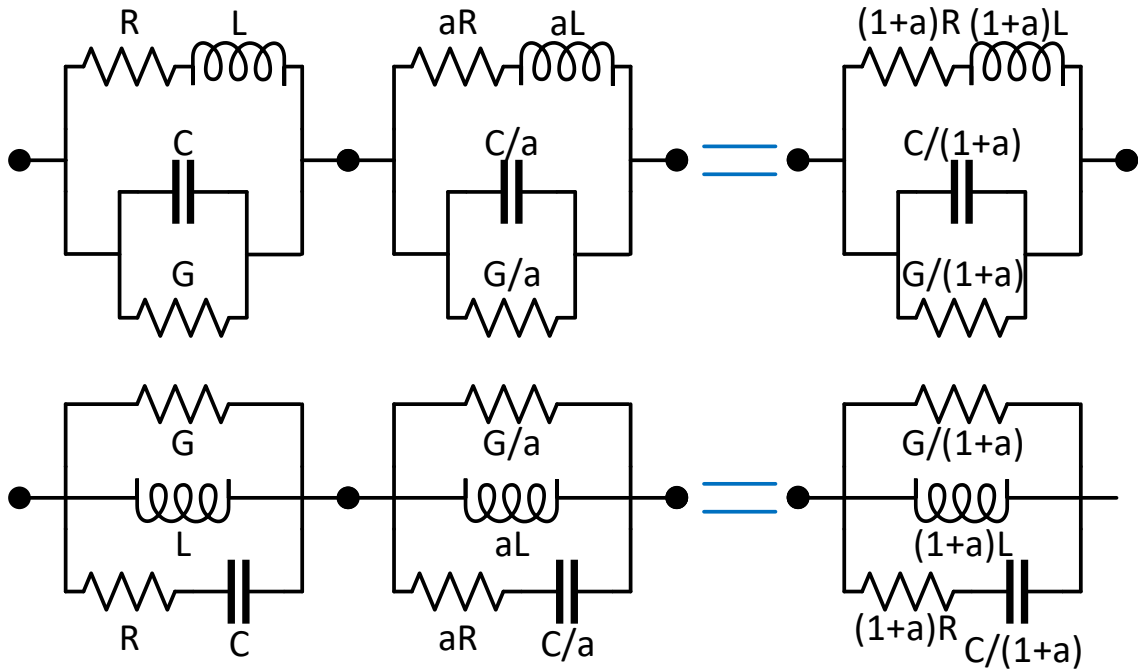
Source: Compiled by author

Figure 58 – First-order equivalent circuit



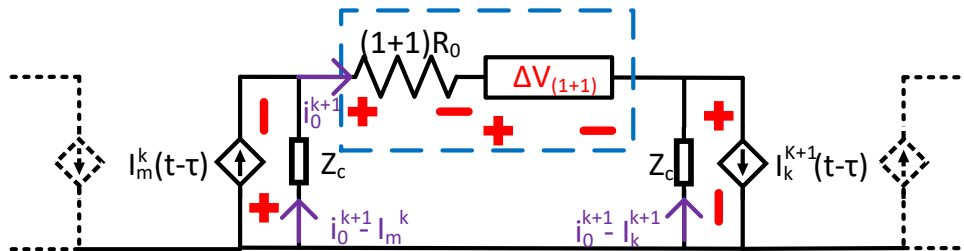
Source: Compiled by author

Figure 59 – Second-order equivalent circuit



Source: Compiled by author

Figure 60 – Simplified connection mesh



Source: Compiled by author

Substituting (321) in (292) results in the following values for the state-system (294)-(297)

$$\mathbf{E} = \mathbf{E}_2 \tag{322}$$

$$\mathbf{C} = \frac{-1}{2R_0 + 2Z_c + H_1} \mathbf{G}_2 \tag{323}$$

$$\mathbf{F} = \mathbf{F}_2 \tag{324}$$

$$\frac{d}{dt} \mathbf{x} = \mathbf{A} \mathbf{x} + \mathbf{B} \mathbf{u} \quad (341)$$

$$i_0 = \mathbf{C} \mathbf{x} + \mathbf{D} \mathbf{u} \quad (342)$$

where state vector \mathbf{x} contains the state variables associated to each inductor or capacitor, input vector \mathbf{u} is constituted by voltage sources and historic values. By discretizing time, the state-space model of each mesh is solved through any numerical integration method⁴⁰.

Among the most common numerical integration methods, Runge-Kutta is faster than Heun's method (explicit trapezoidal rule) or Simpson's rule. Nonetheless, Heun's method is the most robust because its accuracy is less sensible to the time step¹⁰². Therefore, Heun's formula is recommended over other numerical methods to solve the state-space equations (341)-(342).

6.6.1 Heun's method

Heun's formula allows the computation of \mathbf{x} in (341) for a discrete time $n + 1$ using previous discrete time point n as follows

$$\mathbf{x}_{n+1} = \mathbf{x}_n + \frac{\Delta t}{2} (\mathbf{A} \mathbf{x}_n + \mathbf{B} \mathbf{u}_n + \mathbf{A} \mathbf{x}_{n+1} + \mathbf{B} \mathbf{u}_{n+1}) \quad (343)$$

where time step $\Delta t = t_{n+1} - t_n$. \mathbf{x}_{n+1} isolated from equation (343) is

$$\mathbf{x}_{n+1} = \mathbf{A}_{Heun} \mathbf{x}_n + \mathbf{B}_{Heun} (\mathbf{u}_n + \mathbf{u}_{n+1}) \quad (344)$$

where

$$\mathbf{A}_{Heun} = \left(\mathbf{U} - \frac{\Delta t}{2} \mathbf{A} \right)^{-1} \left(\mathbf{U} + \frac{\Delta t}{2} \mathbf{A} \right) \quad (345)$$

$$\mathbf{B}_{Heun} = \left(\mathbf{U} - \frac{\Delta t}{2} \mathbf{A} \right)^{-1} \frac{\Delta t}{2} \mathbf{B}. \quad (346)$$

Equation (344) solves \mathbf{x} in (341) for an discrete time $n + 1$. If Δt is constant (fixed integration steps), \mathbf{A}_{Heun} and \mathbf{B}_{Heun} are time invariant.

6.7 FAST IMPLEMENTATION OF THE FREQUENCY-DEPENDENT METHOD OF CHARACTERISTICS

This section introduces the fast implementation of the proposed frequency-dependent method of characteristics. The improvements presented in this section accelerate the model, reduce memory usage and increase the overall accuracy.

6.7.1 Global Solution

A cascade of b blocks has $b + 1$ meshes, each with their own state equations (341)-(342). The solution of all \mathbf{x} for the integration point $n + 1$ using Heun's method is given by

$$\begin{aligned}
 \mathbf{x}_{n+1}^1 &= \mathbf{A}_{Heun}^{in} \mathbf{x}_n^1 + \mathbf{B}_{Heun}^{in} (\mathbf{u}_n^1 + \mathbf{u}_{n+1}^1) \\
 \mathbf{x}_{n+1}^2 &= \mathbf{A}_{Heun}^{conn} \mathbf{x}_n^2 + \mathbf{B}_{Heun}^{conn} (\mathbf{u}_n^2 + \mathbf{u}_{n+1}^2) \\
 \mathbf{x}_{n+1}^3 &= \mathbf{A}_{Heun}^{conn} \mathbf{x}_{n+1}^3 + \mathbf{B}_{Heun}^{conn} (\mathbf{u}_n^3 + \mathbf{u}_{n+1}^3) \\
 &\vdots \\
 \mathbf{x}_{n+1}^{b+1} &= \mathbf{A}_{Heun}^{out} \mathbf{x}_{n+1}^{b+1} + \mathbf{B}_{Heun}^{out} (\mathbf{u}_n^{b+1} + \mathbf{u}_{n+1}^{b+1})
 \end{aligned} \tag{347}$$

One method to solve (347) is to solve each mesh individually for each time step. This method is referred as *iterative* method.

Another approach is to assemble a global matrix as given by

$$\begin{bmatrix} \mathbf{x}^1 \\ \mathbf{x}^2 \\ \vdots \\ \mathbf{x}^{b+1} \end{bmatrix}_{n+1} = \begin{bmatrix} \mathbf{A}_{Heun}^{in} & & & \\ & \mathbf{A}_{Heun}^{conn} & & \\ & & \ddots & \\ & & & \mathbf{A}_{Heun}^{out} \end{bmatrix} \begin{bmatrix} \mathbf{x}^1 \\ \mathbf{x}^2 \\ \vdots \\ \mathbf{x}^{b+1} \end{bmatrix}_n + \begin{bmatrix} \mathbf{B}_{Heun}^{in} \\ \mathbf{B}_{Heun}^{conn} \\ \vdots \\ \mathbf{B}_{Heun}^{out} \end{bmatrix} \left(\begin{bmatrix} \mathbf{u}^1 \\ \mathbf{u}^2 \\ \vdots \\ \mathbf{u}^{b+1} \end{bmatrix}_n + \begin{bmatrix} \mathbf{u}^1 \\ \mathbf{u}^2 \\ \vdots \\ \mathbf{u}^{b+1} \end{bmatrix}_{n+1} \right) \tag{348}$$

$$\begin{bmatrix} i_0^1 \\ i_0^2 \\ \vdots \\ i_0^{b+1} \end{bmatrix}_{n+1} = \begin{bmatrix} \mathbf{C}^{in} & & & \\ & \mathbf{C}^{conn} & & \\ & & \ddots & \\ & & & \mathbf{C}^{out} \end{bmatrix} \begin{bmatrix} \mathbf{x}^1 \\ \mathbf{x}^2 \\ \vdots \\ \mathbf{x}^{b+1} \end{bmatrix}_{n+1} + \begin{bmatrix} \mathbf{D}_{Heun}^{in} \\ \mathbf{D}_{Heun}^{conn} \\ \vdots \\ \mathbf{D}_{Heun}^{out} \end{bmatrix} \begin{bmatrix} \mathbf{u}^1 \\ \mathbf{u}^2 \\ \vdots \\ \mathbf{u}^{b+1} \end{bmatrix}_{n+1} \tag{349}$$

and solve all meshes at once for each iteration point. Directly solving (348)-(349) is referred as *block* method. Equations (348)-(349) can also be computed considering matrices as sparse. This method is referred as *sparse* method.

Computing (347) has less mathematical operations than computing (348) because all matrices in (347) are full matrices. Matrices containing empty spaces as in (348) have more unnecessary operations while performing multiplications.

However, in computational terms, solving (347) takes more time than (348) for small matrices. That is because the system of equations (347) has to access the memory b more times to retrieve \mathbf{x} and \mathbf{u} than (348), which only retrieves those values once. Accessing the memory is one of the most computationally expensive tasks.

To show the difference between the three methods aforementioned, we present in Table 5 the *floating-points operations* or *flop* count and the number of memory accesses for each method. We also present the *flop* difference between each method and the *iterative* method, which is the fastest in terms of *flops*.

Table 5 – A comparison of flops per iteration for different methods. b is the number of cascaded blocks and m is the number of poles used to fit the longitudinal impedance.

	Flops per iteration	Flops difference compared to the iterative method	Number of memory accesses per iteration
Iterative	$2m^2b + 2m^2 + 3mb + m + 2b + 1$	n/a	$3b + 9$
Block	$4mb^2 + 2m^2b^2 + 4m^2b + 2m^2 + 5mb + m + 2b + 1$	$4mb^2 + 2m^2b^2 + 2m^2b + 2mb$	5
Sparse	$2m^2b + 2m^2 + 3mb + 3m + 2b + 1$	$2m$	5

Source: Compiled by author

Our proposal is to solve the system (348) using sparsity techniques (Matlab sparse libraries), which will save some memory space and unnecessary operations. This way both models are combined: have almost as few flops as the system (347) and being immensely faster in computational terms as system (348) for small cases.

We implemented the three solution proposals: sequential solution, single-block solution and sparse solution for 10 scenarios, each one more complex than the previous one (more elements, more processing time). The processing times for all three methods are presented in Table 6.

Table 6 – Simulation times

	Iterative Solution	Block Solution	Sparse Solution
Scenario 1	1.0723	0.044635	0.13745
Scenario 2	1.9208	0.093261	0.16493
Scenario 3	2.7391	0.20188	0.22722
Scenario 4	3.6181	0.4256	0.31717
Scenario 5	4.5529	0.93253	0.45525
Scenario 6	5.3905	4.1734	0.7239
Scenario 7	6.3249	8.6278	1.0207
Scenario 8	7.2081	14.5813	1.418
Scenario 9	8.3134	23.6439	1.7887
Scenario 10	9.1378	36.306	2.4582

Source: Compiled by author

Table 6 shows that the iterative solution is the slowest from the three solutions for simple scenarios. The Block solution is considerably faster for not-so-complex scenarios but the savings involved in less memory accesses are overcome by the increased flops of more complex scenarios. The sparse solution combines both advantages: is faster than the iterative solution in all scenarios and almost as fast as the block solution for “simpler” scenarios.

6.7.2 Variable storage

Each one of the $b + 1$ systems of equations (341)-(342) is solved using an input vector \mathbf{u}^k . For a time step n , one practical way of managing all \mathbf{u} is to store it in a column vector as follows

$$\mathbf{u}_n = \begin{bmatrix} \mathbf{u}^1 \\ \mathbf{u}^2 \\ \mathbf{u}^3 \\ \vdots \\ \mathbf{u}^b \\ \mathbf{u}^{b+1} \end{bmatrix}_n = \begin{bmatrix} V_{in}[n] \\ I_k^1[n - \tau] \\ I_m^1[n - \tau] \\ I_k^2[n - \tau] \\ I_m^2[n - \tau] \\ I_k^3[n - \tau] \\ \vdots \\ I_m^{b-1}[n - \tau] \\ I_k^b[n - \tau] \\ I_m^b[n - \tau] \\ V_{out}[n] \end{bmatrix} \quad (350)$$

Input vector must be stored for all integration steps.

At time step n , historical current sources are calculated using (278) and (280) as follows

$$\mathbf{u}_n = \begin{bmatrix} V_{in}[n] \\ I_k^1[n - \tau] \\ I_m^1[n - \tau] \\ I_k^2[n - \tau] \\ \vdots \\ I_m^b[n - \tau] \\ V_{out}[n] \end{bmatrix} = \begin{bmatrix} V_{in}[n] \\ -\frac{V_m^1[n - \tau]}{Z_c} + i_0^2[n - \tau] \\ \frac{V_k^1[n - \tau]}{Z_c} + i_0^1[n - \tau] \\ -\frac{V_m^2[n - \tau]}{Z_c} + i_0^3[n - \tau] \\ \vdots \\ \frac{V_k^b[n - \tau]}{Z_c} + i_0^{b+1}[n - \tau] \\ V_{out}[n] \end{bmatrix} \quad (351)$$

However, as stated before, accessing the memory is one of the most delayed tasks in computational terms so avoiding it is mandatory. Therefore the calculation of the variable \mathbf{u}_n using (351) is highly inefficient because:

- All voltages V_k and V_m for all b blocks need to be stored in memory
- All $b + 1$ input currents i_0 need to be stored in memory

Therefore, for each time step, it would be necessary to access the memory $6b + 1$ times to gather the data needed to assemble \mathbf{u} .

Our proposal skips the calculation of voltages V_k and V_m in (351). Instead, we take advantage of the time discretization and of the physical properties of the circuit. At time $n + \tau$, \mathbf{u}^q requires the voltages V_m^q and V_k^q at time n as given by

$$\frac{V_m^q[n]}{Z_c} = i_0^{q+1}[n] - I_m^q[n - \tau] \quad (352)$$

$$\frac{V_k^q[n]}{Z_c} = i_0^q[n] - I_k^q[n - \tau] \quad (353)$$

that can be obtained from the circuit shown in Figure 53.

Implementing (352)-(353) in (351) at time $n + \tau$ and rearranging terms for convenience leads to

$$\mathbf{u}_{n+\tau} = \begin{bmatrix} \mathbf{u}^1 \\ \mathbf{u}^2 \\ \mathbf{u}^3 \\ \vdots \\ \mathbf{u}^b \\ \mathbf{u}^{b+1} \end{bmatrix}_{n+\tau} = \begin{bmatrix} V_{in}[n + \tau] \\ 2i_0^2[n] - I_m^1[n - \tau] \\ 2i_0^1[n] - I_k^1[n - \tau] \\ 2i_0^3[n] - I_m^2[n - \tau] \\ \vdots \\ 2i_0^{b+1}[n] - I_k^b[n - \tau] \\ V_{out}[n + \tau] \end{bmatrix} = \begin{bmatrix} V_{in}[n + \tau] \\ \mathbf{H}_n \\ V_{out}[n + \tau] \end{bmatrix} \quad (354)$$

$$\mathbf{H}_n = \begin{bmatrix} 2i_0^2[n] - I_m^1[n - \tau] \\ 2i_0^1[n] - I_k^1[n - \tau] \\ 2i_0^3[n] - I_m^2[n - \tau] \\ \vdots \\ 2i_0^{b+1}[n] - I_k^b[n - \tau] \end{bmatrix} = 2 \begin{bmatrix} i_0^2 \\ i_0^1 \\ i_0^3 \\ \vdots \\ i_0^{n+1} \end{bmatrix}_n - \begin{bmatrix} I_m^1 \\ I_k^1 \\ I_m^2 \\ \vdots \\ I_k^n \end{bmatrix}_{n-\tau} \stackrel{\text{def}}{=} 2\mathbf{i}_{mod}[n] - \mathbf{u}_{mod}[n - \tau] \quad (355)$$

It can be noticed that vector \mathbf{i}_{mod} is \mathbf{i}_0 sorted in a specific way, and vector \mathbf{u}_{mod} is \mathbf{u} at time $n - \tau$ sorted in a specific way. The indexes \mathbf{i}_{index} and \mathbf{u}_{index} that sort \mathbf{i}_0 and \mathbf{u} into \mathbf{i}_{mod} and \mathbf{u}_{mod} , respectively, are constructed as follows

- \mathbf{i}_{index} is constructed by alternating between 2 vectors: one that counts from 2 to $b + 1$ and one that counts from 1 to b .
- \mathbf{u}_{index} is constructed by switching places every 2 elements from a vector that counts from 1 to $2b + 1$.

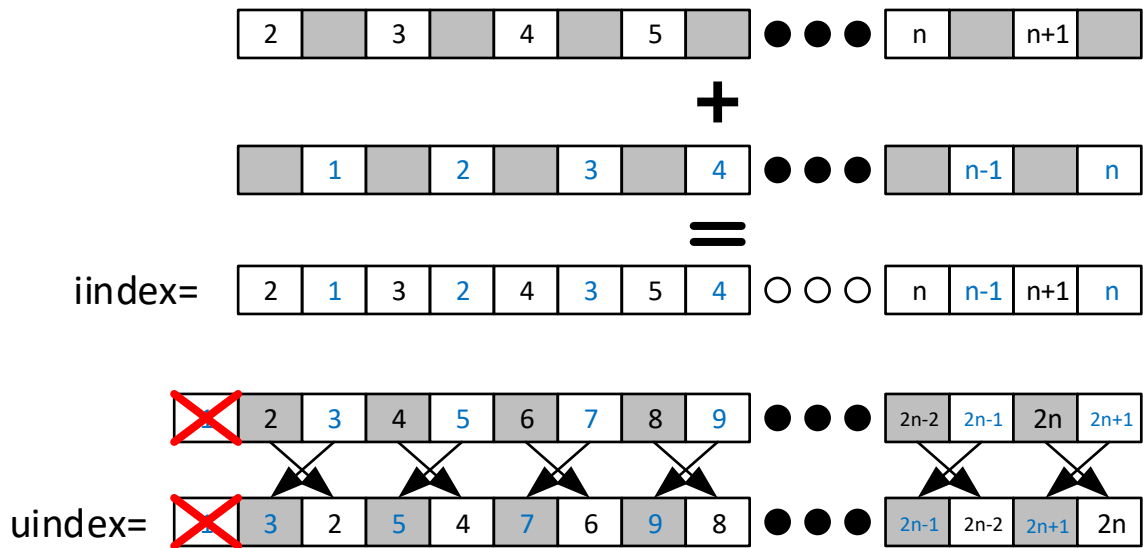
We show a graphical guide to assemble \mathbf{i}_{index} and \mathbf{u}_{index} in Figure 61.

Implementation of (354)-(355) results in the following algorithm:

- i) At current time n , vector \mathbf{u} is ready for use. Vector \mathbf{u} contains the current sources I_k and I_m at time $n - \tau$.
- ii) Load vector \mathbf{x} at time $n - 1$, and load vector \mathbf{u} at times $n - 1$ and n (current time).
- iii) Compute \mathbf{x} at current time n using (348) and the sparse method.
- iv) Compute node currents \mathbf{i}_0 at current time n using (349).

- v) Sort \mathbf{i}_0 into \mathbf{i}_{mod} .
- vi) Sort \mathbf{u} at current time n into \mathbf{u}_{mod} .
- vii) Compute \mathbf{H} using (355).
- viii) Preallocate \mathbf{u} at time $n + \tau$ using (354). Write \mathbf{H} into the preallocated $\mathbf{u}_{n+\tau}$. This action leaves \mathbf{u} at time $n + \tau$ ready for use.

Figure 61 – Guide to assemble vectors of indexes



Source: Compiled by author

Input vector \mathbf{u} must be allocated with a scope of 2τ time steps.

By implementing the previous algorithm, we reduce the number of times the program accesses the memory by 6 times.

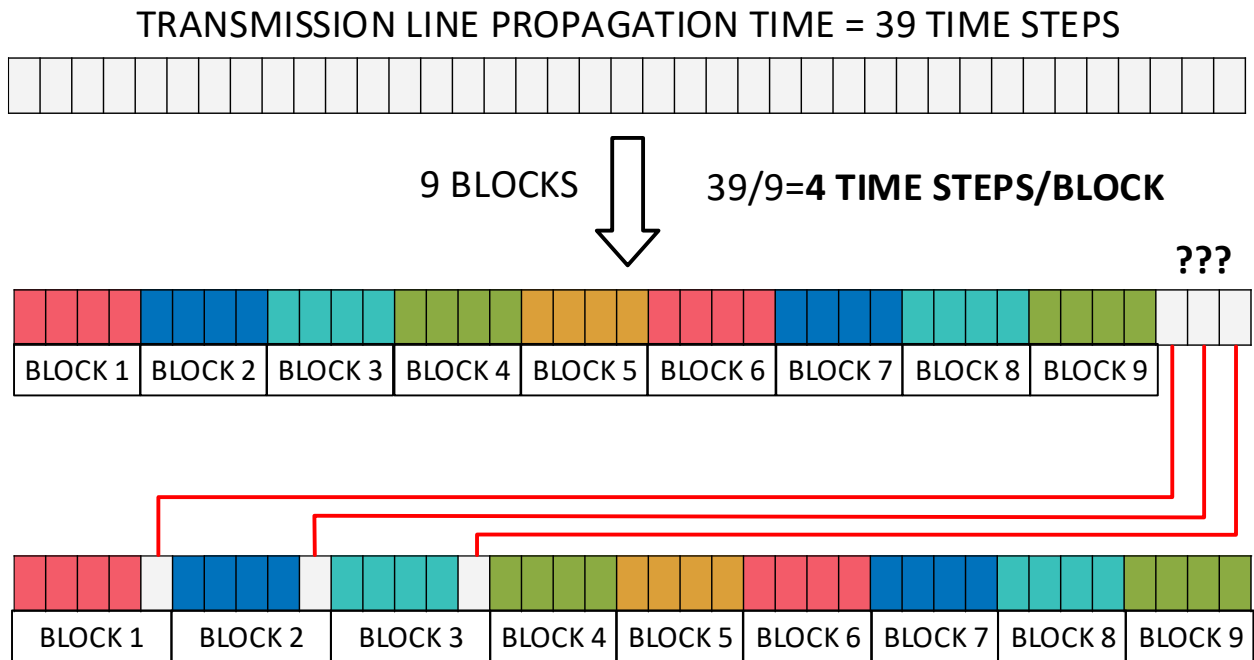
6.7.3 Correction due to Time Discretization

The cascaded model divides the line in b segments. Thus, the line propagation time τ is also divided in b segments. For fixed-time numerical methods such as Heun's ¹⁰³, a problem arises when τ/b is not proportional to the time step Δt .

For example: a transmission line with a propagation time of $39\Delta t$ represented by 9 cascaded blocks would have a propagation time of $4\Delta t$ for each block. The propagation time of the segmented line would be $4\Delta t$, and not $39\Delta t$. During the first iterations, there would be no difference but that gap of $3\Delta t$ would stack over time to produce lag between the line's "ideal response" and its simulation.

To avoid this, we propose to distribute the remainder $\Delta t \text{ MOD} \{\tau, b\}$ between the first cascaded blocks. Applying that technique to our example increases the propagation time of the first 3 blocks by one time step Δt . We show the example discussed in Figure 62.

Figure 62 – Error stacked due to time discretization and proposed solution.



Source: Compiled by author

6.8 MODAL TRANSFORMATION APPLIED TO THE MODEL

In order to simulate MTL, modal transformation must be incorporated into the model presented in this chapter. We propose to use a scheme similar to the one presented in section 3.8: use frequency dependent transformation matrices to obtain mode parameters, and constant transformation matrices to transform currents and voltages.

The matrices used to transform currents and voltages must be constant and real. Amongst all constant matrices presented in section 3.6.2, Clarke's matrix gives the most accurate results. However, since it is an approximation, like all other constant transformation matrices, it adds error to the model.

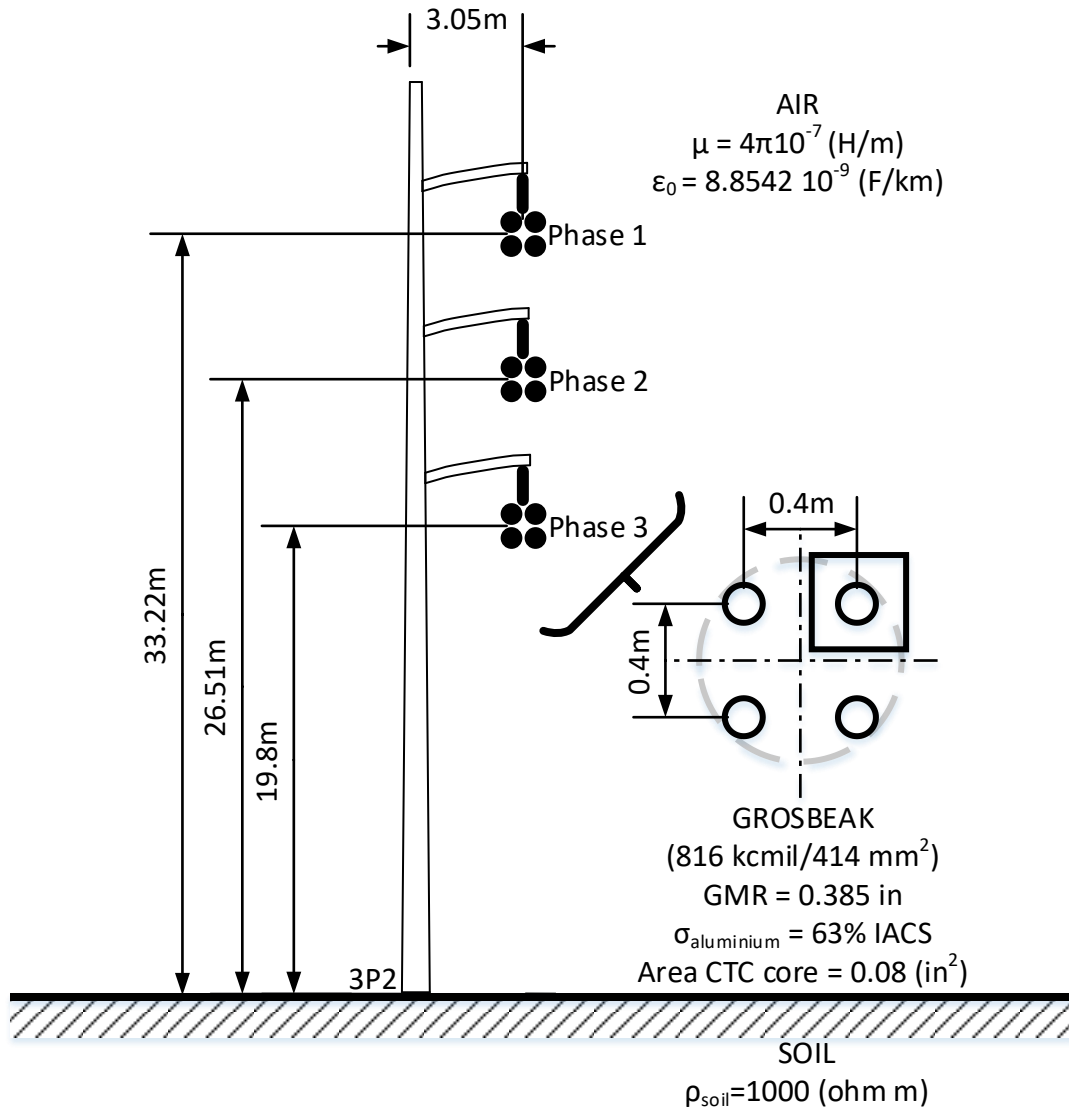
Instead, we propose to calculate the transformation matrices at a fix frequency and disregard its imaginary part. This approach significantly reduces the error caused by using any of the transformation matrices presented in 3.6.2. This approach also produces very accurate transformation matrices for asymmetrical and vertical line configurations.

In order to compare this approach with Clarke's matrix, we simulated the MTL shown in Figure 63. The MTL has its terminals connected as in Figure 64. Phase 1 is connected to a 1 MHz full width at half maximum (FWHM) voltage source and the line length is 2 km. The induced voltages at the receiving end of phase 2 are shown in Figure 65.

Clarke's matrix, as shown in section 3.6.2, gives best results when the MTL has vertical symmetry. When applied to MTL with vertical configuration, as it can be seen in Figure 65, Clarke's matrix has a poor performance whereas our approach is accurate.

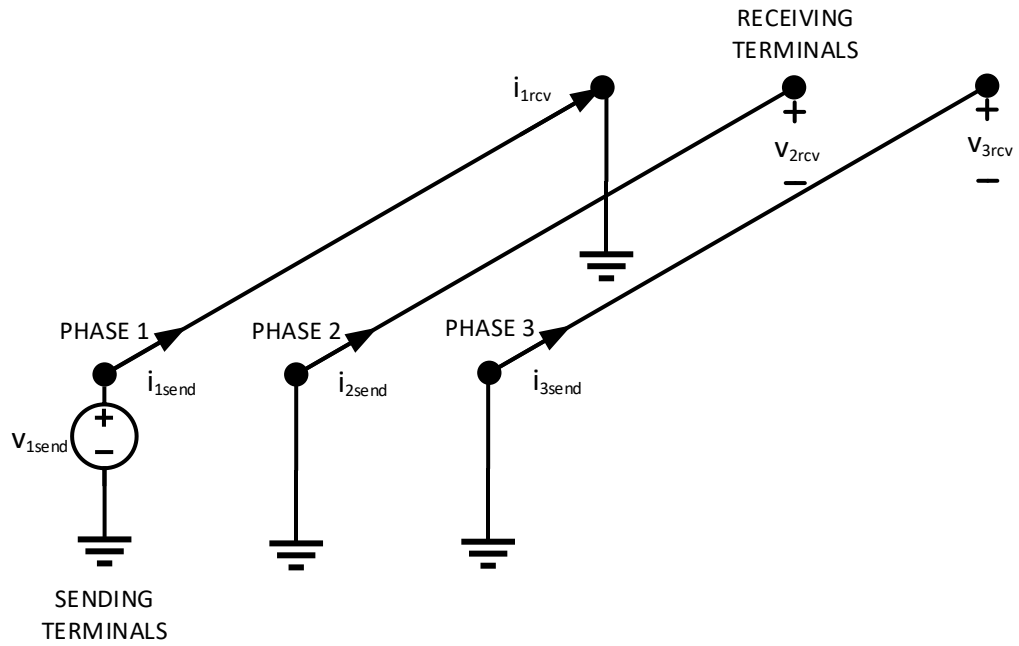
Figure 66 shows the error between the "exact" response and the proposed approach when the transformation matrices are calculated at various frequencies. The error (normalized root-mean-square deviation) was calculated for all 3 line configurations: MTL with vertical symmetry, vertical configuration and asymmetrical. In all cases, the error of our approach never exceeds 0.4%. Therefore, the proposed approach is accurate and works with diverse line configurations.

Figure 63 – Multiconductor transmission line with vertical configuration.



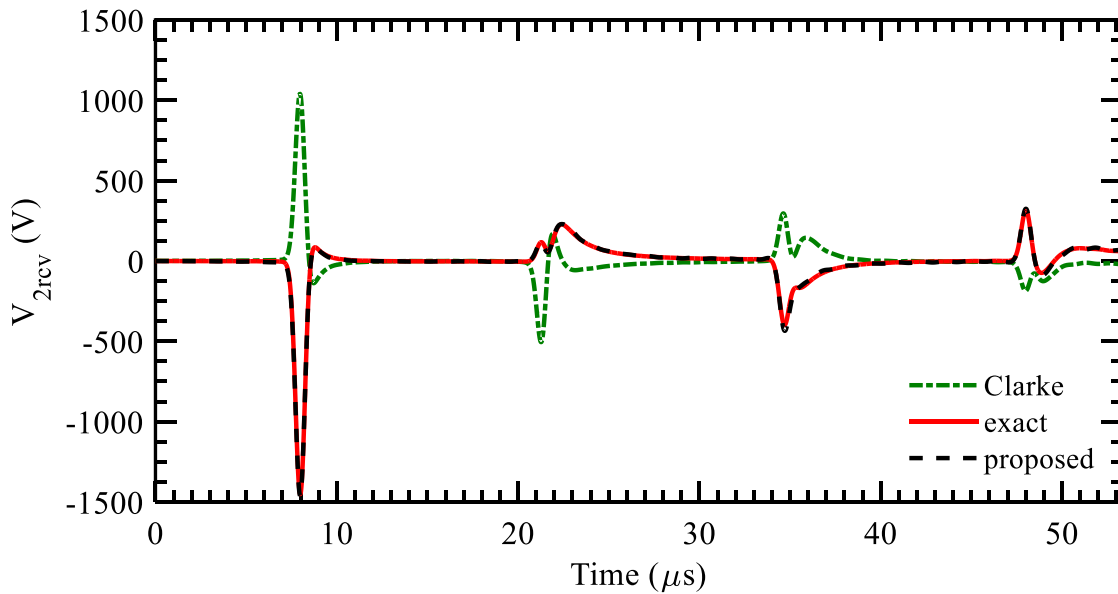
Source: Compiled by author

Figure 64 – Multiconductor transmission line layout.



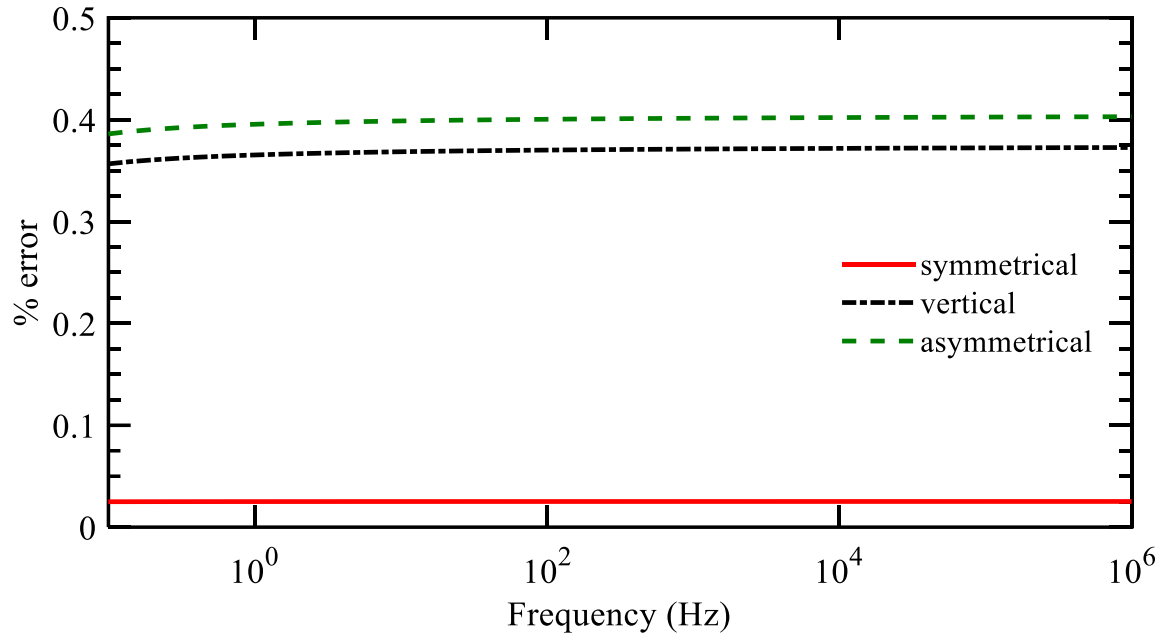
Source: Compiled by author

Figure 65 – Induced voltage in a transmission line with vertical configuration.



Source: Compiled by author

Figure 66 – Induced error as a function of the frequency at which the transformation matrices are calculated.



Source: Compiled by author

6.9 CONCLUSION

In this chapter all the equations needed to include the frequency effect in the method of characteristics were presented. Additionally, a fast implementation of the method was described. The modal transformation method proposed decouples transmission lines with various configurations without exceeding 0.4% of error.

7 VALIDATION AND RESULTS

In this chapter, we will present the results obtained by simulating the three-phase overhead transmission line presented in section 2.8.

7.1 TRANSMISSION LINE USED AND VALIDATION

For the simulations presented in this chapter, the CESP's transmission line presented in section 2.8 of this document is used. The simulations obtained for various scenarios are validated by comparing them to a model whose accuracy is undisputed⁷⁷, the frequency-domain solution of the transmission line, where differential equations are transformed to the time domain using the Numeric Laplace Transform, which for convenience will be referenced for this chapter as NLT (chapter 3)^{52,53}.

A few considerations are taken into account in order to compare both models:

- They both have the same step size and simulation time
- They both receive as input data the same transmission line parameters, although the NLT model samples the data in the frequency-domain as shown in Figure 27.

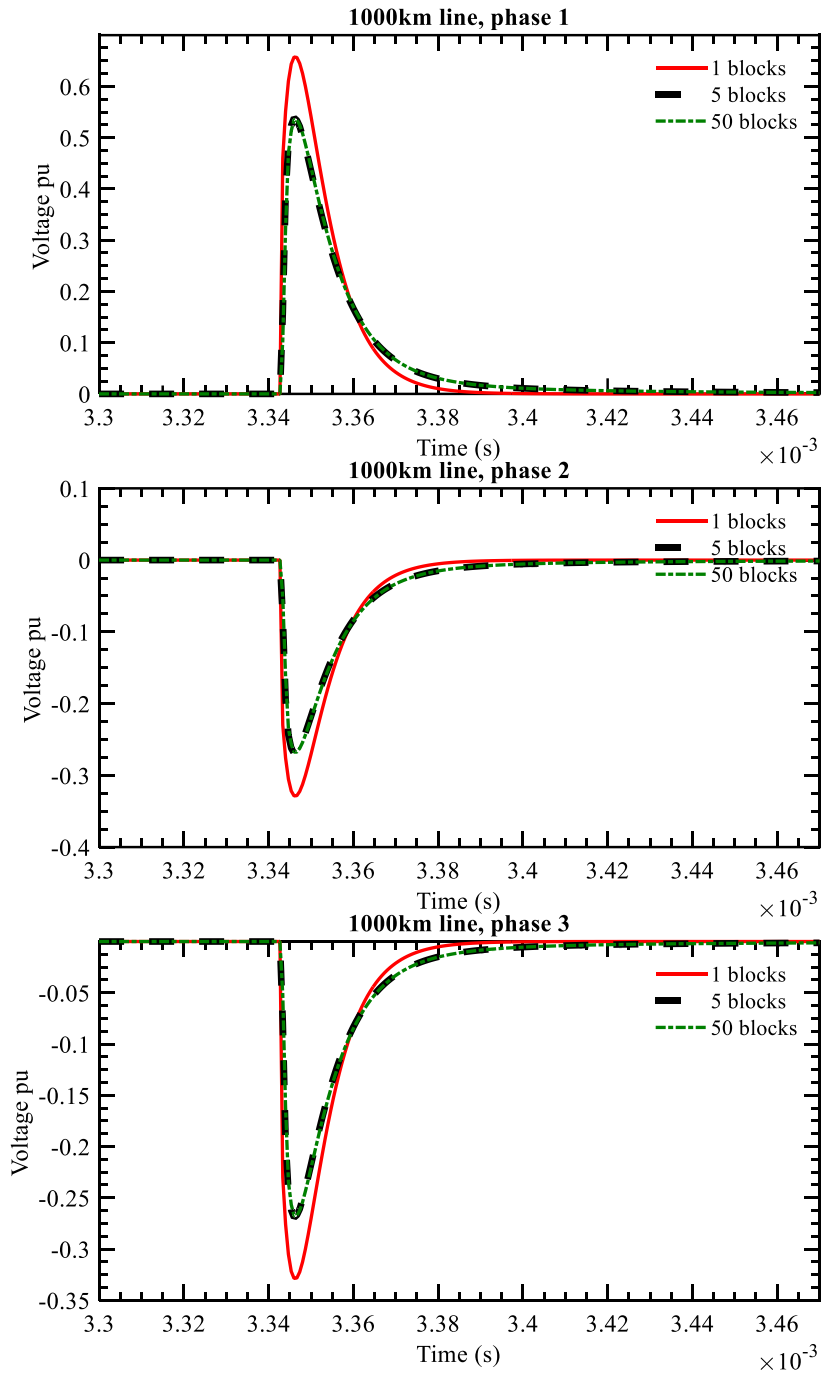
Clarke's matrix is intended to be used in symmetrical lines but it is a common practice^{48,47,88,100} to use it also with asymmetrical lines in acknowledge that it has certain limitations. Our proposal uses transformation matrices calculated at 1 kHz.

7.2 QUANTITY OF CASCADED BLOCKS

The quantity of cascaded blocks n alleviates the effect of concentrating losses.

Figure 67 and Figure 68 show the influence of segmenting a transmission line in b blocks. Figure 67 shows the receiving voltage of the MTL shown in section 2.8 that is 1000km long. The MTL has a 1.2/50 μ s surge waveform applied to one of its phases and all of its receiving terminal open circuited. The MTL is simulated using 1, 5 and 50 blocks of the proposed model. Figure 67 shows that the response of the model converges rapidly as the number of cascaded blocks increase. Figure 68 shows the error of the proposed model as a function of the number of cascaded blocks.

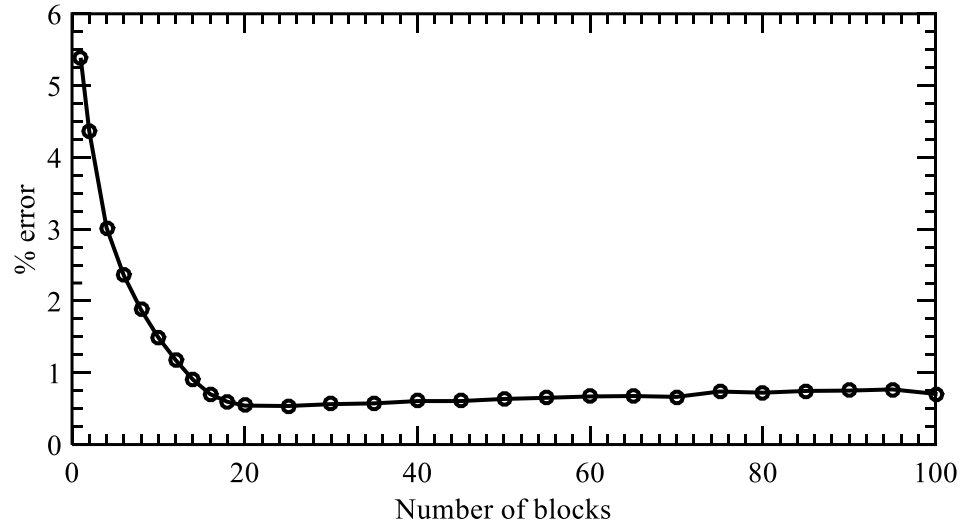
Figure 67 – Response of the proposed model segmenting the line in 1, 5 and 50 blocks.



Source: Compiled by author

Figure 68 shows that 25 cascaded blocks are enough to simulate most transients.

Figure 68 – Error of the proposed model as a function of the number of cascaded blocks.



Source: Compiled by author

7.3 STEP SIZE

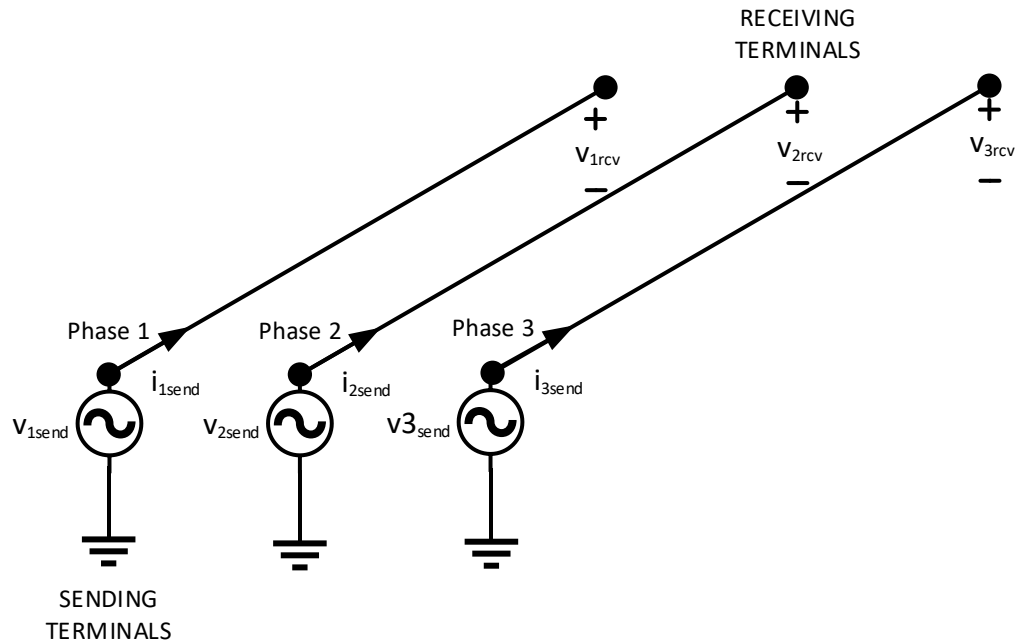
The step size must be at least equal to τ/b , where τ is the propagation time and b the number of cascaded blocks. To give best results, the step size should be at least 3 times smaller than τ/b as given by

$$\Delta t \leq \frac{1}{3} \frac{\tau}{b} \quad (356)$$

7.4 LONG VS. SHORT LINES

In order to show the accuracy of our approach with long and short lines, we simulated the energizing of the MTL shown in section 2.8 when it is 100km (short) and 1000km long. We validated the results of the proposed model when the line is segmented in 25 blocks by comparing it with the reference model described in chapter 3 (NLT exact). The line has its terminals connected as shown in Figure 69. The voltage curves at the receiving terminals of the 100 km MTL and 1000 km line are shown in Figure 70 and Figure 71, respectively.

Figure 69 – Multiconductor transmission line layout.



Source: Compiled by author

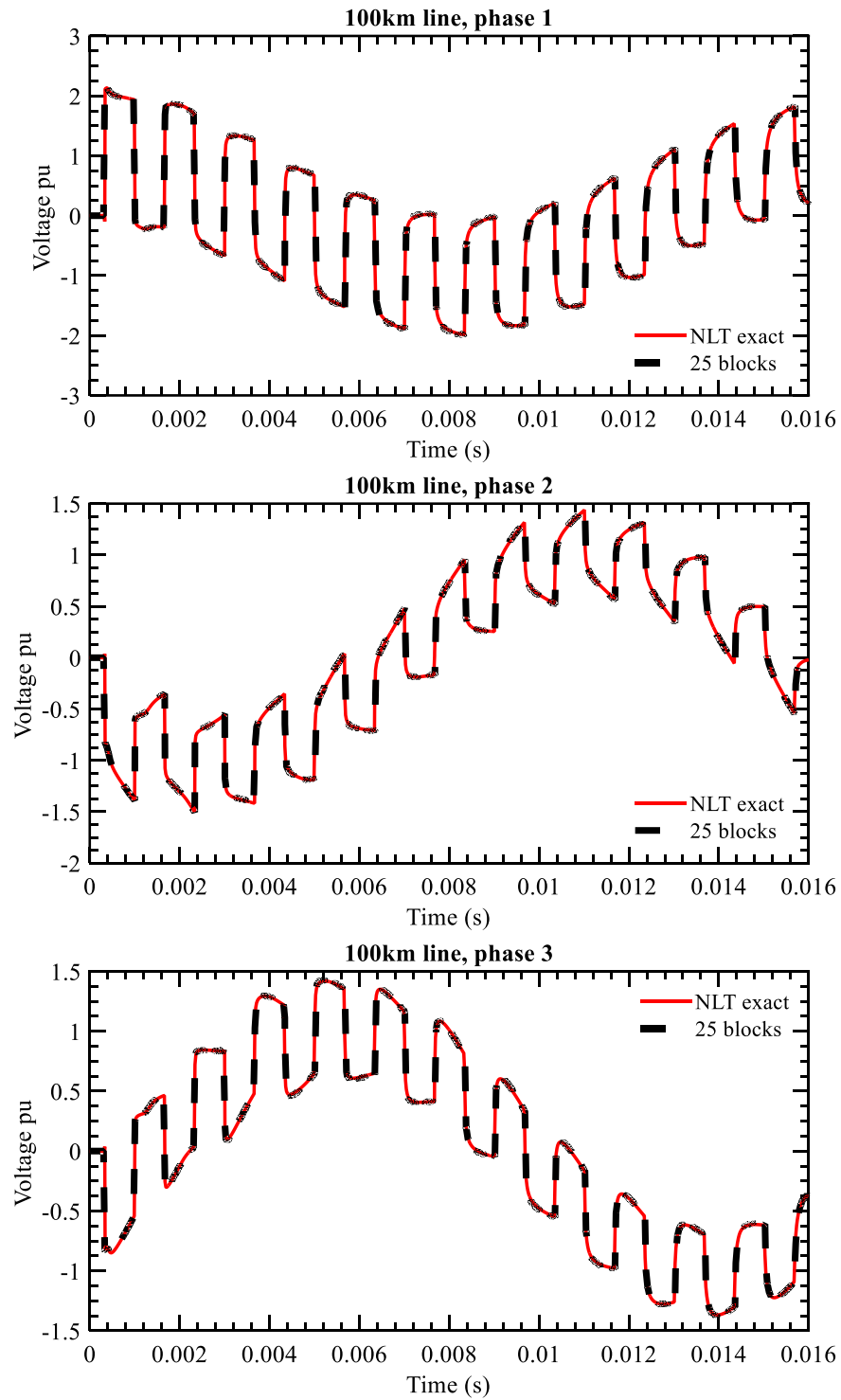
The response of the proposed model is very similar to the reference model, which proves its accuracy.

7.5 FAST TRANSIENTS

In order to show the accuracy of the proposed model when fast transients are involved, we simulate the extreme scenario shown in Figure 72 when the MTL of section 2.8 is 2 km long. The proposed model is simulated using 10 and 25 blocks. The induced voltages in phase 2 V_{2rcv} (and 3) is shown in Figure 73. The input and output currents of phase 1 are shown in Figure 74 and Figure 75, respectively. The voltage source V_{1send} is a delayed Gaussian voltage source with a FWHM of 1 MHz as shown in Figure 23 (section 3.4).

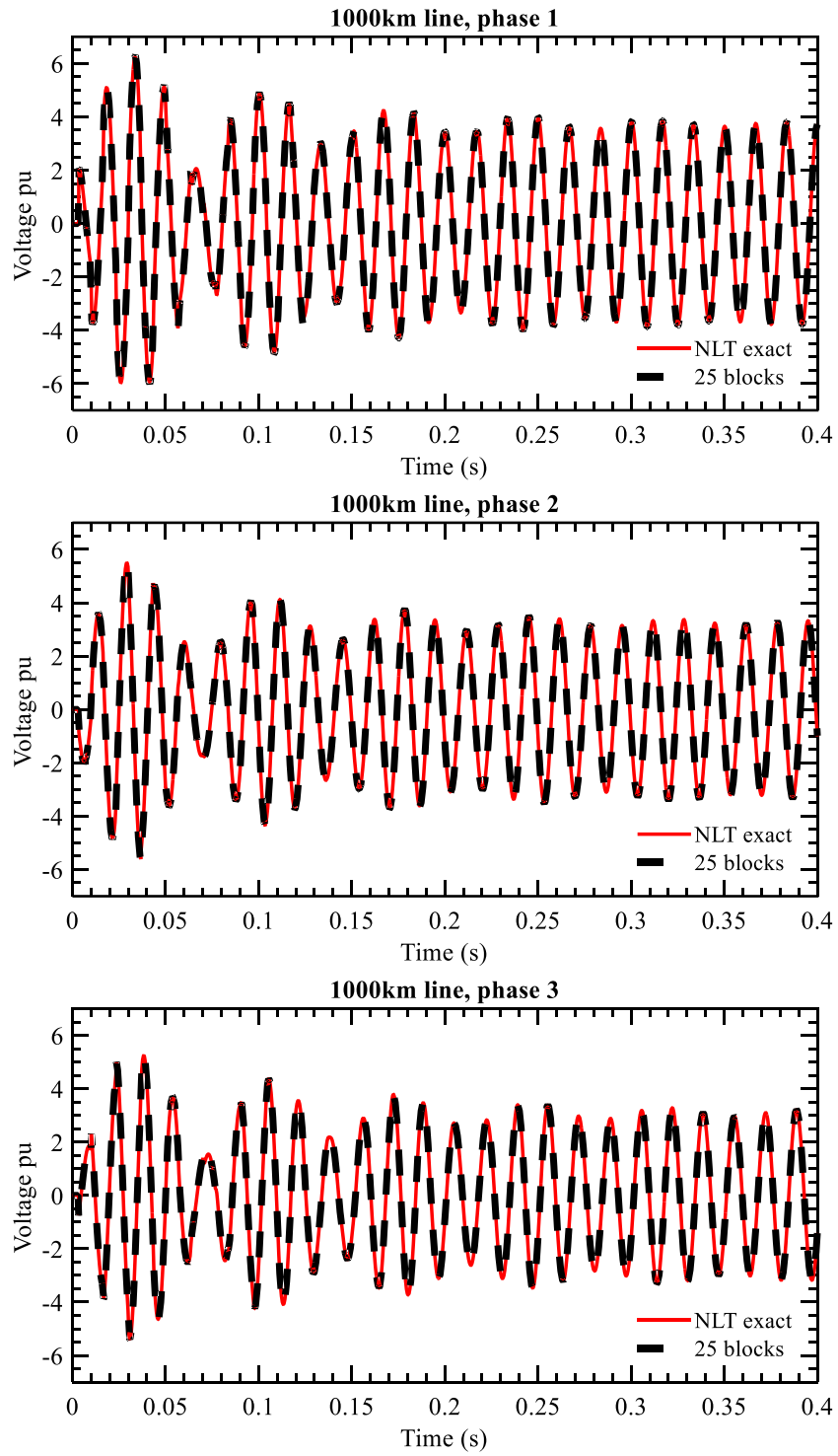
As it can be seen in Figure 73, Figure 74 and Figure 75, 25 blocks give a very accurate answer, which was also shown in Figure 68.

Figure 70 – Energizing of a 100km open-circuited transmission line.



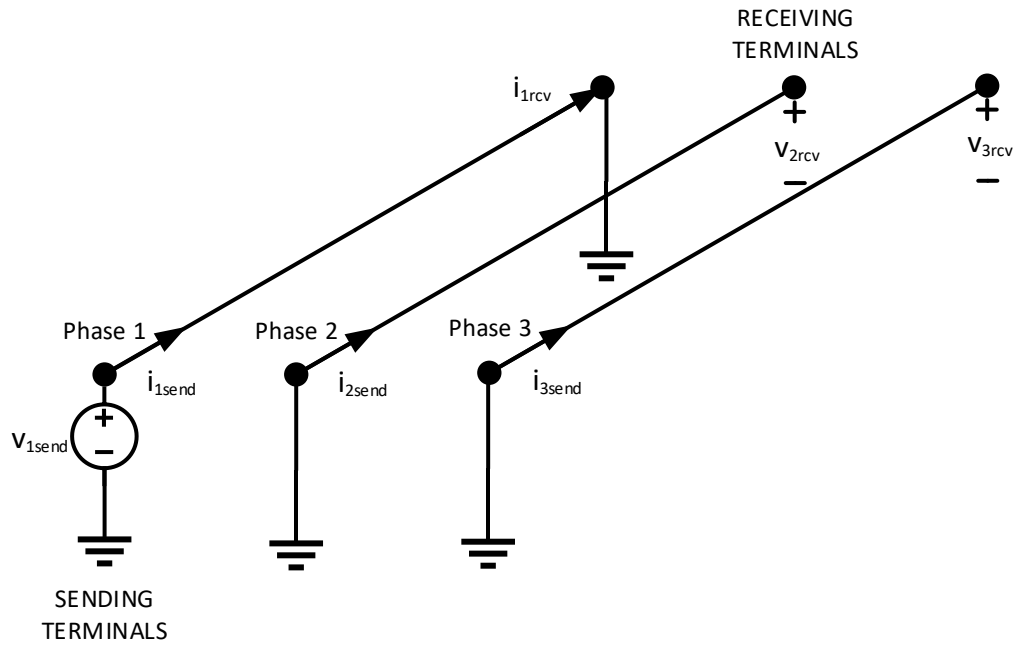
Source: Compiled by author

Figure 71 – Energizing of a 1000km open-circuited transmission line.



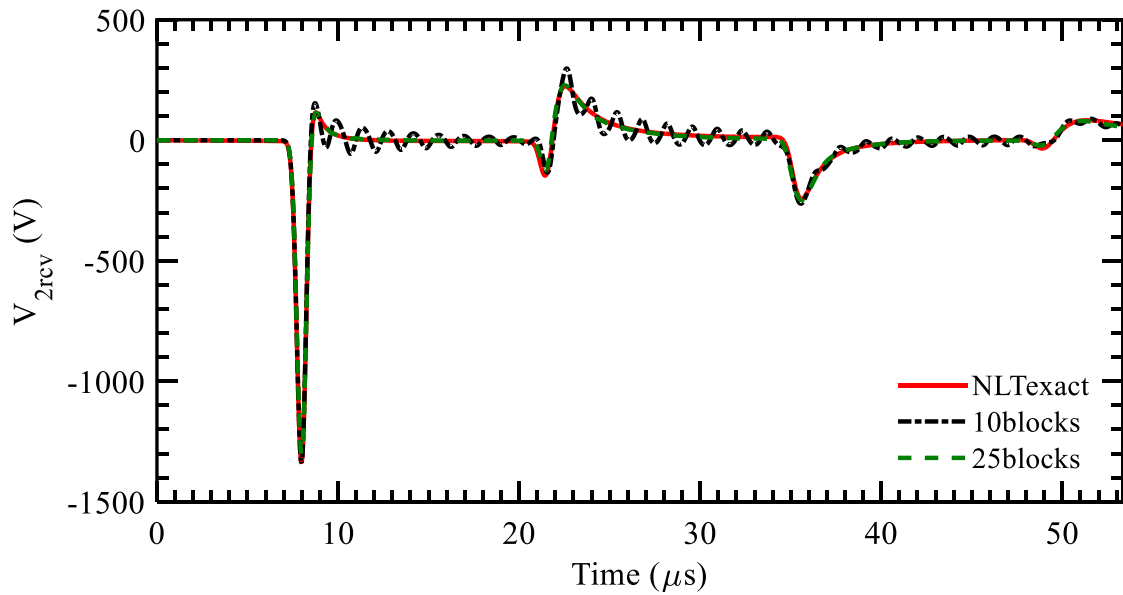
Source: Compiled by author

Figure 72 – High frequency test layout.



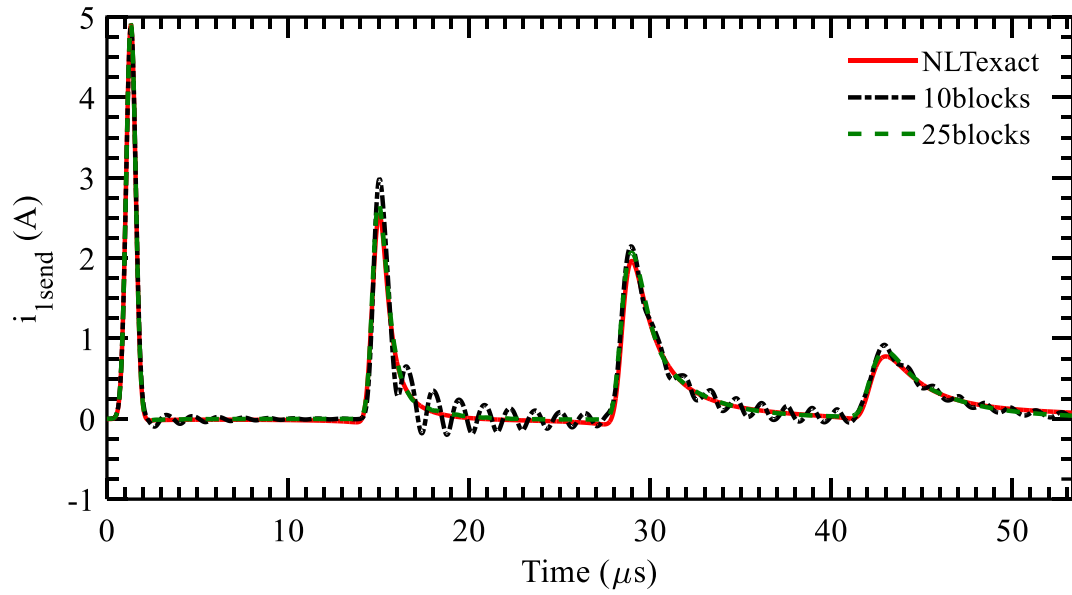
Source: Compiled by author

Figure 73 – Induced voltage during a fast transient.



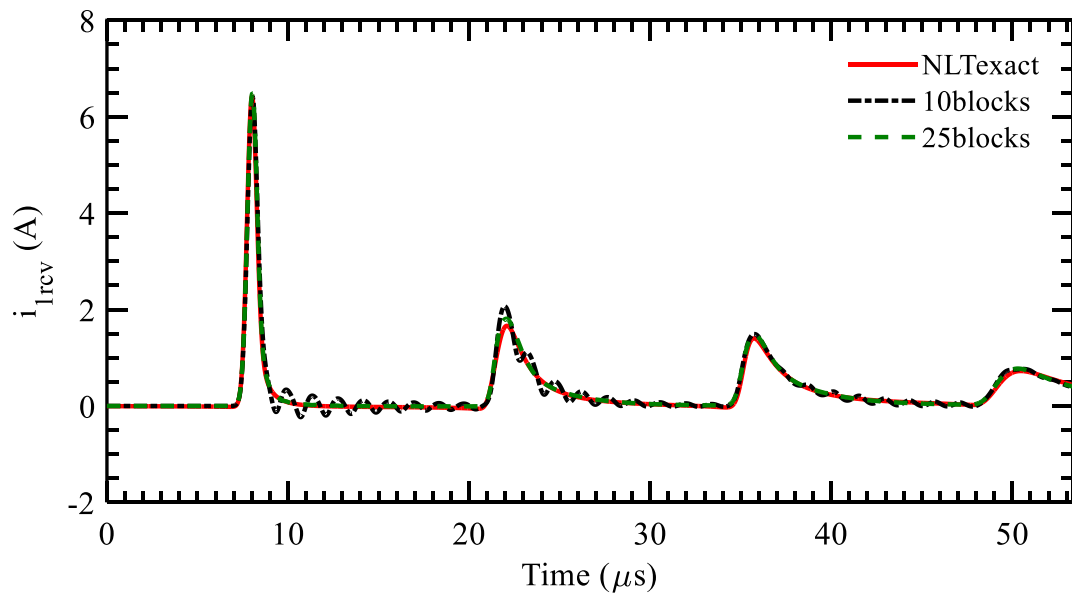
Source: Compiled by author

Figure 74 – Input current during a fast transient.



Source: Compiled by author

Figure 75 – Output current during a fast transient.



Source: Compiled by author

7.6 QUALITY AND PROCESSING TIMES

The overall processing time of the model is determined by the amount of integration points (time steps). Small time steps let us appreciate with more detail the transients at the expense of higher processing times.

The fast implementation of the proposed model (section 6.7) reduced the computation complexity from $O(n^2)$ to $O(n)$, and also reduced the amount of memory accesses from $3b + 9$ to 5. The techniques proposed in this research reduce the overall computation time and memory consumption while increasing the accuracy of the proposed model.

Even though it is difficult to compare models because of differences in programming environments and algorithm implementations, we simulated the transmission line shown in section 7.5 using other time-domain models, and measured the processing time needed to produce responses with the same quality of the one shown in Figure 73. The processing times are shown in Table 7. Table 7 shows that the proposed model is faster than the Universal Line Model ²³ and the cascade of frequency-dependent π circuits ⁴⁸.

Table 7 – Processing times for various transmission line models

	Processing times in seconds	Ratio to the proposed model
Proposed model	7.53	1
Universal Line Model ULM	8.14	1.08
Cascade of frequency dependent π circuits	19.71	2.62
Numeric Laplace Transform (reference model)	10.05	1.33

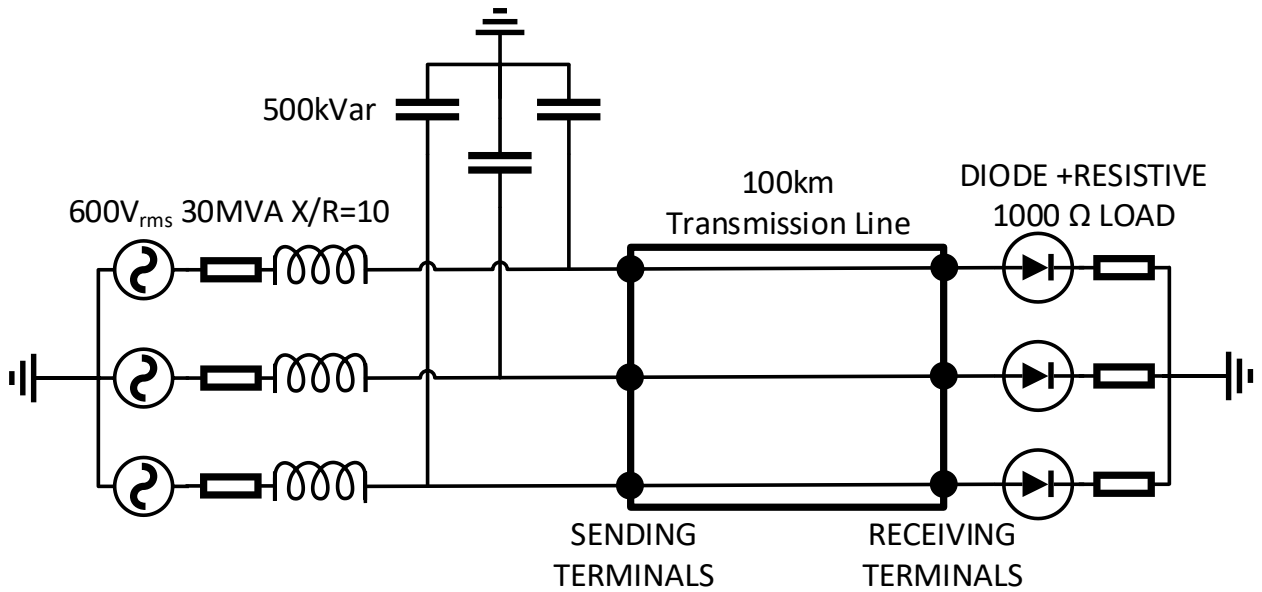
Source: Compiled by author

7.7 COMPATIBILITY

To show the compatibility of the proposed, accelerated approach with electromagnetic transient (EMT) simulators, we simulate a 100-km long MTL with the geometry shown in 2.8 that transmits power from a 600-V three-phase source to a non-linear load as shown in Figure 76. The voltages and currents simulated are shown in Figure 77 and Figure 78. The accelerated model

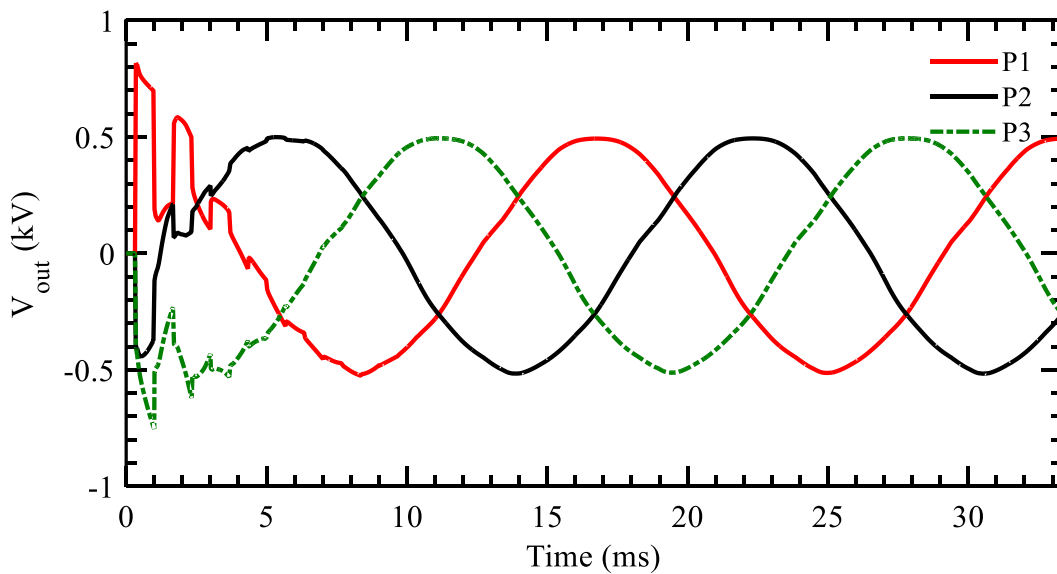
presented in this paper is considerably faster, computationally less expensive, and more accurate due to the techniques described in section 6.7.

Figure 76 – A three phase transmission line terminated by a nonlinear load.

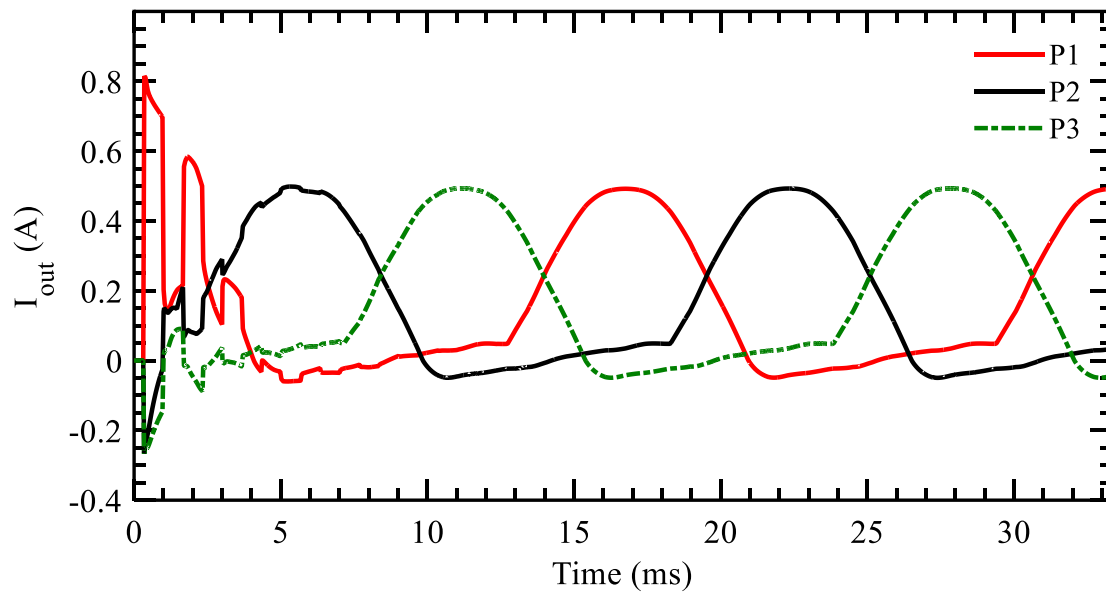


Source: Compiled by author

Figure 77 – Simulation Results: Voltages at the receiving terminal.



Source: Compiled by author

Figure 78 – Simulation Results: Currents at the receiving terminal.

Source: Compiled by author

7.8 CONCLUSION

All the scenarios simulated confirm that the MTL proposed in this research are accurate for simulating slow and fast transients in short and long transmission lines. Furthermore, the proposed model is computationally more efficient than other time domain MTL models and has a good compatibility with electromagnetic simulators.

8 CONCLUSIONS

The frequency-dependence of the longitudinal parameters was included in the method of characteristics Line Model. First, a deep review of the technical literature on fitting parameters and rational functions was done. We combined what in our opinion was the best fitting procedure, the Fast Relaxed Vector Fitting, with the best circuit topologies available in the literature, one that we enhanced to represent pairs of complex conjugate poles-residues.

In order to couple the method of characteristics with the circuit topologies that represent the longitudinal parameters, the classical method of characteristics was reformulated to reduce the number of unnecessary flops. Then, the state space representation of the circuit topologies that represent the longitudinal parameters was combined with the the modified method of characteristics. The resulting state space model was segmented and cascaded to reduce the effect of lumping the losses. The equations that describe the cascaded model are solved in an efficient manner by assembling a global matrices and treating input data. This efficient implementation reduces the computational complexity from $O(n^2)$ to $O(n)$ and the number of memory accesses from $3b + 9$ to 5. The accuracy of the proposed model is further enhanced by correcting the error due to time discretization.

The p.u.l. modal series impedance of a MTL was decoupled using its frequency-dependent modal transformation matrices. The voltages and currents at the terminals were transformed to the mode domain using a real transformation matrix sampled at a low frequency e.g. 1 kHz.

The simulation results proved the accuracy of the proposed model for overhead transmission lines when simulating long or short MTL under slow or fast transients.

We propose to expand the capabilities of the proposed to simulate cables as further research.

REFERENCES

1. BERGERON, L. Propagation d'ondes le long des lignes électriques: méthode graphique. **Bulletin de la société française des électriciens**, [S. l.], v. 1, p. 26, 1937.
2. BRANIN, F. H. J. Transient analysis of lossless transmission lines. **Proceedings of the IEEE**, Piscataway, v. 55, n. 11, p. 2012–2013, 1967. ISSN 0018-9219. DOI 10.1109/PROC.1967.6033.
3. DOMMEL, H. W. Digital Computer Solution of Electromagnetic Transients in Single-and Multiphase Networks. **IEEE Transactions on Power Apparatus and Systems**, Piscataway, v. PAS-88, n. 4, p. 388–399, 1969. ISSN 0018-9510. DOI 10.1109/TPAS.1969.292459.
4. DOMMEL, H. W. **Electromagnetic transients program theory book**. Portland: Bonneville Power Administration, 1986.
5. CARSON, J. R. Wave propagation in overhead wires with ground return. **Bell system technical journal**, Piscataway, v. 5, n. 4, p. 539–554, 1926. ISSN 00058580. DOI 10.1002/j.1538-7305.1926.tb00122.x.
6. BUDNER, A. Introduction of Frequency-Dependent Line Parameters into an Electromagnetic Transients Program. **Power Apparatus and Systems, IEEE Transactions on**, Piscataway, v. PAS-89, n. 1, p. 88–97, 1970. ISSN 0018-9510. DOI 10.1109/TPAS.1970.292674.
7. MEYER, W. S.; DOMMEL, H. W. Numerical Modelling of Frequency-Dependent Transmission-Line Parameters in an Electromagnetic Transients Program. **IEEE Transactions on Power Apparatus and Systems**, Piscataway, v. PAS-93, n. 5, p. 1401–1409, 1974. ISSN 0018-9510. DOI 10.1109/TPAS.1974.293870.
8. SAIED, M. M.; AL-FUHAID, A. Electromagnetic transients in a line-transformer cascade by a numerical laplace transform technique. **IEEE Transactions on Power Apparatus and Systems**, Piscataway, v. PAS-104, n. 10, p. 2901–2909, 1985. DOI 10.1109/TPAS.1985.319135.
9. SEMLYEN, A.; DABULEANU, A. Fast and accurate switching transient calculations on transmission lines with ground return using recursive convolutions. **IEEE Transactions on Power Apparatus and Systems**, Piscataway, v. PAS-94, n. 2, p. 561–571, 1975. ISSN 0018-9510. DOI 10.1109/T-PAS.1975.31884.
10. SEMLYEN, A. Contributions to the Theory of Calculation of Electromagnetic Transients on Transmission Lines with Frequency Dependent Parameters. **IEEE Transactions on Power Apparatus and Systems**, Piscataway, v. PAS-100, n. 2, p. 848–856, 1981. ISSN 0018-9510. DOI 10.1109/TPAS.1981.316943.

11. MARTI, L. Simulation of transients in underground cables with frequency-dependent modal transformation matrices. **IEEE Transactions on Power Delivery**, Piscataway, v. 3, n. 3, p. 1099–1110, 1988. ISSN 19374208. DOI 10.1109/61.193892.
12. BREITHOLTZ, C.; MOLANDER, M.; NAVARRO-ADLEMO, R. Space and time continuous lumped transmission line model. **IEE Proceedings G - Circuits, Devices and Systems**, Stevenage, v. 138, n. 6, p. 661–670, 1991. ISSN 09563768.
13. SNELSON, J. K. Propagation of travelling waves on transmission lines: frequency dependent parameters. **IEEE Transactions on Power Apparatus and Systems**, Piscataway, v. PAS-91, n. 1, p. 85–91, 1972. ISSN 00189510. DOI 10.1109/TPAS.1972.293294.
14. MARTI, J. R. Accurate modeling of frequency-dependent transmission lines in electromagnetic transient simulations. **IEEE Transactions on Power Apparatus Systems**, Piscataway, v. PAS-101, n. 1, p. 147–157, 1982. ISSN 0272-1724. DOI 10.14288/1.0095571.
15. AMETANI, A. et al. A simple and efficient method for including a frequency-dependent effect in a transmission line transient analysis. In: INTERNATIONAL CONFERENCE ON POWER SYSTEMS TRANSIENTS, 1995, Lisbon. **Anais** [...] Lisbon: IPST, 1995. p. 11-16.
16. MARTI, J. R.; TAVIGUI, A. Frequency Dependent Multiconductor Transmission Line Model with Collocated Voltage and Current Propagation. **IEEE Transactions on Power Delivery**, Piscataway, v. PP, n. 99, p. 1–1, 2017. DOI 10.1109/TPWRD.2017.2691343.
17. COLVIN, D. H. Computationally Efficient Method of Calculations Involving Lumped-Parameter Transmission-Line Models. **IEEE Transactions on Electromagnetic Compatibility**, Piscataway, v. EMC-27, n. 1, p. 41–43, 1985. ISSN 1558-187X. DOI 10.1109/TEMC.1985.304244.
18. NELMS, R. M. et al. Simulation of transmission line transients using a personal computer. In: IEEE CONFERENCE RECORD OF THE 1988 EIGHTEENTH POWER MODULATOR SYMPOSIUM, 1988, Hilton Head. **Proceedings** [...] Piscataway: IEEE, 1988. DOI 10.1109/MODSYM.1988.26275. p. 239-222.
19. NELMS, R. M. et al. Using a personal computer to teach power system transients. **IEEE Transactions on Power Systems**, Piscataway, v. 4, n. 3, p. 1293–1294, 1989. ISSN 1558-0679. DOI 10.1109/59.32630.
20. NEWTON, S. R. et al. A modular state variable approach to the electromagnetic transients problem. In: SOUTHEASTERN SYMPOSIUM ON SYSTEM THEORY, 21., 1989, Tallahassee. **Proceedings** [...] Piscataway: IEEE, 1989. DOI 10.1109/SSST.1989.72445.

21. TANG, Y. et al. **Transmission line models used in travelling wave studies**. In: IEEE TRANSMISSION AND DISTRIBUTION CONFERENCE, 1999, New Orleans. **Proceedings** [...] Piscataway: IEEE, 1999. DOI 10.1109/TDC.1999.756151.
22. GUSTAVSEN, B.; SEMLYEN, A. Combined phase and modal domain calculation of transmission line transients based on vector fitting. **IEEE Transactions on Power Delivery**, Piscataway, v. 13, n. 2, p. 596–601, 1998. ISSN 08858977. DOI 10.1109/61.660936.
23. MORCHED, A.; GUSTAVSEN, B.; TARTIBI, M. A universal model for accurate calculation of electromagnetic transients on overhead lines and underground cables. **IEEE Transactions on Power Delivery**, Piscataway, v. 14, n. 3, p. 1032–1037, 1999. ISSN 08858977. DOI 10.1109/61.772350.
24. MARTI, J. R.; MARTI, L.; DOMMEL, H. W. Transmission line models for steady-state and transients analysis. In: JOINT INTERNATIONAL POWER CONFERENCE, 1993, Athens. **Proceedings** [...] Piscataway: IEEE, 1993. DOI 10.1109/APT.1993.673895.
25. GUSTAVSEN, B.; SEMLYEN, A. Rational approximation of frequency domain responses by vector fitting. **IEEE Transactions on Power Delivery**, Piscataway, v. 14, n. 3, p. 1052–1059, 1999. ISSN 08858977. DOI 10.1109/61.772353.
26. TAVARES, M. C.; PISSOLATO, J.; PORTELA, C. M. Quasi-modes multiphase transmission line model. **Electric Power Systems Research**, Amsterdam, v. 49, n. 3, p. 159–167, 1999. ISSN 03787796. DOI 10.1016/S0378-7796(98)00105-9.
27. MAMIŞ, M. S.; KÖKSAL, M. Solution of eigenproblems for state-space transient analysis of transmission lines. **Electric Power Systems Research**, Amsterdam, v. 55, n. 1, p. 7–14, 2000. ISSN 03787796. DOI 10.1016/S0378-7796(99)00092-9.
28. PAUL, C. R. Decoupling the multiconductor transmission line equations. **IEEE transactions on Microwave Theory and Techniques**, Piscataway, v. 44, n. 8, p. 1429–1440, 1996. ISSN 00189480. DOI 10.1109/22.536026.
29. FARIA, J. A. B. A New Generalized Modal Analysis Theory for Nonuniform Multiconductor Transmission Lines. **IEEE Transactions on Power Systems**, Piscataway, v. 19, n. 2, p. 926–933, maio 2004. ISSN 0885-8950. DOI 10.1109/TPWRS.2004.826726.
30. ROYCHOWDHURY, J. S.; PEDERSON, D. O. **Efficient transient simulation of lossy interconnect**. In: CONFERENCE ON ACM/IEEE DESIGN AUTOMATION CONFERENCE - DAC '91, 28., 1991, New York. **Proceedings** [...] New York: ACM Press, 1991. DOI 10.1145/127601.127762.

31. ROYCHOWDHURY, J. S.; NEWTON, A. R.; PEDERSON, D. O. Algorithms for the transient simulation of lossy interconnect. **IEEE Transactions on Computer-Aided Design of Integrated Circuits and Systems**, Piscataway, v. 13, n. 1, p. 96–104, 1994. ISSN 02780070. DOI 10.1109/43.273746.
32. LIN, S.; KUH, E. S. Transient simulation of lossy interconnects based on the recursive convolution formulation. **IEEE Transactions on Circuits and Systems I: Fundamental Theory and Applications**, Piscataway, v. 39, n. 11, p. 879–892, 1992. ISSN 10577122. DOI 10.1109/81.199887.
33. JUN-FA MAO; ZHENG-FAN LI. Waveform relaxation solution of the ABCD matrices of nonuniform transmission lines for transient analysis. **IEEE Transactions on Computer-Aided Design of Integrated Circuits and Systems**, Piscataway, v. 13, n. 11, p. 1409–1412, 1994. ISSN 02780070. DOI 10.1109/43.329269.
34. GUSTAVSEN, B.; SEMLYEN, A. Simulation of transmission line transients using vector fitting and modal decomposition. **IEEE Transactions on Power Delivery**, Piscataway, v. 13, n. 2, p. 605–614, abr. 1998. ISSN 08858977. DOI 10.1109/61.660941.
35. NODA, T.; NAGAOKA, N.; AMETANI, A. Phase domain modeling of frequency-dependent transmission lines by means of an ARMA model. **IEEE Transactions on Power Delivery**, Piscataway, v. 11, n. 1, p. 401–411, 1996. ISSN 08858977. DOI 10.1109/61.484040.
36. CASTELLANOS, F.; MARTI, J. R. Full frequency-dependent phase-domain transmission line model. **IEEE Transactions on Power Systems**, Piscataway, v. 12, n. 3, p. 1331–1339, 1997. ISSN 08858950. DOI 10.1109/59.630478.
37. GUSTAVSEN, B.; SEMLYEN, A. Calculation of transmission line transients using polar decomposition. **IEEE Transactions on Power Delivery**, Piscataway, v. 13, n. 3, p. 855–862, jul. 1998. ISSN 08858977. DOI 10.1109/61.686984.
38. RAMIREZ, A. et al. Electromagnetic transients in overhead lines considering frequency dependence and corona effect via the method of characteristics. **International Journal of Electrical Power and Energy System**, London, v. 23, n. 3, p. 179–188, 2001. ISSN 01420615. DOI 10.1016/S0142-0615(00)00056-9.
39. MAMIŞ, M. S.; NACAROĞLU, A. Transient voltage and current distributions on transmission lines. **IEE Proceedings - Generation, Transmission and Distribution**, Piscataway, v. 149, n. 6, p. 705–712, 2002. ISSN 1350-2360. DOI 10.1049/ip-gtd:20020625.

40. MAMIŞ, M. S.; KAYGUSUZ, A.; KÖKSAL, M. State variable distributed-parameter representation of transmission line for transient simulations. **Turkish Journal of Electrical Engineering and Computer Sciences**, Ankara, v. 18, n. 1, p. 31–42, 2010an. ISSN 13000632. DOI 10.3906/elk-0905-2.
41. GUTIÉRREZ, J. A. et al. Fast transients analysis of nonuniform transmission lines through the method of characteristics. **International Journal of Electrical Power and Energy Systems**, London, v. 24, n. 9, p. 781–788, 2002. ISSN 01420615. DOI 10.1016/S0142-0615(01)00084-9.
42. DÁVILA, M. et al. The effects of non-uniformities and frequency dependence of line parameters on electromagnetic surge propagation. **International Journal of Electrical Power and Energy Systems**, London, v. 28, n. 3, p. 151–157, 2006. ISSN 01420615. DOI 10.1016/j.ijepes.2005.09.006.
43. MAMIŞ, M. S. Computation of electromagnetic transients on transmission lines with nonlinear components. **IEE Proceedings - Generation, Transmission and Distribution**, Piscataway, v. 150, n. 2, p. 200–204, 2003. ISSN 13502360. DOI 10.1049/ip-gtd:20030115.
44. MACIAS, J. A. R.; EXPOSITO, A. G.; SOLER, A. B. A Comparison of Techniques for State-Space Transient Analysis of Transmission Lines. **IEEE Transactions on Power Delivery**, Piscataway, v. 20, n. 2, p. 894–903, 2005. ISSN 0885-8977. DOI 10.1109/TPWRD.2005.844271.
45. MAMIŞ, M. S.; MERAL, M. E. State-space modeling and analysis of fault arcs. **Electric Power Systems Research**, Amsterdam, v. 76, n. 1–3, p. 46–51, 2005. ISSN 0378-7796. DOI 10.1016/j.epsr.2005.04.002.
46. KUROKAWA, S. et al. Representação de linhas de transmissão por meio de variáveis de estado levando em consideração o efeito da frequência sobre os parâmetros longitudinais. **Controle & Automação**, Campinas, v. 18, n. 3, p. 337–347, 2007. ISSN 0103-1759.
47. KUROKAWA, S. et al. Using state-space techniques to represent frequency dependent single-phase lines directly in time domain. 2008 In: IEEE/PES TRANSMISSION AND DISTRIBUTION CONFERENCE AND EXPOSITION: LATIN AMERICA, 2008, Bogotá. **Anais [...]** Bogota: [s. n.], 2008. p. 1-5. DOI 10.1109/TDC-LA.2008.4641842.
48. KUROKAWA, S. et al. Inclusion of the frequency effect in the lumped parameters transmission line model: State space formulation. **Electric Power Systems Research**, Amsterdam, v. 79, n. 7, p. 1155–1163, 2009. ISSN 03787796. DOI 10.1016/j.epsr.2009.02.007.
49. MORENO, P. et al. Frequency domain transient analysis of transmission networks including non-linear conditions. **International Journal of Electrical Power & Energy Systems**, London, v. 27, n. 2, p. 139–146, 2005. ISSN 01420615. DOI 10.1109/PTC.2003.1304291.
50. HENRIKSEN, T. Approximations introduced by lumped resistances in a transmission line

model. **Electric Power Systems Research**, Amsterdam, v. 76, n. 8, p. 602–607, 2006. ISSN 03787796. DOI 10.1016/j.epsr.2005.12.007.

51. COELHO MARQUES DA COSTA, E.; PRADO, A. J. DO; BOVOLATO, L. F. **Parâmetros discretos e distribuídos para o estudo de transitórios eletromagnéticos**. In: CONGRESSO BRASILEIRO DE AUTOMÁTICA, 18., 2010, Bonito. **Anais** [...] Bonito: [s. n.], 2010. p. 3911-3916.

52. MORENO, P.; RAMIREZ, A. Implementation of the numerical Laplace transform: A review. **IEEE Transactions on Power Delivery**, Piscataway, v. 23, n. 4, p. 2599–2609, 2008. ISSN 08858977. DOI 10.1109/TPWRD.2008.923404.

53. GÓMEZ, P.; URIBE, F. A. The numerical Laplace transform: An accurate technique for analyzing electromagnetic transients on power system devices. **International Journal of Electrical Power and Energy Systems**, London, v. 31, n. 2–3, p. 116–123, 2009. ISSN 01420615. DOI 10.1016/j.ijepes.2008.10.006.

54. GUSTAVSEN, B. Improving the pole relocating properties of vector fitting. **IEEE Transactions on Power Delivery**, Piscataway, v. 21, n. 3, p. 1587–1592, 2006. ISSN 08858977. DOI 10.1109/TPWRD.2005.860281.

55. DESCHRIJVER, D. et al. Macromodeling of multiport systems using a fast implementation of the vector fitting method. **IEEE Microwave and Wireless Components Letters**, Piscataway, v. 18, n. 6, p. 383–385, 2008. ISSN 1531-1309. DOI 10.1109/LMWC.2008.922585.

56. DUESTERHOEFT, W. C.; SCHULZ, M. W.; CLARKE, E. Determination of Instantaneous Currents and Voltages by Means of Alpha, Beta, and Zero Components. **Transactions of the American Institute of Electrical Engineers**, New York, v. 70, n. 2, p. 1248–1255, 1951. ISSN 0096-3860. DOI 10.1109/T-AIEE.1951.5060554.

57. PINHEIRO, M. G.; TAVARES, M. C. Análise de sensibilidade de parâmetros elétricos de linhas de transmissão dependentes na frequência. **Sba: Controle & Automação**, Sociedade Brasileira de Automatica, v. 20, n. 3, p. 335-344, 2009.

58. TORREZ CABALLERO, P.; COSTA, E. C. M.; KUOKAWA, S. Frequency-dependent multiconductor line model based on the Bergeron method. **Electric Power Systems Research**, Amsterdam, v. 127, p. 314–322, 2015. ISSN 03787796. DOI 10.1016/j.epsr.2015.05.019.

59. TORREZ CABALLERO, P.; COELHO MARQUES DA COSTA, E.; KUOKAWA, S. Using the frequency-dependent bergeron line model to simulate transients. In: CONFERÊNCIA BRASILEIRA SOBRE QUALIDADE DA ENERGIA ELÉTRICA, 11., Campina Grande. **Anais** [...] Campina Grande: CBQEE, 2015. p. 1-6.

60. TORREZ CABALLERO, P.; MARQUES COSTA, E. C.; KUOKAWA, S. Frequency-

dependent line model in the time domain for simulation of fast and impulsive transients.

International Journal of Electrical Power and Energy Systems, London, v. 80, p. 179–189, 1 set. 2016. DOI 10.1016/j.ijepes.2016.01.051.

61. TORREZ CABALLERO, P.; COELHO MARQUES DA COSTA, E.; KUROKAWA, S. Análise de desempenho de modelos de linhas de transmissão a parâmetros discretos. In: SIMPÓSIO BRASILEIRO DE SISTEMAS ELÉTRICOS, 6., Natal. **Anais [...]** Natal: SBSE, 2016. p. 1-5.

62. HAFNER, A. A. et al. Modeling of Power Cables with Arbitrary Cross Section: From Parameter Calculation to Electromagnetic Transients Simulation. **Journal of Control, Automation and Electrical Systems**, Heidelberg, v. 28, n. 3, p. 405–417, 22 jun. 2017. ISSN 2195-3880. DOI 10.1007/s40313-017-0308-0.

63. TORREZ CABALLERO, P.; MARQUES COSTA, E. C.; KUROKAWA, S. Modal decoupling of overhead transmission lines using real and constant matrices: Influence of the line length. **International Journal of Electrical Power & Energy Systems**, London, v. 92, p. 202–211, nov. 2017. ISSN 01420615. DOI 10.1016/j.ijepes.2017.05.006.

64. TORREZ CABALLERO, P.; KUROKAWA, S.; KORDI, B. Routine for simulating transmission lines with symmetrical and asymmetrical configurations using a real and constant modal transformation matrix. In: ANNUAL IEEE CANADA ELECTRICAL POWER AND ENERGY CONFERENCE, 18., 2018, Toronto. **Proceedings [...]** Piscataway: IEEE, 2018. p. 1-6.

65. TORREZ CABALLERO, P.; KUROKAWA, S.; KORDI, B. Accelerated frequency-dependent method of characteristics for the simulation of multiconductor transmission lines in the time domain. **Electric Power Systems Research**, Amsterdam, v. 168, p. 55–66, mar. 2019. ISSN 03787796. DOI 10.1016/j.epsr.2018.11.006.

66. HOFMANN, L. Series expansions for line series impedances considering different specific resistances, magnetic permeabilities, and dielectric permittivities of conductors, air, and ground. **IEEE Transactions on Power Delivery**, Piscataway, v. 18, n. 2, p. 564–570, 2003. ISSN 0885-8977. DOI 10.1109/TPWRD.2003.810493.

67. ASTI, G. A. **Um procedimento de estimação de parâmetros de linhas de transmissão baseado na teoria de decomposição modal**. 2010. Dissertação (Mestrado em Engenharia Elétrica) - Faculdade de Engenharia, Universidade Estadual Paulista, Ilha Solteira, 2010.

68. DWIGHT, H. B. Skin Effect in Tubular and Flat Conductors. **Transactions of the American Institute of Electrical Engineers**, Piscataway, v. 37, n. 2, p. 1379-1403, 1918. ISSN 0096-3860. DOI 10.1109/T-AIEE.1918.4765575.
69. FUCHS, R. D. **Transmissão de Energia Elétrica: linhas aéreas**. Itajuba: Escola Federal de engenharia de Itajuba, 1977.
70. MINGLI, W.; YU, F. Numerical calculations of internal impedance of solid and tubular cylindrical conductors under large parameters. **IEE Proceedings - Generation, Transmission and Distribution**, Stevenage, v. 151, n. 1, p. 67–72, 2004. ISSN 1350-2360. DOI 10.1049/ip-gtd:20030981.
71. STEVENSON, W. D. J. **Elements of power system analysis**. 4. ed. New York: McGraw Hill, 1955.
72. BRYANT, D. **ACSR and ACCC**. Disponível em: <https://commons.wikimedia.org/wiki/File:ACSR_and_ACCC.JPG>. Acesso em: 10 fev. 2018bs.
73. TLEIS, N. **Power Systems Modelling and Fault Analysis**. Boston: Newnes, 2007.
74. YAMANAKA, F. N. R. **Inclusão do efeito da frequência nas equações de estado de linhas bifásicas: análise no domínio do tempo**. 2009. 108 f. Dissertação (Mestrado em Engenharia Elétrica) - Faculdade de Engenharia, Universidade Estadual Paulista, Ilha Solteira, 2009.
75. KUROKAWA, S. et al. Behavior of overhead transmission line parameters on the presence of ground wires. **IEEE Transactions on Power Delivery**, Piscataway, v. 20, n. 2, p. 1669–1676, 2005. ISSN 08858977. DOI 10.1109/TPWRD.2004.833916.
76. CHIPMAN, R. A. **Schaum's outline of theory and problems of transmission lines**. New York: McGraw Hill, 1968.
77. GUSTAVSEN, B. Validation of frequency-dependent transmission line models. **IEEE Transactions on Power Delivery**, Piscataway, v. 20, n. 2, p. 925–933, 2005. ISSN 0885-8977. DOI 10.1109/TPWRD.2004.837676.
78. DORF, R. C.; BISHOP, R. H. **Modern control systems**. 13th ed. New York: Pearson, 2016. 1032 p.
79. CENTRE, M. H. R. **Standard surge waveforms**. PSCAD X4 (v4.6). [S. l.: s. n.], 2018. Disponível em: [https://hvdc.ca/webhelp/ol-help.htm#Master_Library_Models/CSMF/Surge_Generators/Wavelet_Transformation_\(WT\).htm](https://hvdc.ca/webhelp/ol-help.htm#Master_Library_Models/CSMF/Surge_Generators/Wavelet_Transformation_(WT).htm) Acesso em: 11 fev. 2018.
80. AMETANI, A. et al. **Power system transients: theory and applications**. Boca Raton: CRC

Press, 2013.

81. EXPOSITO, A. G.; CONEJO, A. J.; CAÑIZARES, C. **Electric energy systems analysis and operation**. Boca Raton: Taylor & Francis Group, 2009.

82. FERNANDES, A. B.; NEVES, W. L. A. Phase-domain transmission line models considering frequency-dependent transformation matrices. **IEEE Transactions on Power Delivery**, Pistacaway, v. 19, n. 2, p. 708–714, abr. 2004. ISSN 0885-8977. DOI 10.1109/TPWRD.2003.822536.

83. WEDEPOHL, L. M.; NGUYEN, H. V. Frequency-dependent transformation matrices for untransposed transmission lines using newton-raphson method. **IEEE Transactions on Power Systems**, Pistacaway, v. 11, n. 3, p. 1538–1546, 1996. ISSN 08858950. DOI 10.1109/59.535695.

84. HIGHAM, N. J. **Cholesky factorization wiley interdisciplinary reviews computational statistics**. Manchester: The University of Manchester, 2008. DOI 10.1002/wics.18.

85. BOYD, S.; VANDENBERGHE, L. **Convex optimization**. Cambridge: Cambridge University Press, 2004.

86. GOLUB, G. H.; VAN LOAN, C. F. **Matrix computations physics today**. [S. l: s. n.], 1996. ISSN 00036935. DOI 10.1063/1.3060478.

87. CLARKE, E. **Circuit analysis of A-C power systems**. New York: John Wiley & Sons, 1943. v. 1.

88. COELHO MARQUES DA COSTA, E. et al. Simplified computational routine to correct the modal decoupling in transmission lines and power systems modelling. **IET Science, Measurement & Technology**, Stevenage, v. 7, n. 1, p. 7–15, 2013. ISSN 1751-8822. DOI 10.1049/iet-smt.2012.0057.

89. DOMMEL, H. W.; MEYER, W. S. Computation of electromagnetic transients. **Proceedings of the IEEE**, Pistacaway, v. 62, n. 7, p. 983–993, 1974. ISSN 15582256. DOI 10.1109/PROC.1974.9550.

90. ABDELAZIZ, A. Y. et al. Modern approaches for protection of series compensated transmission lines. **Electric Power Systems Research**, London, v. 75, n. 1, p. 85–98, 2005. ISSN 03787796. DOI 10.1016/j.epsr.2004.10.016.

91. FARIA, J. A. B.; BRICENO, J. H. On the modal analysis of asymmetrical three-phase transmission lines using standard transformation matrices. **IEEE Transactions on Power Delivery**, Pistacaaway, v. 12, n. 4, p. 1760–1765, 1997. DOI 10.1109/61.634202.

92. WEDEPOHL, L. M. Application of matrix methods to the solution of travelling-wave

phenomena in polyphase systems. **Proceedings of the Institution of Electrical Engineers**, Stevenage, v. 110, n. 12, p. 2200–2212, 1963. DOI 10.1049/piee.1963.0314.

93. SWOKOWSKI, E. W. **Cálculo com geometria analítica**. Rio de Janeiro: Brasil Editora, 1995.

94. MARTINEZ, J. A.; GUSTAVSEN, B.; DURBAK, D. Parameter determination for modeling system transients--part i: overhead lines. **IEEE Transactions on Power Delivery**, Piscataway, v. 20, n. 3, p. 2038–2044, 2005. ISSN 0885-8977. DOI 10.1109/TPWRD.2005.848678.

95. BRANIN, F. H. J. Computer methods of network analysis. **Proceedings of the IEEE**, Piscataway, v. 55, n. 11, p. 1787–1801, 1967. ISSN 0018-9219. DOI 10.1109/PROC.1967.6010.

96. MARTINEZ-VELASCO, J. A. Digital computation of electromagnetic transients in power systems: current status. In: EUROPEAN EMTP-ATP USERS GROUP (EEUG), 1997, [S. l.]. **Proceedings** [...] [S. n.: s. n.], 1997. p. 1-19.

97. SARTO, M. S.; SCARLATTI, A.; HOLLOWAY, C. L. On the use of fitting models for the time-domain analysis of problems with frequency-dependent parameters. In: IEEE INTERNATIONAL SYMPOSIUM ON ELECTROMAGNETIC COMPATIBILITY, 2001, Montreal. **Proceedings** [...] Piscataway: IEEE, 2001. p. 588-593. ISSN 01901494. DOI 10.1109/IEMC.2001.950710.

98. ANTONINI, G. SPICE equivalent circuits of frequency-domain responses. **IEEE Transactions on Electromagnetic Compatibility**, Piscataway, v. 45, n. 3, p. 502–512, 2003. ISSN 00189375. DOI 10.1109/TEMC.2003.815528.

99. LI, B. et al. Equivalent circuit model of frequency-domain responses with external field. **IEEE International Symposium on Electromagnetic Compatibility**, Piscataway, v. 2015–Septm, p. 761–766, 2015. ISSN 21581118. DOI 10.1109/IEMC.2015.7256259.

100. TORREZ CABALLERO, P.; MARQUES COSTA, E. C.; KUROKAWA, S. Fitting the frequency-dependent parameters in the Bergeron line model. **Electric Power Systems Research**, Amsterdam, v. 117, p. 14–20, 2014. ISSN 03787796. DOI 10.1016/j.epsr.2014.07.023.

101. TORREZ CABALLERO, P. **Representação de linhas de transmissão por meio do modelo de bergeron**: inclusão do efeito da frequência nos parâmetros longitudinais. 2014. 100 f. Dissertação (Mestrado em Engenharia Elétrica) - Faculdade de Engenharia, Universidade Estadual Paulista, Ilha Solteira, 2014.

102. SILVA, R. C. DA et al. Integration Methods Used in Numerical Simulations of Electromagnetic Transients. **IEEE Latin America Transactions**, Piscaway, v. 9, n. 7, p. 1060–1065, 2011. ISSN 1548-0992. DOI 10.1109/TLA.2011.6129703.
103. FATHONI, M. F.; WURYANDARI, A. I. Comparison between euler, heun, runge-kutta and adams-bashforth-moulton integration methods in the particle dynamic simulation. In: INTERNATIONAL CONFERENCE ON INTERACTIVE DIGITAL MEDIA (ICIDM), 4th., 2015, [S. l.]. **Anais [...]** Piscaway: IEEE, 2015. DOI 10.1109/IDM.2015.7516314.